Dietrich Kohlheyer

# Microfluidic free-flow electrophoresis for proteomics-on-a-chip


MESA+
Institute for Nanotechnology

# MICROFLUIDIC FREE-FLOW ELECTROPHORESIS FOR PROTEOMICS-ON-A-CHIP

MESA+
Institute for Nanotechnology

University of Twente
The Netherlands

The described research was performed at the "Sensorsystems for biomedical and environmental applications" group (BIOS) of the MESA+ Research Institute for Nanotechnology at the University of Twente, Enschede, The Netherlands. This research was financially supported by the Dutch technology foundation STW project 06209.

Samenstelling promotiecommissie:

| | | |
|---|---|---|
| *Voorzitter* | | |
| | Prof. Dr. Ing. M. Wessling | Universiteit Twente |
| *Promotor* | | |
| | Prof. Dr. Ir. A. van den Berg | Universiteit Twente |
| *Assistent Promotor* | | |
| | Dr. Ir. R.B.M. Schasfoort | Universiteit Twente |
| *Leden* | | |
| | Dr. J.C.T. Eijkel | Universiteit Twente |
| | Prof. Dr. Ir. J.G.E. Gardeniers | Universiteit Twente |
| | Prof. Dr. A. Manz | ISAS, Institute for Analytical Sciences |
| | Prof. Dr. G.J. de Jong | Universiteit Utrecht |
| | PD Dr. C. Eckerskorn | BD Diagnostics, Munich |

Title: Microfluidic Free-Flow Electrophoresis for Proteomics-on-a-chip
Cover: Free-flow isoelectric focusing of fluorescently labeled molecules
Author: Dietrich Kohlheyer
ISBN: 978-90-365-2666-1

# MICROFLUIDIC FREE-FLOW ELECTROPHORESIS FOR PROTEOMICS-ON-A-CHIP

DISSERTATION

to obtain
the degree of doctor at the University of Twente
on the authority of the rector magnificus,
prof. dr. W.H.M. Zijm,
on account of the decision of the graduation committee,
to be publicly defended
on Friday the 20th of June 2008 at 16:45 hrs

by

**Dietrich Kohlheyer**
born on the 17th of December 1979
in Cologne, Germany.

Dit proefschrift is goedgekeurd door

Promotor: prof. dr. ir. Albert van den Berg

Assistent promotor: dr. ir. Richard B. M. Schasfoort

# Table of Content

# 1 Introduction

*This introduction chapter gives a broad overview on various aspects included in this thesis. Besides the general research description as well as the specific objectives, some underlying theory and principles are explained. Furthermore, the development process towards the application of microfluidic free-flow electrophoresis as a tool for future proteome research is briefly described. Finally an outline of this thesis is given.*

## 1.1 Proteomics-on-a-Chip for Monitoring Autoimmune Diseases

With the increasing requirement for fast and accurate analytical tools for proteomics, as will be explained in the following section, the researched project: "Proteomics-on-a-chip for monitoring autoimmune diseases" was engaged in 2004 by three cooperating Dutch Universities, namely: University of Twente, University of Utrecht and University of Nijmegen. This project was funded by the national technology foundation STW after a positive advise of the IOP Genomics program committee of the Dutch Ministry of Economic Affairs.

### 1.1.1 Primary and Secondary Project Goals

The research in the project "Proteomics-on-a-chip for monitoring autoimmune diseases" was driven by the need for alternative rapid methods for separation and analysis of the highly complex protein mixtures that are inherent to proteomics research.

The primary objective was to develop a device for screening the auto antibody repertoire of Rheumatoid Arthritis patients for monitoring typical autoimmune fingerprints. The proposed goal was to implement surface plasmon resonance imaging as a label free biosensing principle for screening the autoantibody repertoire of RA patients in only one step. Therefore a prespotted chip with biomarker ligands was

exposed to diluted patient serum and the biomolecular interactions should be monitored directly as a result of the specific binding of autoimmune antibodies.

The secondary objective was to discover new potential biomarkers which are typical for a class of autoimmune diseases by using an integrated proteomics-on-a-chip device. The device should mimic classical two dimensional gel electrophoresis based on separation of a mixture of proteins/peptides by charge and molecular weight differences. It was proposed to develop successive on-chip separations combined with surface plasmon resonance (SPR) imaging as a prescreening step for identification of potential biomarkers using mass spectrometry. The feasibility of this new approach has to be demonstrated for autoantibody interactions in autoimmune diseases. The integrated proteomics-on-a-chip technology will be applied to discover new autoimmune biomarkers and to develop diagnostic applications based on these new autoantigens. [Project description, STW project 06209]

### 1.1.2 Complementary Tasks

In order to fulfill this challenging task with its high diversity in technological and bio-chemical aspects and multidisciplinary disciplines, the project was divided into several complementary tasks carried out at the three universities for the primary and secondary goals of the project, as briefly described in the following:

1. *University of Twente, Expertise of microfluidic separation and detection technologies:*
   a) SPR imaging in combination with spotting microfluidics b) **microchip electrophoresis using continuous sample flow microfluidics and microarray surface plasmon resonance imaging**.
2. *University of Utrecht, Expertise of separation (CE) and identification (MS) methodologies:*
   a) Capillary electrophoresis with focus on capillary isoelectric focusing (cIEF) and other sample pre-treatment strategies with regard to autoimmune diseases. b) Hyphenating SPR and MS
3. *University of Nijmegen, Expertise of autoimmune diseases on a molecular level:*
   Supply of relevant recombinant autoantigens and autoantibodies and screening methods for the autoimmune repertoire in patient serum

In this thesis the more technical results of task 1.b (highlighted in bold) are given and discussed, whereby the main focus is on free-flow electrophoresis as a new tool for proteomics-on-a-chip.

## 1.2 Proteomics-on-a-Chip

The successful sequencing of the human genome provided researchers with information on the construction of human beings. However, the genome, the entire genetic code, does not itself perform any active role in building the organism. The sequence of individual subunits (bases) of the DNA only determines hereditary features. By a complex series of interactions, this series is translated into the production of all the proteins of the organism in the appropriate time and place. These proteins form part of the human body, build the body and perform necessary metabolic reactions [1]. In order to allow further insight in the relevant processes and the proteins involved, the relatively young research field *proteomics* is expanding rapidly.

> *Proteomics is the analysis of amounts and types of proteins produced by a genome and the study of their interactions and biological functions [2].*

Unfortunately, gene expression and protein interactions are very dynamic processes, which make the study of the proteome more complex than exploring the information lying in the genome. Furthermore, the increasing importance of proteomics has not been accompanied by a corresponding improvement in analytical tools. Proteomics still relies primarily on the low throughput technique of two-dimensional slab gel electrophoresis, spot excision, digestion, mass spectrometry (MS) and database interrogation [3, 4]. The analytical challenge of proteomics becomes clear when investigating the vast amount of proteins present in e.g. a mammalian sample. Such samples contain often more than 20.000 different proteins with some in very low concentrations, therefore putting high demands on the analytical identification procedure. Due to the enormous complexity of the proteome, focus in proteomics shifts more and more from attempting to study the complete proteome towards the targeted analysis of parts of the proteome [5].

In recent years, new microfluidic and microarray technologies have appeared for proteomics. These miniaturized proteomics-on-a-chip devices benefit from short

analysis times, high surface to volume ratios and small amounts of required sample. Due to the high sample complexity emphasis is put on fractionation and separation technologies and enrichment of relevant compounds in microfluidic platforms but also on dense microarray technology in order to process high amounts of sample on the same substrate. Since MS plays a major role in proteomics the coupling of separation devices with ESI-MS but also other hyphenated systems have been investigate for years now.

As an example of microarray based proteomics one is referred to the article published by project coworkers of the University of Nijmegen and University of Twente. Lokate et al. [6] applied microarray technology with the affinity-based detection method SPR (briefly introduced in section 1.5) to monitor biomolecular interactions of autoantibodies, as shown in Fig. 1.1. The project partners have run tests on the blood serum of 50 RA patients as well as a control group of 29 persons. Diluted serum was flushed over a special gold coated microchip containing different spots with a specific peptide coating. Whenever these peptides interacted with auto-antibodies present in the serum, this process was monitored by SPR imaging. The authors concluded that the applicability of this scanning SPR technology goes beyond monitoring the presence of autoantibodies in sera of autoimmune patients. Real-time monitoring of the binding allows the user to study the association and dissociation rate constants for determining the affinity constants of the biomolecular interactions. This new scanning SPR technique will be of great use in any field that requires high-detection power and high-throughput analyses [6, 7].

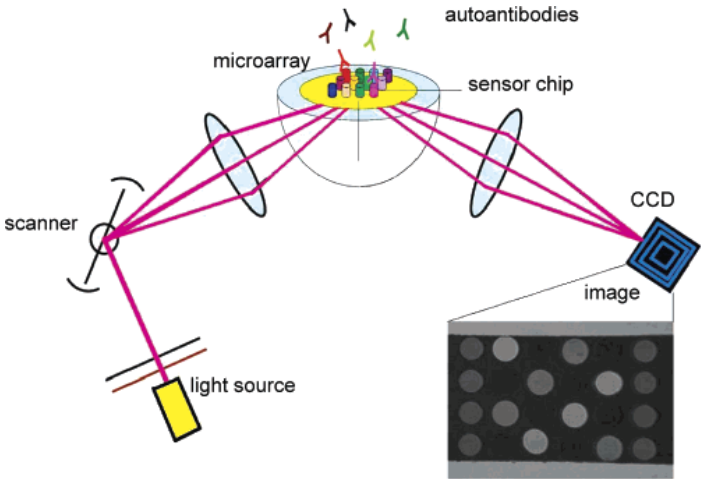


Fig. 1.1 Schematic representation of the optical configuration of the scanning angle SPR imaging instrument. Citrullinated peptides and control peptides are chemically anchored on discrete spots of the microarray. Autoantibodies from diluted rheumatoid arthritis patient serum were flushed over the sensor chip. The incident light is being reflected by the angle operated mirror before reaching the hemispheric prism and gold sensor, and the microarray is imaged on a CCD. [6]

For more information on proteomics-on-a-chip in general and relevant publications, the reader is referred to recent reviews [2-4, 8-10].

## 1.3 Electrokinetics

### 1.3.1 Electrical Double Layer and Related Phenomena

Many substances generate a surface charge when brought into contact with an electrolyte (e.q. aqueous medium), the possible charging mechanisms being ionization, ion adsorption and ion dissolution. In case of the commonly applied material glass and similar materials, silanol groups dissociate protons resulting in a negative surface charge. This acquired surface charge influences the ion distribution near the surface by attracting counter ions (ions of opposite charge) and repelling co-ions (same charge-ions). This accumulation of ions at the charged surface forms what is known as the electrical double layer, as shown in Fig. 1.2 and Fig. 1.3.

*Electroosmotic flow is the motion of the bulk liquid relative to a stationary charged surface with an electrical double layer (e.g. a capillary or microchannel) induced by en electrical field.*

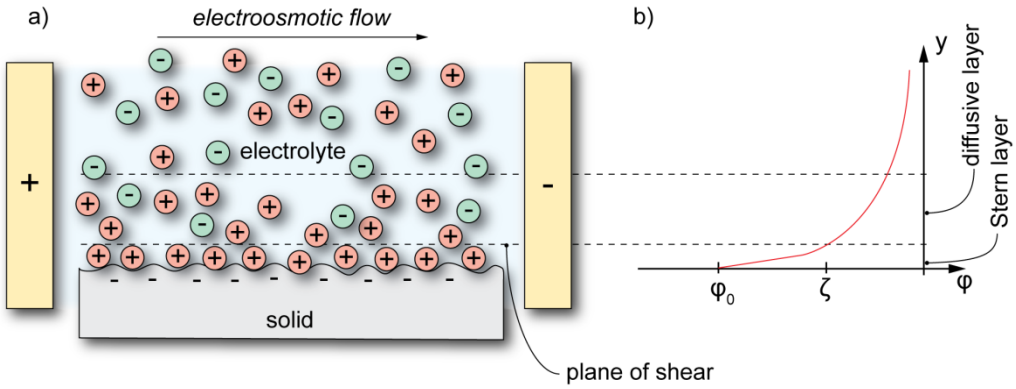


Fig. 1.2 (a) Electrical double layer formation at a negatively charged wall and electroosmotic flow. The Stern layer is a single-ion layer of ions adherent to the surface, the diffuse layer is the adjacent charged layer with freely moving hydrated ions. (b) Resulting potential distribution; $\varphi_0$ is the surface potential, $\zeta$ is the potential at the position of the first mobile ions in the diffuse layer.

The ions immediately next to the surface, so strongly attracted that they become (partly) immobile, form the Stern layer. The thickness of the Stern layer is approximately equal to an ionic diameter. The diffuse double layer contains mobile hydrated ions distributed according to the influence of electrical forces and random thermal motion. The thickness of the diffusive layer is also referred to as Debye length. The shear plane separates the Stern and the diffuse double layer and in simple models of the EDL, it is the location where fluid slips along the surface. The electrical potential at the shear plane is called zeta potential ($\zeta$).

When an electrical field is applied parallel to a charged wall with an EDL the mobile ions in the diffusive layer show a net migration into the opposite direction dragging the solvent with them, thus causing flow referred to as electroosmotic flow, as illustrated in Fig. 1.2.

*Electrophoresis is the motion of dispersed* charged particles *and dissolved molecules relative to a stationary fluid under the influence of a uniform* electric field*.*

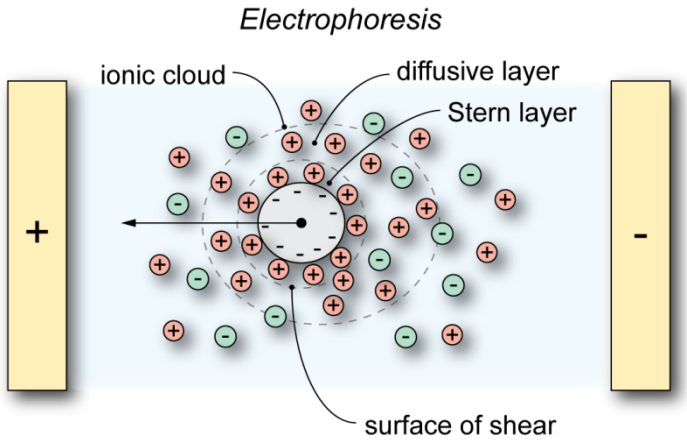


Fig. 1.3 Electrical double layer formation at a negatively charged sphere. When an electrical field is applied the charged particle migrates into the direction of the opposite charged electrode. This effect is referred to as electrophoresis.

When an electrical field is applied to a charged dispersed particle with an electrical double layer present, the particle is set into motion and migrates towards the electrode of opposite electrical charge. This phenomenon is known as electrophoresis, as shown in Fig. 1.3. Assuming that dissolved bio-molecules to be massive particles with a shape comparable to a sphere, this idealized model of the EDL formation is also applicable for proteins. For more specific particle and molecule related EDL aspects, one is referred to the book by Bier [11].

For more information on electrokinetic phenomena the reader is referred to the relevant literature, e.g. [12, 13].

### 1.3.2 Electrophoresis

To reduce the high sample complexity in proteomics research *electrophoresis* is the most applied method to separated protein samples. The most common methods in CE are slab gel electrophoresis, capillary electrophoresis and free-flow electrophoresis. For particles and molecules whereby the Debye length (width of the diffusive layer) is small compared to the particle size the electrophoretic mobility $\mu_{ep}$ ($m^2/(Vs)$) of the particle is usually expressed by the Smoluchowski equation:

$$\mu_{ep} = \frac{\varepsilon_r \varepsilon_0 \zeta_p}{\eta} \tag{1.1}$$

where $\varepsilon_r$ is the dielectric constant, $\varepsilon_0$ the permittivity of free space, $\zeta_p$ the zeta potential of the particle and $\eta$ the viscosity of the fluid

### 1.3.3 Electroosmotic Flow

The flow velocity induced by the electrical force acting on the mobile ions of the electrical double layer is proportional to the applied electrical field $E$ (V/m), the surface charge and the viscosity of the liquid. Usually it is expressed by

$$u_{EOF} = \frac{\varepsilon_r \varepsilon_0 \zeta_{wall}}{\eta} E \tag{1.2}$$

in which $\zeta_p$ is the zeta potential of the wall.

## 1.4 Continuous Flow Microfluidics

*Continuous flow microfluidics is based on the control of continuous liquid flow through micromachined channels. The liquid flow can be generated either by external pressure sources, external mechanical pumps, integrated mechanical micropumps, or by electroosmotic flow. Continuous-flow devices are adequate for many well-defined and simple biochemical applications, and for certain tasks such as pre-fractionation.*

One of the main goals of this research project was the coupling of a miniaturized separation unit with an affinity based detection array possibly for surface plasmon resonance. The preliminary concept, as illustrated in Fig. 1.4, was to integrate capillary electrophoresis, the bio-sensing array and the introducing sample steering capability. In that way fractionated sample plugs could be guided over specific bio-sensing regions. However, separation by capillary electrophoresis leads to the formation of discrete sample plugs of nanoliter volume. The amount of relevant bioactive material and the sample contact time as a result are so limited, that the demands on the detection system are too high. Therefore, with the proposed concept as indicated in figure 1.4 it was calculated that the project partners should not be able to detect low abundant protein/peptides and therefore it was decided in an early stage to reject the concept of the CE-SPR as hyphenation technology. In order to achieve long contact times of low abundant separated protein material it was foreseen

that a continuous separation method such as free-flow electrophoresis might offer an interesting and viable alternative. In this thesis not only the separation unit but also interconnects and other relevant sub-units of the proteomics on a chip device were designed and investigated for use in a continuous flow system.

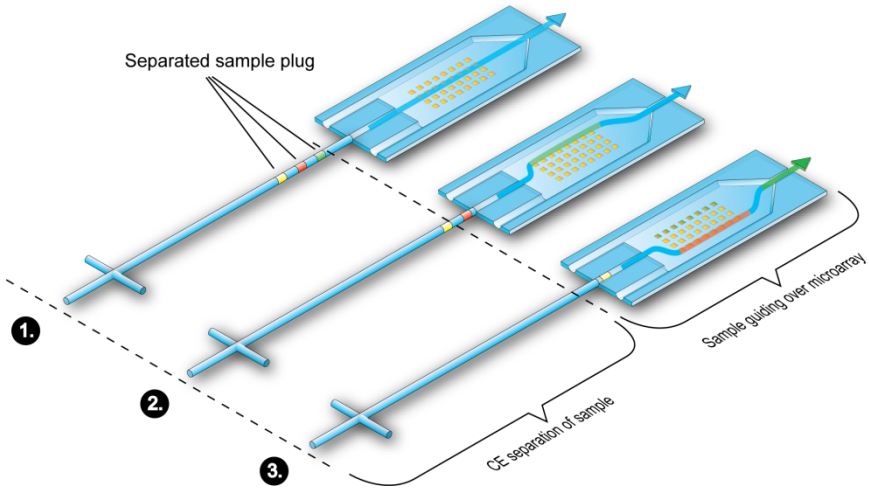


Fig. 1.4 Preliminary concept of the proteomics-on-a-chip device, later discarded: Microchip capillary electrophoresis coupled to an affinity based bio-sensing array with sample steering capability. (1), (2) and (3): different sample components are guided over sensing lanes by hydrodynamic focusing. Final concept: see Fig. 1.6.

## 1.5 Surface Plasmon Resonance

At the interface between two transparent media of different refractive index, light coming from the side of higher refractive index is partly reflected and partly refracted. Above a certain critical angle of incidence, no light is refracted across the interface, and total internal reflection is observed. While the incident light is totally reflected, the electromagnetic field component penetrates a short (about half the wavelength of the light) distance into the medium of lower refractive index creating an exponentially decreasing evanescent wave. If the interface between the media is coated with a thin layer of metal (e.g. gold), and light is monochromatic and p-polarized, the light induces oscillations of the free electrons (so-called plasmons) in the thin layer of gold. As a result of these induced oscillations, the intensity of the reflected light is reduced at a specific incident angle producing a sharp shadow (called surface plasmon resonance, SPR).

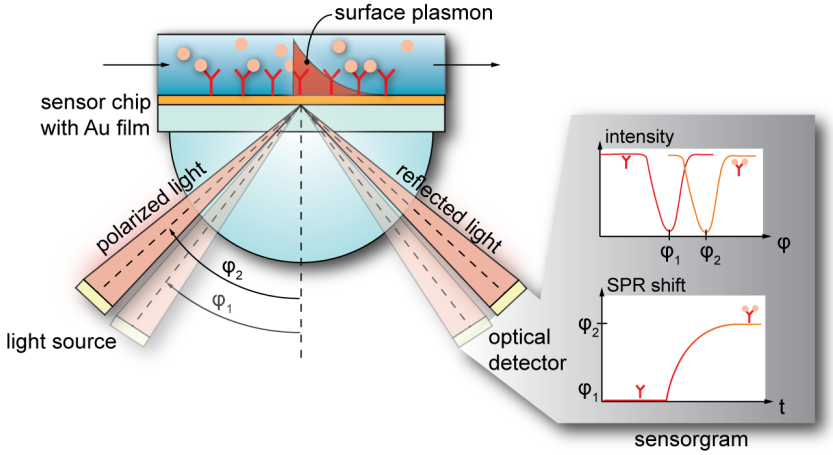


Fig. 1.5 Principle of surface plasmon resonance (SPR): P-polarized light is reflected under total internal reflection at the glass-gold interface. At a specific incident angle light energy is transferred into plasmons resulting in a light reflection intensity dip. Immobilization of molecules on the surface causes an angle shift, which can be followed in time to obtain the sensorgram giving information about association and dissociation of molecules.

The SPR conditions are influenced by the refractive index of the material adsorbed onto the thin metal film, as illustrated in Fig. 1.5 and an example given in Fig. 1.1. A satisfactory linear relationship is found between refractive index shift and mass of biochemically relevant molecules such as proteins adsorbed to the surface and changing the dielectric constant of the evanescent field. The SPR signal which is

expressed in millidegree units is therefore a measure of mass density at the sensor chip surface. This means that the analyte and ligand association and dissociation can be observed and ultimately rate constants as well as equilibrium constants can be calculated.

## 1.6 Overall Objective of the Research

As briefly described in the previous sections 1.3, 1.4 and 1.5 the major aspects to be developed in this thesis were: electrophoresis (sample preparation and separation), continuous flow microfluidics (sample control and supply) and array based SPR (detection). Microfluidic free-flow electrophoresis was chosen as the sample preparation and separation method. Since previously published results on microfluidic free-flow electrophoresis seemed insufficient for the proteomics-on-a-chip system, emphasis was put on the development of an improved free-flow electrophoresis chip device for protein separation. Therefore, most of the work performed is related to free-flow electrophoresis and minor sub projects were dedicated to the investigation of microfluidic systems for micro-array approaches and bio-sensing related systems. However, the overall system as illustrated in Fig. 1.6 remained the guiding objective throughout the project. This device should be capable of: 1. separating a purified sample mixture of interest, e.g. sample fluid from patients suffering from autoimmune disease; 2. Immobilizing lanes of fractionated compounds; and 3. Monitoring of interaction while flushing the device with relevant anti ligands. Eventually, in investigations which were not part of this project, immobilized fractions which were found to give a positive response in the interaction step would then analyzed further by MS. It is obvious, that this challenging project involved taking many hurdles, in which very good progress was made, while some hurdles still remain to be taken.

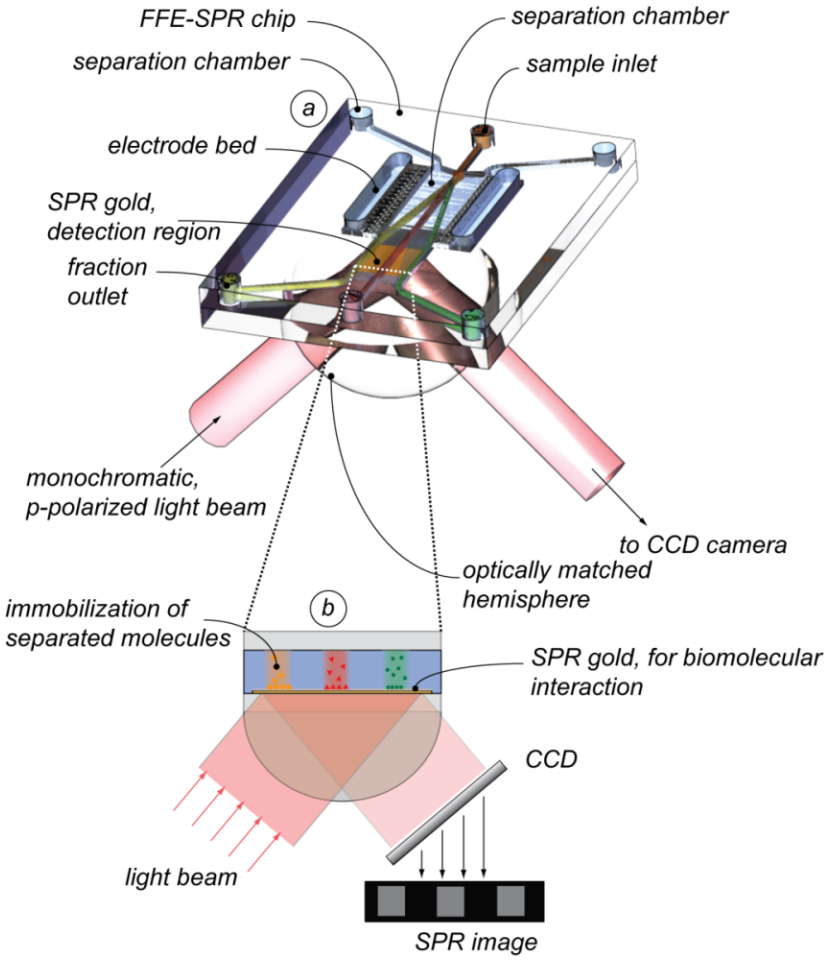


Fig. 1.6 Concept of the proteomics-on-a-chip device: (a), Separation of sample is performed in a continuous manner, by free-flow electrophoresis. (b), Separated fractions are guided over an affinity based detection array whereby immobilization of molecules is followed real-time by surface plasmon resonance.

## 1.7 Outline of this Thesis

Besides the introduction chapter, this thesis contains one theoretical and literature chapter and seven experimental chapters, which mainly focus on the development of free-flow electrophoresis chips but also, as explained in the previous sections, of related continuous-flow devices.

Chapter 2 describes the principle of miniaturized free-flow electrophoresis, gives related theory and a literature overview on results published so far.

In chapter 3 a new free-flow electrophoresis chip is presented and experimental results are discussed.

Several chip improvements, with respect to the previous design presented in chapter 3 led to increased separation efficiency, in particular in the mode of free-flow isoelectric focusing. These results are shown and discussed in chapter 4.

Furthermore, a new FFE chip design and results are presented in chapter 5. In this chip gas formation was suppressed by supplying a redox couple to the electrode area, obviating the need for special membranes as implemented in the previous designs.

A digression concerning a new microfluidic patterning approach was investigated to form a biosensing microarray inside the chip device. Although not further investigated with respect to a possible integration in the total device, the results are given in chapter 6.

Furthermore, based on the same technical principle applied in chapter 6 a microfluidic chip was developed to manipulate two sample streams, with the future intention of further integration. This device is demonstrated and evaluated in chapter 7.

Chapter 8 gives the results on the final hyphenation approach, integrating separation and detection units into one chip device.

Finally overall conclusions are drawn and possible future developments are briefly discussed in chapter 9.

Since most of the chapters are based on published articles, information especially in the introduction sections, is repeated more often throughout this thesis. This allows a good readability of chapters separately.

# 2 Miniaturizing Free-Flow Electrophoresis

*This chapter gives an introduction on the research field of miniaturized free-flow electrophoresis systems and related theory. Furthermore, various µ-FFE devices are compared with respect to technological achievements and separation capability. This literature survey was conducted 2007 and is based on published articles as well as own research results. This review was published in Electrophoresis in 2008.*

## 2.1 Abstract

Free-flow electrophoresis separation methods have been developed and investigated for around 50 years and have been applied to many types of analytes for various biomedical applications, but also for the separation of inorganic and organic substances. Its continuous sample preparation and mild separation conditions makes it also interesting for online monitoring and detection applications. Since 1994 several microfluidic, miniaturized free-flow electrophoresis devices were developed and experimentally characterized. In contrast to their large-scale counterparts microfluidic FFE devices offer new possibilities due to the very rapid separations within several seconds or below and the requirement for sample volumes in the micro liter range. Eventually, these microfluidic FFE systems might find application in so called lab-on-a-chip devices for real-time monitoring and separation applications. This review gives detailed information on the results so far published on microfluidic free-flow electrophoresis chips, comprising its four main modes, namely free-flow zone electrophoresis (FFZE), free-flow isoelectric focusing (FFIEF), free-flow isotachophoresis (FFITP) and free-flow field-step electrophoresis (FFFSE). The principles of the different FFE modes and the basic underlying theory are given and discussed with special emphasis on miniaturization. Different designs as well as fabrication methods and applied materials are discussed and evaluated. Furthermore,

the separation results shown indicate that similar separation quality and better with respect to conventional FFE systems, as defined by the resolution and peak capacity can be achieved with microfluidic FFE separations when applying much lower electrical voltages. Furthermore innovations still occur and several approaches for hyphenated, more integrated systems have been proposed so far, some of which are discussed here. This review is intended as an introduction and early compendium for research and development within this field.

## 2.2 Introduction

Since the introduction of free-flow electrophoresis (FFE) in the 1960s [14], this separation method has found a permanent position among analytical and preparative methods in biochemistry and chemistry for the separation of e.g. cells, organelles, peptides, proteins, inorganic and organic compounds [15-18]. In free-flow electrophoresis, analytes are separated continuously in an electrical field applied perpendicular to a thin pressure driven carrier electrolyte flow between two insulating plates, as shown in Fig. 2.1. The sample mixture is injected into the carrier electrolyte flow and with increasing residence time the differently charged components split up into diverging lanes which can be collected at various device outlets.

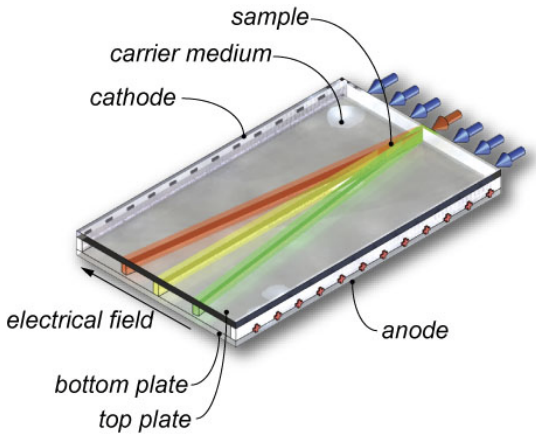


Fig. 2.1 Illustrative principle of free-flow zone electrophoresis and main components

Commercially available large scale FFE systems (e.g. BD Diagnostics, Germany) were originally developed as standalone sample clean up devices, e.g. as a pre-fractionation

step prior to 2D gel electrophoresis or other detection and identification methods. Size reduced mini-FFE systems were developed later and were coupled to mass spectrometry and liquid chromatography enabling continuous separation with online detection possibilities [19, 20]. This combination of FFE as a continuous separation method with online detection would allow for real-time monitoring of analytes, such as patients samples, reaction products and more. These size reduced systems are still complicated and slow in operation and downscaling would be very promising. Eventually such microfluidic FFE systems might find application in small portable devices and point-of-care (POC) tools [21]. With the upcoming trend of miniaturization and the development of lab-on-a-chip systems [22], also microfluidic, chip-based FFE systems have been developed and demonstrated. The miniaturization of FFE implies several advantages especially considering sample volume and separation speed. In contrast to the tens of milliliters of sample consumed by conventional large scale FFE devices, microfluidic FFE systems require only tens of nanoliters up to hundreds of microliters of sample. This is especially interesting in clinical analysis where often only low sample volumes are available. Furthermore, instead of residence times of up to tens of minutes, microfluidic FFE (μ-FFE) devices separate within several seconds. Scaling laws predict a 100-fold increase in speed for a 10-fold (linear) downscaling of a FFE experiment [23]. Such short analysis times would be very beneficial in POC devices. The shallower separation chambers of several micrometers enable good heat dissipation allowing higher electrical field strengths necessary for rapid separations. According to theory, the quality of the separation, as defined by the resolution does not decline with reduced separation geometry [24], as shown for capillary isoelectric focusing. Due to the mentioned advantages of miniaturizing FFE and due to the availability of new fabrication technologies, the interest in this field has recently grown rapidly indicated by the relatively large number of μ-FFE publications in 2005 and in 2006. This review has its focus mainly on micro FFE systems, while for a more general overview the reader is referred to the recent review by N. Pamme [25] on continuous flow separations in microfluidic devices.

This review gives detailed information about the recent developments in the field of microfluidic FFE systems including various modes of FFE. The different technological solutions and developments are critically analyzed and compared with respect to design, fabrication methods and separation quality. Furthermore, detection methods

and hyphenation aspects are discussed. In this chapter, we will first describe the common separation modes of free-flow electrophoresis and discuss basics of the related theory. In Section 2.4 we will describe different technological approaches that have been applied for FFE micro chips. In Section 2.5 recent separation results are shown and hyphenation and detection aspects are discussed in Section 2.6.

## 2.3 FFE Modes and Related Theory

Most of the modes of standard capillary electrophoresis [26] can be applied in free-flow electrophoresis (FFE) as well. The four common ones are free-flow zone electrophoresis (FFZE), free-flow isoelectric focusing (FFIEF), free-flow isotachophoresis (FFITP) and free-flow field step electrophoresis (FFFSE) [27, 28].

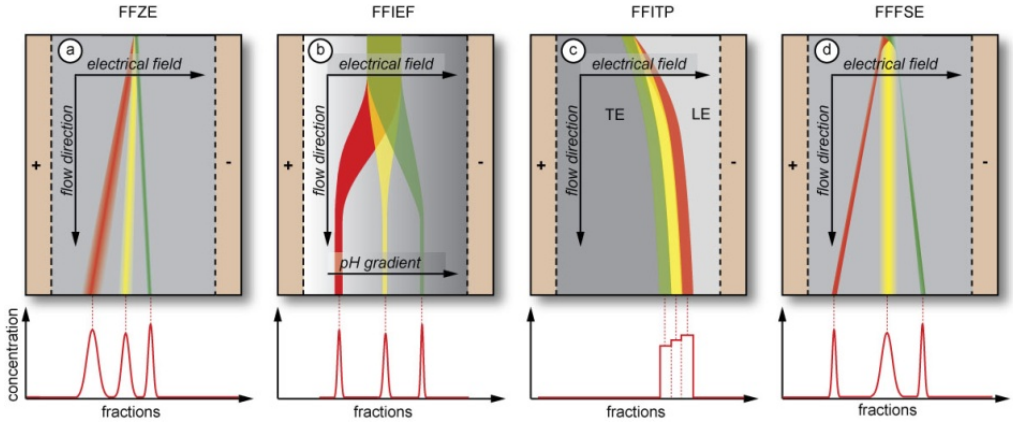


Fig. 2.2 Modes of FFE: (a) free-flow zone electrophoresis, (b) free-flow isoelectric focusing, (c) free-flow isotachophoresis, (d) free-flow field step electrophoresis.

### 2.3.1 FFZE

Free-flow zone electrophoresis implies the usage of a carrier electrolyte flow of constant composition of pH and electrical conductivity in which components are separated according to their mobility (determined by the charge-to-size ratio; Fig. 2.2a). It has been found that there is a direct correlation between capillary zone electrophoresis (CZE) as used for analytical applications and free-flow zone electrophoresis as used for preparative ones. The theory of this correlation can be found in the references [29, 30]. In FFZE the analyte to be separated is deflected

linearly under a constant angle determined by the electrical field strength, the analyte mobility and the flow velocity. The migration distance *d* of the analyte moving through the electrical field is given by

$$d = \mu_p E t \tag{2.1}$$

where $\mu_p$ is the apparent electrophoretic mobility, *E* is the electrical field strength, *t* is the residence time of molecules in the separation chamber [31].

The goal of FFZE is to achieve high resolution, which is reached by analytes migrating in narrow zones with sharp boundaries. However, several phenomena negatively influence the separation quality. The following sources of band broadening are common in FFZE: the width of the injected sample stream leads to a band standard deviation $\sigma_{INJ}$, and further types of band broadening are diffusional broadening ($\sigma_D$), hydrodynamic broadening ($\sigma_{HD}$), electrodynamic broadening ($\sigma_{ED}$), Joule heating ($\sigma_{JH}$) and electromigration dispersion ($\sigma_{EMD}$) [17, 32]. Not all sources of band broadening are discussed here and the reader is referred to the literature for more details. The variance $\sigma_T^2$ of a separated analyte band is then given by the sum of the variances of all broadening contributing factors:

$$\sigma_T^{\,2} = \sigma_{INJ}^{\,2} + \sigma_D^{\,2} + \sigma_{HD}^{\,2} + \sigma_{ED}^{\,2} + \sigma_{JH}^{\,2} + \sigma_{EMD}^{\,2}\,. \tag{2.2}$$

The variance due to the sample injection width $w_i$ is usually expressed by [33]

$$\sigma_{INJ}^{\,2} = \frac{w_i^2}{12}\,. \tag{2.3}$$

Reducing the sample injection width is often easier in microfluidic systems than in larger fluidic systems for example by the precise control of the neighboring laminar flow streams causing hydrodynamic focusing of the sample as for example shown in reference [34].

The variance caused by lateral diffusion is directly related to the residence time *t* of the analyte in the separation chamber, and can be expressed by

$$\sigma_D^{\,2} = 2Dt \tag{2.4}$$

where *D* is the analyte diffusion coefficient [35]. Short residence times, as usually involved in microfluidic FFE systems therefore reduce this effect.

The parabolic flow profile, which is caused by the pressure driven flow leads to unequal velocity regions inside the separation chamber. The analytes flowing near to

the top and the bottom plate spend more time in the electrical field, and thus are deflected more than analytes flowing near the chamber center. This effect is called hydrodynamic broadening and leads to a crescent shaped deformation of the sample. The variance due to hydrodynamic band broadening equals

$$\sigma_{HD}{}^2 = \frac{h^2 t}{105D} E^2 \mu_p^2 \tag{2.5}$$

where $h$ is the chamber height [35]. Eq. (2.5) shows that a shallower separation chamber, as used in microfluidic FFE devices does strongly reduce the effect of hydrodynamic band broadening.

The applied electrical field together with an electrical double layer present at the separation chamber surfaces leads to electroosmotic flow (EOF) inside the separation chamber. Normally, in an open channel EOF results in a plug shaped flow profile from the anode towards the cathode. However, in many FFE systems the electroosmotic flow generated at the upper and lower cover plates results in a hydrodynamic counterflow in the center of the chamber due to a high transport resistance in the direction of the electroosmotic flow (e.g. due to incorporated membranes). This hydrodynamic flow perpendicular to the separation axis often results in crescent shaped sample deformation comparable to that caused by hydrodynamic band broadening. This effect is generally referred to as electrodynamic band broadening. As discussed later, not all microfluidic FFE systems are subject to this type of band broadening, therefore we will not discuss the theory in more detail here and one is referred to [16].

As the electrical current heats the separation medium (Joule heating) inside the FFE device a temperature gradient is established between the two cover plates with the maximum in the center. This temperature change leads to a viscosity decrease in the center locally affecting the analyte mobility, and thus leading to band broadening. In contrast to actively cooled conventional FFE systems the shallower separation region of µ-FFE systems favors fast heat dissipation reducing this type of sample distortion and usually also much lower electrical currents are involved. Experiments have confirmed that µ-FFE separations could be performed without noticeable influence of Joule heating applying electrical field strengths of up to 60 V $mm^{-1}$ [35, 36] with an exception given by [37].

Zones of different electrical conductivity in sample and carrier electrolyte will lead to electromigration dispersion [17, 32]. This type of distortion results from different migration velocities of the analytes in zones having different electrical field strengths. This effect can be minimized by choosing appropriate buffer systems with similar conductivities for sample and carrier electrolyte.

An interesting approach was shown by Fonslow et al. [35] in which the authors derived an analogue of the van Deemter equation describing the separation in FFZE. They showed that linear velocity, electric field, and migration distance must all be considered to optimize bandwidth and resolution.

The separation resolution *Rs* of two adjacent peaks is defined by

$$Rs = \frac{d_1 - d_2}{2(\sigma_{T1} + \sigma_{T2})} \tag{2.6}$$

Assuming that the band broadening is dominated by diffusion and inserting Eq. (2.1) and Eq. (2.4) one can derive (assuming equal diffusion coefficients)

$$Rs = \frac{(\mu_{t1} - \mu_{t2})Et}{4\sqrt{2Dt}}. \tag{2.7}$$

Substituting the residence time $t$ with $L/v$, where $L$ is the length of the separation chamber in the flow direction and $v$ is the linear flow velocity, and substituting $E$ with $V_{eff}/W$, where $V_{eff}$ is the effective separation voltage (the effective voltage utilized for separation) and $W$ the separation chamber width one obtains

$$Rs = \underbrace{\frac{(\mu_{t1} - \mu_{t2})}{4\sqrt{2D}}}_{Analytes} \cdot \underbrace{\sqrt{\frac{L}{W^2}}}_{\substack{Device \\ geometry}} \cdot \underbrace{\frac{V_{eff}}{\sqrt{v}}}_{\substack{Tunable \\ parameters}} . \tag{2.8}$$

This equation shows that when scaling down FFZE devices, the separation resolution is independent of the device size (assuming a constant device aspect ratio $L/W$) and is dependent only on the applied separation voltage and the linear flow velocity. In the derivation of this equation many assumptions were made and it is just intended to guide the reader and to demonstrate that resolution eventually is independent of the actual device size and does not have to suffer from downscaling. Of course at the same time the separation time $L/v$ decreases proportionally with downscaling.

### 2.3.2 FFIEF

In free-flow isoelectric focusing, the used carrier electrolyte is composed of a mixture of ampholytes, which lead in the presence of the applied voltage and a natural pH gradient (mostly achieved by low and high pH anodic and cathodic electrode electrolytes), to the formation of a linear pH-gradient perpendicular to the flow direction. Sample components migrate within this pH gradient due to the electrical field until they reach the point where their isoelectric point (pI) is equal to the local pH value of the buffer, where they become neutrally charged and focus (Fig. 2.2b). Unlike the linear separation technique FFZE where the standard deviation of the band increases as the separation continues, the standard deviation of a sample fraction band width in FFIEF stays constant once equilibrium is reached. Band broadening e.g. due to diffusion is continuously counteracted since species leaving the equilibrium zone become charged again and migrate back to the location of zero charge [38]. Therefore, the sample injection width and band broadening factors as discussed for FFZE play a minor role in FFIEF. However, the low solubility of analytes at their isoelectric point and therefore precipitation often leads to non-ideal and distorted focusing.

The following differential equation, valid under steady state conditions, describes the equilibrium conditions between simultaneous electrophoretic and diffusional mass transport during IEF,

$$\frac{d(C\mu E)}{dx} = \frac{d}{dx} D \frac{dC}{dx} \tag{2.9}$$

where $C$ is the analyte concentration at position $x$ in the separation channel, $\mu$ is its mobility at that point, $E$ the electrical field strength and $D$ is the diffusion coefficient [39].

Useful parameter to express the quality of an equilibrium gradient separation system such as an isoelectric focusing system, include the standard deviation of the peak width $\sigma$ *(Eq.* (2.10)), minimum pI value that can be resolved $\Delta(pI)_{min}$ (Eq. (2.12)) and peak capacity $n$ (Eq. (2.14)). The solution to the differential Eq. (2.9) at final steady state gives a Gaussian concentration distribution, with a standard deviation expressed by

$$\sigma = \pm\sqrt{\frac{D}{pE}} \tag{2.10}$$

where $D$ is the diffusion coefficient, $E$ the electrical field strength, and

$$p = -\frac{d\mu}{d(pH)} \cdot \frac{d(pH)}{dx} \tag{2.11}$$

where $d(pH) / dx$ is the pH gradient and $d\mu / d(pH)$ the mobility slope of the analyte [39]. A way to express the resolving power of IEF is given by Eq. (2.12) which expresses the minimum difference in isoelectric point of two species that still can be separated (peak distance 3σ) [39].

$$\Delta(pI)_{\min} = 3 \cdot \sqrt{\frac{D(d(pH)/dx)}{E(-d\mu / d(pH)}} \,. \tag{2.12}$$

By replacing $d(pH) / dx$ with $\Delta pH / L$, where $L$ is the length of the pH gradient and $\Delta pH$ the total difference of the applied pH gradient, and replacing $E$ with $V_{eff} / L$, where $V_{eff}$ (see eq. (2.16)) is the voltage drop utilized for separation one can rewrite Eq. (2.12) to

$$\Delta(pI)_{\min} = 3 \cdot \underbrace{\sqrt{\frac{\Delta pH}{V_{eff}}}}_{Device} \cdot \underbrace{\sqrt{\frac{D}{-\frac{d\mu}{dpH}}}}_{Analyte} \,. \tag{2.13}$$

This approach has been utilized for capillary isoelectric focusing by Das et al. [24]. One can see from Eq. (2.13) that only $\Delta pH$ *and* $V_{eff}$ are device related parameters while the others depend on the analyte. It thus becomes clear that the resolution $\Delta(\mathrm{pI})_{\min}$ is independent of the device dimensions but increases with total applied voltage, a result similar to that for FFZE. Assuming ideal separation conditions, such as no Joule heating one can therefore conclude that microfluidic FFIEF systems can achieve similar and better resolution compared to their larger counterparts. Obviously, a good resolution is favored by a high separation voltage and a narrow pH gradient. The separation time however benefits from downscaling, since it decreases linearly with the chamber length.

A common method to express the number of peaks that can be resolved is the peak capacity $n$, defined by

$$n = \frac{L}{4\bar{\sigma}} \tag{2.14}$$

where $L$ is the total length of the pH gradient [38]. Also the peak capacity is theoretically independent of the device dimensions as it can be rewritten to

$$n = \underbrace{\sqrt{\Delta pH \cdot V_{eff}}}_{Device} \cdot \underbrace{\sqrt{\frac{-d\mu/dpH}{16D}}}_{Analytes}. \tag{2.15}$$

### 2.3.3 FFITP

In free-flow isotachophoresis, the sample is introduced between leading and terminating buffers respectively having the highest and the lowest mobility of their ions with respect to the mobility of the analytes. During FFITP separation the analytes form adjacent regions according to their descending electrophoretic mobility (Fig. 2.2c). For more theory about ITP the reader is referred [40-42].

### 2.3.4 FFFSE

A fourth mode is free-flow field step electrophoresis (FFFSE), in which an electrical field step gradient is built up by introducing a less conductive buffer in the centre of the separation chamber, enclosed by more conductive buffers on the sides. The analytes to be separated move relatively fast through the centre zone with high electrical field strength until they reach the boundary with the high ionic buffer concentration and lower electrical field strength (Fig. 2.2d). This field step results in a drastic reduction of the analyte electrophoretic velocity and the components therefore become concentrated and focus [16, 43].

## 2.4 Device Technology

### 2.4.1 General Aspects

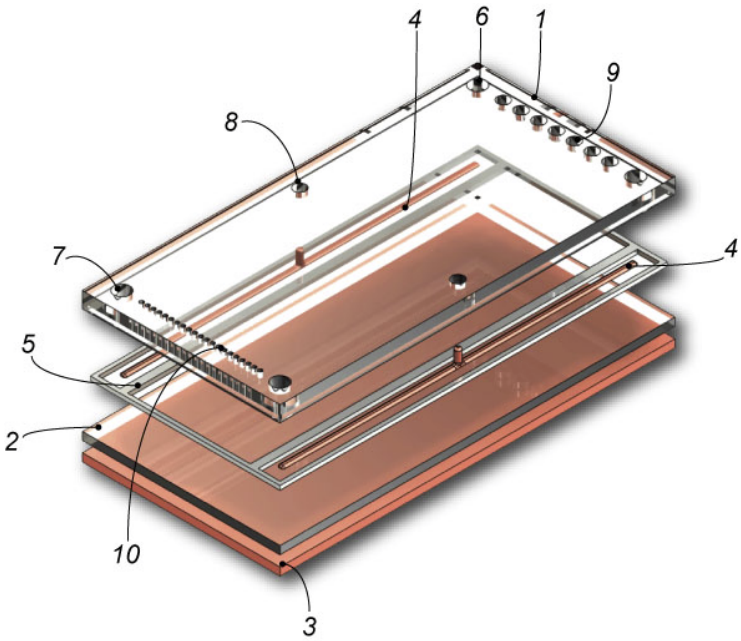


Fig. 2.3 Illustration of a disassembled conventional FFE separation unit: 1, top plate; 2, bottom plate; 3, cooling plate; 4, electrode; 5, membrane spacer; 6, electrode electrolyte inlet; 7, electrode electrolyte outlet; 8, electrode connection; 9, sample + carrier electrolyte inlet; and 10, fraction collector.

A conventional large scale FFE separation device, as illustrated in Fig. 2.3, consists of two insulating plates (often glass or acrylic glass (PMMA)) which are separated by a membrane spacer (e.g. cellulose nitrate [20]) of up to several hundred µm in thickness. This spacer defines the separation chamber height and is conductive for an electrical current but due to its internal structure acts as a confinement for the pressure-driven fluid inside the separation chamber. In this configuration it spatially defines three regions: the separation region, the anode bed and the cathode bed. Electrodes are placed outside the separation region avoiding the disturbance of generated gas bubbles and minimizing the interference of chemical side products migrating into the separation region. Continuous electrolyte flow inside the electrode beds ensure stable electrical properties by flushing away generated oxygen, hydrogen

bubbles and chemical side products. Usually the device is placed on an actively cooled plate in order to efficiently remove heat generated by the electrical current.

To some extent this principle is applicable for smaller FFE systems as well, using traditional micromachining techniques such as injection molding and milling [19, 20, 44]. However, when the lateral feature size decreases to millimeters and the separation chamber heights decrease to tens of micrometers the fabrication of the necessary thin cellulose membranes sheets and their manual handling including device assembly is not practicable anymore. Applying modern cleanroom fabrication technologies new manufacturing principles for FFE micro devices have therefore been developed whereby the developments mainly focused on alternatives to conventional membranes. Generally, three aspects are thereby of main importance: (i) efficient removal of gas and chemical side products formed during electrolysis with no cross contamination between the separation chamber and the side beds; (ii) a stable electrical field over the separation chamber and (iii) good voltage efficiency. The voltage efficiency $\eta_V$ is defined by

$$\eta_V = \frac{V_{eff}}{V_{total}} \tag{2.16}$$

where $V_{total}$ is the total applied voltage and $V_{eff}$ is the voltage effectively utilized for separation. In conventional large scale FFE devices the width of the membranes is much smaller than the actual width of the separation chamber, resulting in a negligible voltage loss across the membranes when the separation voltage is applied. In contrast to this, in microfluidic FFE chips the membrane-replacing structures often have widths of the same size as the separation chamber causing a large extent of voltage loss, resulting in low voltage efficiency. Unfortunately, reducing the width of the membranes or similar structures to achieve low electrical resistance normally leads to structures with low hydrodynamic resistance as well, possibly causing fluid leakage towards the electrode side beds or vice versa.

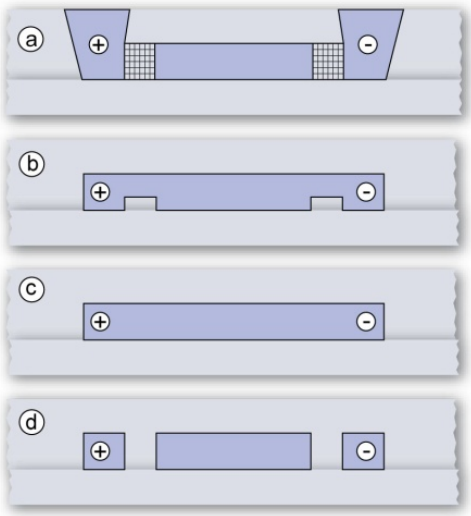


Fig. 2.4 Illustration of various design categories applied for microfluidic FFE systems. (a) open electrode beds with membrane like structure or structures of a similar function; (b) closed electrode beds with membrane-like structures; (c) electrodes inside the separation chamber; and (b) mechanically and electrically insulated separation chamber.

In general, as shown in Fig. 2.4, four different technological approaches were demonstrated in µ-FFE systems trying to full-fill the mentioned criteria: (a) Electrodes were placed in open side reservoirs with membrane like structures of high hydrodynamic resistance isolating the separation chamber. (b) Electrodes were placed in closed side beds with a continuous electrode flow, with a membrane equivalent or different structures to shield the separation chamber. (c) Electrodes were integrated into the separation chamber with no additional structures. (d) The electrodes were electrically and mechanically isolated from the separation chamber. Tab. 2.1 briefly compares the papers using these different approaches which are discussed in the following sections. Comparisons should be taken with care, since many aspects have to be considered that are not always simple to compare in the different approaches.

### 2.4.2 Open Electrode Side Beds with Membrane Equivalent

The implementation of open electrode side beds to place the electrodes allows for an easy ventilation of gas products formed during electrolysis. This design however results in a pressure gradient from the separation chamber towards the electrode side beds which can cause fluid leakage. This fluid leakage has to be compensated by proper shielding of the separation chamber with membrane equivalent structures with high hydrodynamic resistance. Since there is no need for a precise control of electrolyte fluid streams the working setup can be simplified. However, for longer separation times a continuous refreshment of the electrode solutions should be implemented, to avoid electrical conductivity changes.

Zhang et al. [45] developed a FFE chip using PDMS and Pyrex glass. In their design, they used an array of narrow side channels connecting the separation chamber with the electrode side beds. These side channels were of high hydrodynamic resistance acting as a membrane equivalent structure. Gas bubbles were efficiently hindered from entering the separation chamber and eventually left through the open electrode side beds. The design allowed for relatively fast flow rates and furthermore, the usage of glass and PDMS made the application of high voltages possible. This resulted in a FFZE separation of fluorescent components and labeled amino acids with residence times below 2 seconds. The same chip design was used later to demonstrate rapid free-flow isoelectric focusing by Xu et al. [46]. They showed the 400-fold focusing of Angiotensin II at its isoelectric point within 430 ms. Despite the very short separation times, more than 90% of the applied voltage was lost across the side channels. The high hydrodynamic resistance of the side channels, necessary for rapid operation, in a trade off therefore caused a tremendous increase of the electrical resistance of the side channels, making the device less efficient in terms of applied voltage. Applying FFZE in this device, the low voltage efficiency turned out not to be a limiting factor, especially when considering it as a proof-of principle device. However, in FFIEF a large part of the pH gradient was established inside the side channel membranes and not in the separation chamber due to carrier ampholytes migrating into the side channels. Therefore, only the part of the pH gradient which formed inside the separation chamber was available for isoelectric focusing. This effect significantly limited the separation capacity. Janasek et al. [47] applied a comparable PDMS chip to demonstrate for the first time free-flow isotachophoresis of fluorescein and Eosin G.

| Category (related to Fig. 2.4) | Author | Year of publication | Principle | Chamber width (mm) | Voltage efficiency (%) | Removal of bubbles and side products | Stable elec–trical field, separation | Comments |
|---|---|---|---|---|---|---|---|---|
| **a** | Xu, Zhang and Janasek [45-47] | 2003, 2006 | Side channels | 4.07 | 4.5 | o | o | Reduced pH gradient in FFIEF |
| **a** | Kohlheyer [34, 36] | 2006, 2007 | Acrylamide membranes | 3.5 | 63[1] | + | + | Low mechanical stability |
| **a** | Albrecht [37] | 2006 | Acrylamide membranes | 1 | 15[1] | + | + | Joule heating |
| **a** | de Jesus [48] | 2006 | Acrylamide membranes | 18 | 69 | + | + | Laborious electrode connections |
| **b** | Raymond [31, 33] | 1994, 1996 | Side channels | 10 | 60[1] | o | - | Low break-down voltage |
| **b** | Fonslow [49] | 2005 | Side channels | 10 | 50 | - | - | Bubbles distorted separation |
| **b** | Fonslow [35, 50] | 2006 | Deeper electrode beds | 10 | 91 | + | + | Precise flow control required |
| **b** | Kobayashi [51] | 2003 | Shallow side banks | 56.5 | 95[1] | + | + | Relatively large, ø 100mm wafer sized |
| **c** | Lu [52] | 2004 | Integrated electrodes | 1 | 100 | n.a. | + | Only low diffusive analytes, long residence times |
| **c** | Song [53] | 2006 | Diffusion potential | 0.05 | n.a. | n.a. | + | Ampholyte less IEF |
| **d** | Janasek [54] | 2006 | Electrostatic induction | 4.4 | 50 | n.a. | + | Still under investigation |

[1)] Estimated by the author; (-, inefficient; o, fair; + efficient)

Tab. 2.1 Rough comparisons of different FFE design approaches.

In conventional gel electrophoresis, a dense swollen hydrogel made from crosslinked acrylamide monomer is used as a separation matrix. Similar gels were used in microfluidic systems as so called ion-bridges or salt-bridges (e.g. used in electroosmotic pumps [55]) making it a also a suitable membrane material for µ-FFE. This principle was applied by several groups in miniaturized FFE devices to form conductive membranes.

Kohlheyer et al. [34] presented a µ-FFE glass chip with photo–polymerized acrylamide membranes. This device was fabricated by using two wafers of Borofloat glass, one containing the 15 µm high separation chamber as well as inlet and outlets, as shown in Fig. 2.5. The glass wafers were bonded by direct glass wafer bonding with no need for an additional intermediate silicon layer as used for example by Fonslow et al. [49]. The electrodes were placed in open reservoirs to allow the ventilation of gas. Depending on the used separation chamber width, between 60% and 40% of the applied voltage was utilized across the separation region. The stability of the membranes turned out to be the limiting factor. At elevated fluid velocities and especially during FFIEF the membranes eventually broke. An improved version of this FFE chip was developed and used to achieve an increased separation resolution in FFIEF [36].

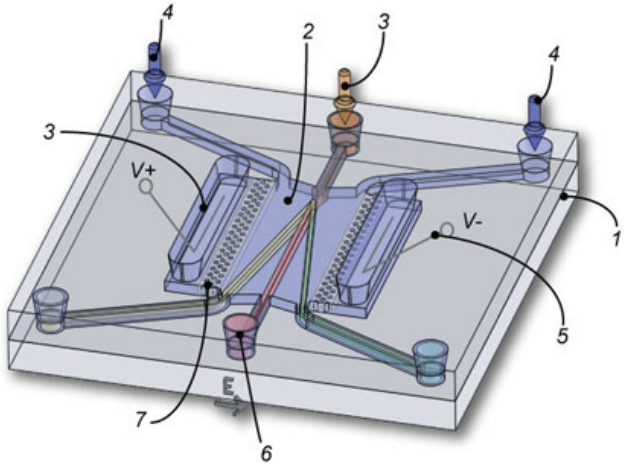


Fig. 2.5 Illustration of the µ-FFE device during FFZE: 1, glass plates; 2, separation chamber; 3, sample inlet; 4, sheath flow inlet; 5, electrode wire; 6, fraction outlet; 7, acrylamide membrane. [34]

Albrecht et al. [37] demonstrated a FFIEF PDMS device with integrated functionalized photo polymerized acrylamide membranes, as shown in Fig. 2.6. These membranes of low and high pH respectively provided buffering capacity during isoelectric focusing to confine a pH gradient between pH 3 – 9 with no need for additional sheath flow streams as used e.g. by Kohlheyer et al. [34]. Furthermore, an integrated cooling system was used to reduce the negative effect of Joule heating at high electrical field strengths. Considering the width of the membranes, the utilized voltage drop across the separation channel is estimated by us to be around 15% of the total applied voltage. Albrecht et al. [37] did not report on low mechanical stability of their membranes.

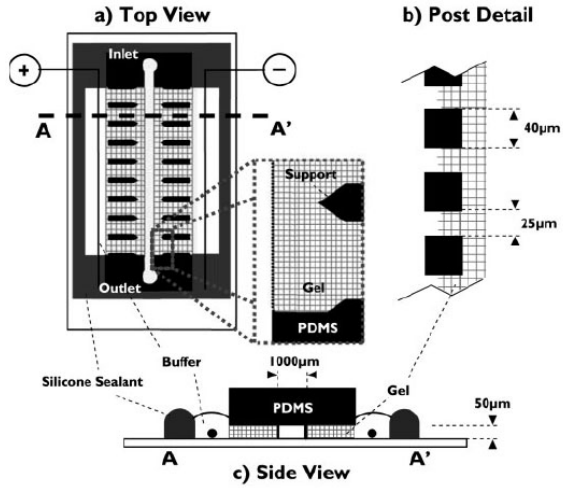


Fig. 2.6 Top view (a) shows the PDMS device with the sample channel bordered by left and right porous material regions (cross-hatched areas) and anode and cathode, respectively. Silicone sealant (solid array) is used to form the reservoirs for the anolyte and catholyte buffers, as well as to hold the platinum electrodes in place. (reproduced from [37] Copyright Wiley-VCH Verlag GmbH & Co. KGaA.)

De Jesus et al. [48] fabricated a low-cost µ-FFE chip using laser printing toner as a structural material on a glass substrate. Furthermore, they used a polymerized hydrogel to fill the electrode reservoirs shielding the separation chamber. The electrodes were placed inside two electrolyte filled syringes connected to the side openings via polyethylene tubing. Gas formation inside the syringes did not enter the side openings nor caused disturbance of the separation. De Jesus et al. achieved a similar voltage efficiency as Kohlheyer et al. [34].

### 2.4.3 Closed Electrode Side Channels

The usage of closed electrode channels requires additional flow streams ensuring an effective removal of produced gas bubbles and chemical side products, and to ensure stable electrical properties. Structures or obstacles also have to be implemented to avoid gas bubbles from entering the separation chamber. In addition, an exact flow balancing of the fluid flow streams in the electrode and separation channels becomes important to avoid cross contamination of fluids between the electrode channels and the separation chamber.

Raymond et al. [31] were the first to develop a microfluidic FFE chip, and it operated with closed side channels. This FFE micro chip incorporated a separation region, inlet and outlet channels, electrode beds and a dense array of micro channels which acted as a membrane, separating the electrodes from the actual separation chamber, as shown in Fig. 2.7. This liquid filled channel array formed a high hydrodynamic resistance for the pressure driven fluid but could conduct the electrical current. This was a very elegant solution, since all channel features could be fabricated in one standard silicon etching step. The chip was used to separate fluorescent markers as well as amino acids during free-flow zone electrophoresis.

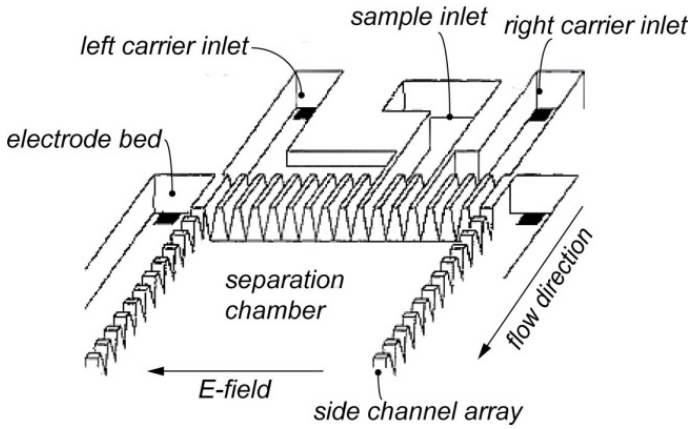


Fig. 2.7 Principal FFE layout used by Raymond et al. [31] A highly dense side channel array acted as membrane between the separation chamber and electrode beds. (reproduced from [31], copyright American Chemical Society)

The same device was used two years later to separate FITC labeled proteins and amino acids with FFZE and was further characterized [33]. The major drawback of this system was the low breakdown voltage of 100-200 volts due to the use of silicon

as chip material, limiting the device in its separation power. Due to low electrical field strength, long residence times of up to one minute were required to achieve good separations. Although the side channels formed a high hydrodynamic resistance, fluid flow from the side beds into the separation chamber, negatively influencing the separation, was still observed. Considering the width of the separation chamber (10 mm) and of the side channels arrays (2 x 1 mm), the estimated actual voltage efficiency was around 80%.

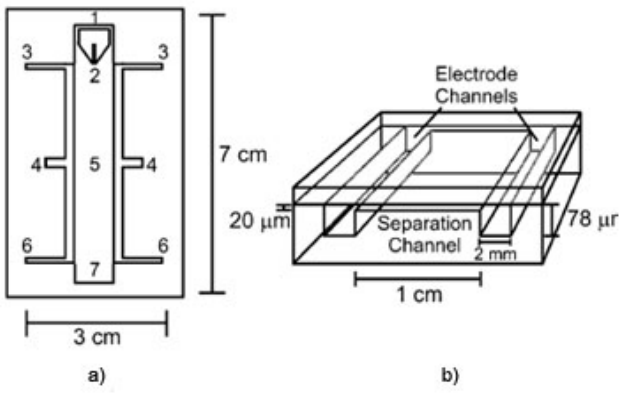


Fig. 2.8 (a) A top view of the µ-FFE mask of Fonslow et al. [50] with the following features: 1, separation buffer inlet; 2, sample inlet; 3, electrode buffer inlets; 4, Au electrodes in electrode channels; 5, separation channel; 6, electrode buffer outlets; and; 7, separation buffer outlet. (b) A side view of the electrode and separation channels etched into the bottom glass wafer and bonded to the top glass wafer (reproduced from [50], copyright American Chemical Society).

Fonslow et al. [49] presented a FFE chip fabricated from two glass plates with an intermediate layer of amorphous silicon (a-Si) for anodic bonding. This device contained closed electrode channels, in which gas bubbles were flushed out by a pressure driven flow passing the integrated micro fabricated gold electrodes. These electrode side channels were separated by connecting side channel arrays comparable to those shown in Fig. 2.7. Due to the side channel arrays and its electrical resistance, 50 % of the applied voltage was utilized across the separation region in this device. Although the device could withstand higher voltages and fluid pressure, the successful separation of several fluorescent dyes was eventually distorted by gas bubbles inside the side channels, since they could not be removed efficiently anymore.

Fonslow et al. [50] subsequently improved their FFE concept as mentioned above and presented a device with a shallow separation region (20 µm deep) and roughly 4

times deeper closed electrode beds, completely avoiding side channel arrays or membrane equivalents. The flow-rate through the electrode channels was now significantly higher, effectively removing electrolysis products without disrupting the flow pattern in the shallow separation channel as shown in Fig. 2.8 [50]. As a complicating consequence, this approach required a precise control over the flow rates and more equipment. In the new design, 91% of the applied voltage was utilized across the separation channel where it actually impacts the separation. Although this multiple-depth μ-FFE device required more fabrication steps, it could be operated continuously at electric fields (in the separation channel) as high as 589 V/cm, a 4-fold improvement over their previous design. They now found that neither Joule heating, nor electrolysis product formation, was a limiting factor when applying high separation potentials. The device was applied to separate several fluorescent standards with FFZE. The chip was additionally used for a more detailed study of FFZE investigating several parameters affecting separation resolution in order to find optimum separation conditions [35].

A third approach to confine the separation region was achieved by Kobayashi et al. [51] who implemented parallel shallow side banks (20 μm) in-between the separation channel (30 μm) and the electrode beds (30 μm). Similar to the side channels discussed before, these shallower regions have a higher hydrodynamic resistance than the separation chamber, thus leading the carrier electrolyte flow through the separation region. Kobayashi et al. [51] presented a 100 mm diameter wafer sized Pyrex FFE device where they implemented this so-called bank shape design. The efficiency of the banks shape of the m-FFE was enough to prevent dispersion to the separation chamber of bubbles generated at the electrodes.

### 2.4.4 Integrated Electrodes Inside the Separation Chamber

The direct integration of electrodes into the separation chamber allows for easy flow control and chip layout. However, in order to avoid the disturbance of gas bubbles one has to operate the device with voltages below the electrolysis potential. Even then the occurrence of electrode reactions cannot be excluded.

As shown in Fig. 2.9, Lu et al. [52] used a microfabricated glass chip with integrated vertical gold electrodes directly inside the separation channel. They demonstrated free-flow isoelectric focusing of subcellular organelles with voltages applied below the potential required for electrolysis, therefore completely avoiding gas formation inside

the channel. However, due to the low electrical field strength available for separation, long residence times of up to several minutes were required. Due to this, most likely only components of low diffusivity, such as cell fractions and organelles could be separated.

Song et al. [53] presented a micro fabricated free-flow electrophoresis chip for isoelectric focusing without the usage of carrier ampholytes. Instead of applying an external electrical field required to run the pI-based sorting the field was generated by the diffusion of buffer ions in situ, at the liquid junction between two laminar flows within the microfluidic channel. However, the separation could be enhanced by applying an additional low voltage of 1.3 V using integrated electrodes as demonstrated.

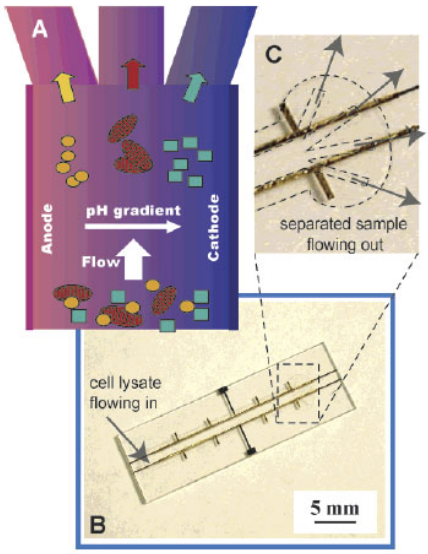


Fig. 2.9 (A) Schematic of free-flow isoelectric focusing (IEF) of organelles. (B) Photograph of the microfabricated device before final assembly with (C) enlarged view of the fractionation end of the device. The device consists of electroplated gold electrodes and microfluidic channels formed in a photopatternable epoxy. (reproduced from [52], copyright American Chemical Society)

### 2.4.5 Mechanically and Electrically Insulated Separation Chamber

A different approach to isolate the electrodes from the separation chamber was investigated by Janasek et al. [54]. Janasek and co-workers faced the question, if it is

possible to achieve a stable electrical field across the FFE separation chamber by electrostatic induction, like in an ideal DC capacitor. A glass FFE chip was fabricated containing integrated aluminum electrodes shielded from the separation chamber by 146 µm wide glass walls.

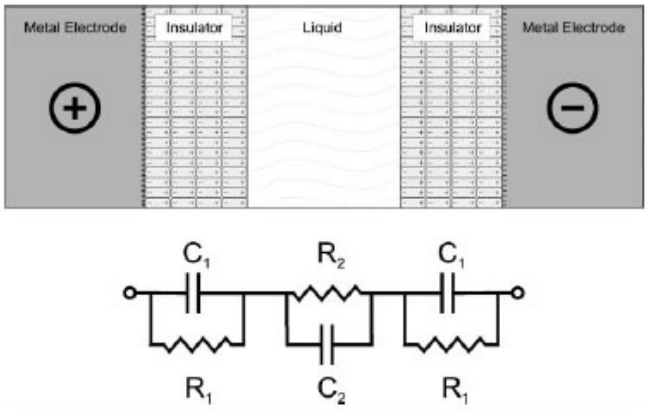


Fig. 2.10 Principle of electrostatic induction by charge displacement caused by dipole orientation. Lower panel: Equivalent circuit diagram. The capacitor C1 and the resistor R1 for the dielectric barrier are in the range of pF and TV, respectively; C2 and R2 for the liquid compartment are in the range of tens of fF and a few V, respectively. (reproduced from [54], copyright The Royal Society of Chemistry)

If an electrical field is applied over an insulator, a rearrangement of the mobile charges in the liquid close to the wall of the insulator will take place. E.g. if a negative potential is applied at the electrode, the amount of positive charge in the double layer adjacent to the wall will increase due to the decrease of the local electrical potential as illustrated for example in the paper of Schasfoort et al. [56]. After a certain charging time it would be expected that the entire electrical field drop will occur over the capacitances formed by the glass walls and the electrical double layer, and that no electrical field would be present in chamber any more (see Fig. 2.10). As a result separations would be impossible. This might be the explanation of the phenomenon, which was observed in the presented FFE device under stagnant conditions, when no flow was applied. However, under flow conditions a stable FFE separation was observed, with which FFITP of fluorescein was demonstrated while no electrical current was measured [54]. The authors concluded that the flow is counteracting the accumulation of charges at the glass walls, but a clear explanation of the phenomenon was not given. More detailed experiments are currently performed, to understand this

phenomenon in more detail. Comparable to earlier devices, the voltage efficiency was approximately 50%.

### 2.4.6 Device Technology - Concluding Remarks

Several technological approaches for microfluidic FFE devices have been demonstrated in literature over the past years, in which the main challenges were to avoid separation interference due to gas bubbles, to establish a stable electrical field and to optimize voltage efficiency. It is difficult to choose a favorite solution, since many aspects have to be compared. A brief comparison of the different approaches can be found in Tab. 2.1.

A FFE chip design with open electrode reservoirs (Fig. 2.4, category a) allows indeed for easy ventilation of gas products. However, such an approach puts higher demands on a proper shielding of the separation chamber. This shielding structure, usually a kind of membrane substitution has to be of low electrical resistance in order to achieve good voltage efficiency but also of high hydrodynamic resistance to prevent for example fluid leakage from the separation chamber towards the open electrodes reservoirs. Therefore, several groups implemented so called side channel arrays which acted as a membrane allowing electrical current flow but preventing fluid flow. Using integrated side channel arrays was an elegant solution since they can be fabricated usually in one step. However, the main drawbacks are a poor voltage efficiency and especially in FFIEF the formation of a pH gradient inside the side channels. As a positive side effect, it has been reported, that with the open characteristics of side channels rather than closed membranes electrodynamic band broadening could be avoided. Another technological solution to isolate the separation chamber from the open electrode reservoirs was the implementation of gel membranes, usually of acrylamide. This more laborious implementation of conductive acrylamide membranes has proven to be an efficient method with good voltage efficiency. Acrylamide gel membranes enable high hydrodynamic resistance with low electrical resistance and a relatively small width which seems very promising for further miniaturization. However, the mechanical stability of the membranes can be the limiting factor in some designs. Generally, it should be noted that a continuous replacement of the electrolyte solutions is of importance for longer separation times, in order to avoid changes of the solutions electrical properties.

A continuous refreshment of the solutions surrounding the electrodes seems straightforward when implementing electrodes into closed channels parallel to the separation chamber (see also Fig. 2.4, category b). Additional pumping equipment is then required to achieve flows in order to remove gas bubbles efficiently. To avoid cross contamination between the main flow inside the separation chamber and the electrode electrolyte flows, a proper flow balancing in this technological approach becomes more important. In these devices also side channel arrays have been used, but of lower hydrodynamic resistance. However, disturbance of the electrical field was reported due to gas bubbles moving along the electrodes and eventually entering and blocking the interconnecting side channels. Furthermore without proper fluid and pressure balancing fluid flow through the side channels occurred. Not many results have been published on the usage of shallower side banks, although this design seemed to work well. The device we reviewed that used this method was relatively large with 100 mm in diameter. Instead of using any membrane substitution the usage of closed deep electrode channels was found to be an efficient method to remove gas bubbles without scarifying voltage efficiency. This method seems very promising, although it requires more and precise control of flow rates. However, it has to be investigated, if the design is also applicable for other FFE methods such as FFIEF.

Electrodes can also be placed directly inside the separation chamber as shown by some groups (see Fig. 2.4, category c). As a result however, only voltages below the electrolysis potential can be applied. This usually leads to long separation times of up to several minutes making this approach only suitable for low diffusivity substances. The usage of a diffusion potential rather than applying an external electrical field forms an interesting method for pI based sorting, although the resolution seemed to be low.

The technological approach where a mechanical and electrical isolation of electrodes from the separation chamber (here electrostatic induction, see also Fig. 2.4, category d) is used, has to be studied more intensively and a clear explanation and understanding of the phenomenon should be found, but might offer an interesting alternative to other methods.

## 2.5 Separation Results

As mentioned, the four standard modes of free-flow electrophoresis include zone electrophoresis, isoelectric focusing, isotachophoresis and field step electrophoresis. All modes have been applied in micro FFE devices, generally as proof of principle. In this section we review the separation results obtained.

### 2.5.1 Free-Flow Zone Electrophoresis

Raymond et al. [31] were the first to publish results on free-flow zone electrophoresis applying their micro fabricated FFE device. The potential of the system was demonstrated by the separation of three rhodamine-B isothiocynate labeled amino acids, namely lysine, glutamine and glutamic acid as shown in Fig. 2.11. A residence time of 73 s was needed to separated the components when 50 V were applied, which resulted in an electrical field strength (estimated by the authors) of 3 V $mm^{-1}$ (I = 7.5 mA). Raymond et al. [31] found that the separation resolution was controllable by varying the side bed electrical conductivity, which was mainly due to the large contribution of the side channels to the total electrical resistance. Higher side bed conductivity resulted in an improved resolution, as the voltage drop across the separation chamber increased. Electroosmotic flow did not significantly affect the experimental baseline widths. This was probably a consequence of using side channels rather than closed membranes for the isolation of the separation chamber. However, this more open characteristic of the side channels resulted in flow from the side beds into the separation chamber, affecting separation. Eventually the bubbles created during electrolysis filled up the side beds resulting in a loss of the electrical field. It was reported, that no apparent Joule heating was observed.

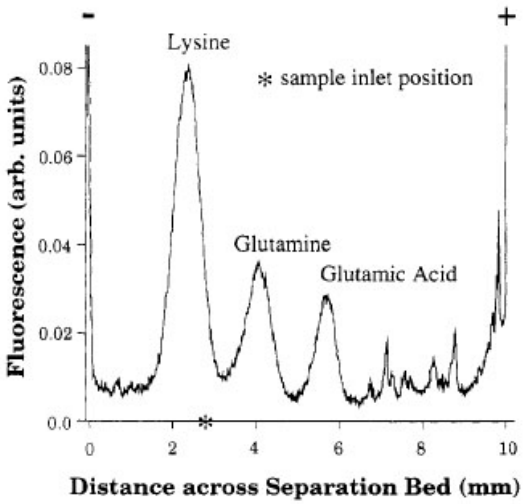


Fig. 2.11 Intensity plot of three labeled amino acids continuously separated by FFZE with a residence time of 73s when 50V were applied (reproduced from [31], copyright American Chemical Society)

For a more detailed separation study Raymond et al. [33] used the same chip design for the continuous separation of high molecular weight compounds with FFZE. In fact, they separated a mixture of FITC labeled human serum albumin (HSA), bradykinin and ribonuclease A. An electrical field strength of 100 V $cm^{-1}$ and a residence time of 62 s was needed to fully separate these components. Furthermore, the authors investigated different sources of band broadening and found that, initial bandwidth, diffusion and hydrodynamic band broadening were the main contributors to the band broadening. Despite some problems, Raymond et al. [33] reported a peak capacity of 8 bands / cm. This was in the same range as reported for conventional systems (10 bands / cm), indicating that miniaturized FFE devices could achieve similar separation results. They also demonstrated that the chip is capable of separating more complex samples such as diluted rat plasma and trypic digests of bovine cytochrome C and melittin.

Kobayashi et al. [51] demonstrated FFZE of two native proteins, cytochrome C and myoglobin. The residence time for a complete separation was 10 s when 2 kV was applied (estimated by the authors: $E$ = 33 V $mm^{-1}$, $I$ = 0.7 mA). The separated analytes were collected at different outlets and analyzed offline by reverse phase HPLC. The authors applied a HPMC coating in order to reduce the glass surface charge, trying to minimize EOF. Although the EOF was suppressed, the coating efficiency was not stable

during longer separations. The device was also used for a theoretical study on the temperature distribution and Joule heating [57].

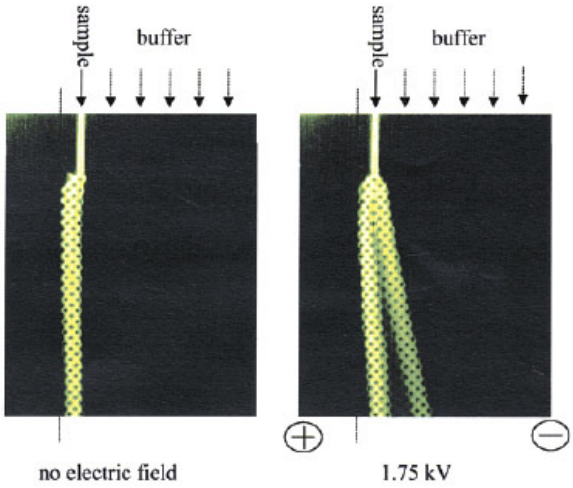


Fig. 2.12 FFZE of rhodamine 110 and fluorescein with a flow velocity of 6 mm $s^{-1}$. The resulting electrical field strength was 135 V $cm^{-1}$ with an induced current of 140 µA. The right separated stream was rhodamine-110 and the left fluorescein. (reproduced from [45], copyright American Chemical Society)

Zhang et al. [45] presented a µ-FFE chip for high speed separations of analytes. With their improved chip design they achieved a full separation of the fluorescent dyes rhodamine 110 and fluorescein within 75 ms. The total residence time (sample flux was 2 nL $s^{-1}$) in the separation chamber was two seconds when 1.75 kV was applied (E = 13.5 V $mm^{-1}$, I = 0.14 mA). As shown in Fig. 2.12, the negatively charged fluorescein (left stream) is slightly deflected towards the negative electrode, which was caused by EOF, as Zhang et al. [45] concluded. The chip has also been used for the separation of FITC labeled amino acids in both aqueous and binary media.

FFZE of a mixture of fluorescent dyes, namely fluorescein, rhodamine 110, a rhodamine 110 impurity and rhodamine 123 was presented by Fonslow et al. [49]. With the application of 515 V ($I$ = 310 µA), resulting in an electrical field strength inside the separation chamber of 25.9 V $mm^{-1}$, the three dyes as well as the impurity clearly separated with a residence time of 9.6 s before detection. In agreement with previous publications, Joule heating was found not to be significant at the studied field strengths.

Fonslow et al. [50] further developed their original FFE chip design in order to apply higher voltages and improve voltage efficiency. As before, they separated fluorescein, rhodamine 110, rhodamine 110 impurity and rhodamine 123 by FFZE. With a linear flow velocity of 5 mm $s^{-1}$ and electrical field strength up to 58.6 V $mm^{-1}$ an improved and more stable separation compared to their previous device was observed. With separation voltages of over 645 V Joule heating became significant. The same chip was used for a more theoretical study to optimize band width and separation resolution in FFZE [35].

Kohlheyer et al. [34] presented free-flow zone electrophoresis of fluorescein and rhodamine B. Both analytes were separated within a total residence time of 3.3 s when 180 V was applied ($E$ = 25 V $mm^{-1}$, $I$ = 50 μA). The linear flow velocity was 3 mm $s^{-1}$. The precise control of two sheath flow streams enabled positioning of the separated components within the separation chamber. Separated components could be steered towards different outlets by varying the sheath flow rates without altering the separation voltage, as shown in Fig. 2.13. This steering technique can be used in future devices to purify a sample mixture in such a way that only the separated component of interest is steered to a specific outlet. Steering of fluorescently labeled, easy visible components seems straightforward. However, it is questionable how to control the precise position in more realistic label-free applications.

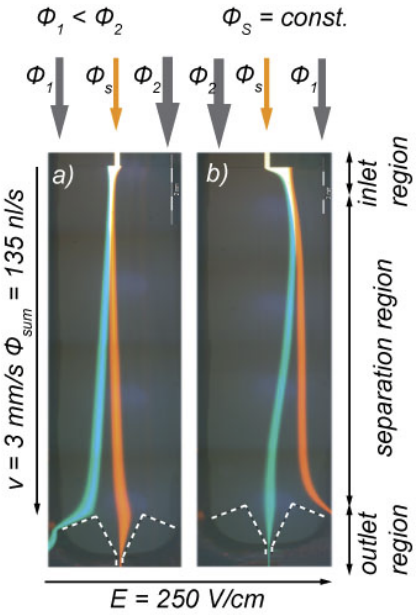


Fig. 2.13 Steering of rhodamine B and fluorescein bands in FFZE. The sample stream is hydrodynamicly focused by two parallel sheath flow streams. By adjusting the flow rates $\Phi_1$ and $\Phi_2$ the sample injection position is shifted. [34]

In order to demonstrate the feasibility of their FFE chip, de Jesus et al. [48] separated a mixture of the ionic dyes bromophenol, brilliant blue and crystal violet. The separation was carried out at a linear flow velocity of 0.54 mm $s^{-1}$ with a total residence time of 18.2 s. 300 V was applied to achieve an electrical field strength inside the separation chamber of app. 11.5 V $mm^{-1}$. During three hours of evaluation under a maximum current of 706 µA a stable separation was observed.

### 2.5.2 Free-Flow Isoelectric Focusing

The first to publish results on microfluidic free-flow isoelectric focusing were Xu et al. [46]. The authors demonstrated the 400-fold isoelectric focusing of fluorescently labeled angiotensin within 430 ms focusing time. They applied 1750 V to realize an electrical field strength of 13.5 V $mm^{-1}$, as shown in Fig. 2.14. To generate the required pH gradient an ampholyte solution was applied. However, due the technical layout, as discussed before, only a part of the pH gradient was available for separation since the low pH and high pH ampholytes migrated into the side channels. The chip could be

operated between 7.7 and 30 V $mm^{-1}$ before Joule-heating became significant and bubbles appeared.

Continuous isoelectric focusing of large molecules such as sub-cellular organelles was presented by Lu at al. [52]. In order to avoid electrolysis low voltages were applied. However, due to this procedure, long residence times were necessary in order to reach stable focusing. The method is therefore suited to separate components with low diffusion constants. Among other results, FFIEF of stained mitochondria from a cell lysate was shown. For this purpose an ampholyte based pH gradient (pH 3 - 6) was utilized and 2 V were applied with a residence time of 6 minutes. Especially with its mild voltage conditions this method is suitable for more sensitive biological components.

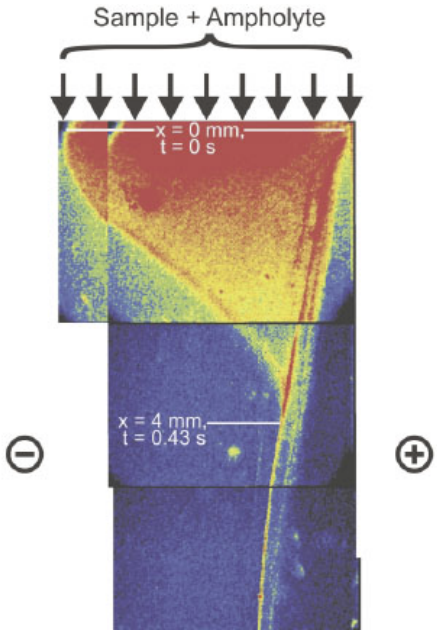


Fig. 2.14 Isoelectric focusing of fluorescently labeled Angiotensin II: Ang II = 10 mM, U = 1750 V; E = 135 $Vcm^{-1}$, picture in false colors (yellow represents high fluorescence intensity, blue no fluorescence). (reproduced from [46], copyright The Royal Society of Chemistry)

Using the same device as used for FFZE, Kohlheyer et al. [34] applied FFIEF for the separation of several fluorescent IEF markers. IEF Markers with isoelectric points at pH 4.5, 5.5, 7.6 and 8.7 were separated and focused. With a residence time at the point of measurement of 3 s (linear flow velocity 2 mm $s^{-1}$) and the application of 20 V (app.

10 V $mm^{-1}$ inside the separation chamber) all components fully focused at their isoelectric points within a 500 µm wide pH gradient (pH 3-10). The full pH gradient was available for separation since outer sheath flows of high pH and low pH respectively formed a border for arranging ampholytes.

Kohlheyer et al. [36] reported later an improved FFIEF chip based on their previous publication. Here, a pre-separated ampholyte buffer was used which reduced the electrical current and the focusing time. FFIEF of various IEF markers ranging from pI 3 to 10 as shown in Fig. 2.15.

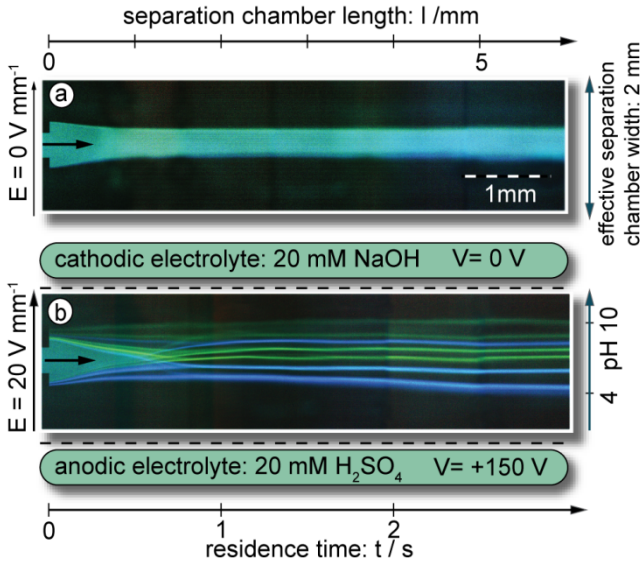


Fig. 2.15 Free-Flow Isoelectric focusing of 7 fluorescent IEF markers: When 150 V (I=50 µA) were applied, the markers (pI 4, 5.1, 6.2, 7.2, 8.1, 9 and 10.3) fully separated within less than two seconds. The sample flow rate was 0.4 µL $min^{-1}$ (v = 2 mm $s^{-1}$). The apparent kinks in the fluorescent tracer paths are caused by merging multiple photographs. [36]

The authors determined, that the device is capable of separating analytes with a minimum difference in isoelectric point of Δ(pH) = 0.23. This resulted in a theoretical peak capacity of 29 peaks within 1.8 mm for a pH gradient pH 2.5 – 11.5. With optimized pI markers, commonly used for calibration, the peak capacity of conventional FFE systems is between 50 and 70 peaks within 70 mm separation width [personal communication, Dr. Gerhard Weber, BD Diagnostics]. In terms of resolution, this would mean for a pH gradient (pH 2.5 – 11.5) a $\Delta(pI)_{min}$ between 0.13 – 0.18 pH units. To achieve this, in the conventional FFE system usually voltages of up to 2 kV

have to be applied, while Kohlheyer et al. applied only 150 V, clearly indicating the potential advantages of microfluidic FFIEF devices. In practice, the resolution is reduced when separating proteins and peptides [58]. This comparison shows that with μ-FFIEF one can achieve comparable and even better resolution with applying much lower voltages.

Instead of using sheath flow streams to confine the pH gradient, Albrecht et al. [37] used functionalized gel membranes with low and high pH buffering capacity respectively. FFIEF of several fluorescent IEF markers (pI 3.5, 5.1, 7.2 and 7.6), with 200 V separation voltage and a residence time of 14 s, was shown. Although a lower resolution than in the publication of Kohlheyer et al. [34] was achieved, the device involved less control over fluid streams and pumps. In contrast to previous results Albrecht et al. [37] were the first to report the need for a thermal cooling system to optimize their separation resolution. Therefore, a thermoelectric element was used to cool the top of the FFE device. A possible explanation is the lower heat dissipation of the chosen material (PDMS) compared with glass devices [59]. Recently, Albrecht et al. [60] also reported a cascaded FFIEF device based on their earlier published results. The streams of separated components from a first FFIEF separation chamber were guided into a second FFIEF stage resulting in an improved separation resolution. Their FFIEF device was used to focus native model proteins, denatured proteins as well as protein complexes.

Song et al. [53] demonstrated successful FFIEF of two different pI markers. This device operated differently than other FFIEF systems, since neither ampholytes nor an external voltage have to be applied. The electrical potential gradient was achieved by diffusion potential in a separation channel of around 100 μm in width.

### 2.5.3 Free-Flow Isotachophoresis

Janasek et al. [47] were the first to report on microfluidic free-flow isotachophoresis, and demonstrated the method by separating fluorescein, acetylsalicylic acid (ASS) and Eosin G, as shown in Fig. 2.16. Since in isotachophoresis the bands flow adjacent to each other, for a clear experimental validation ASS was chosen as a non fluorescent spacer analyte between the two fluorescent components fluorescein and Eosin G. For the experiment the electrical field strength was 21 V $mm^{-1}$. At higher field strength movement of the analytes into the side channels was observed.

As a proof of principle, Janasek et al. [54] applied FFITP of fluorescein to investigate their principle of electrostatic induction for FFE. They successfully focused fluorescein with the application of 150 V, which corresponds to an electrical field strength of 18 V $mm^{-1}$ inside the separation chamber, and a total flow rate of 20 µL $min^{-1}$.

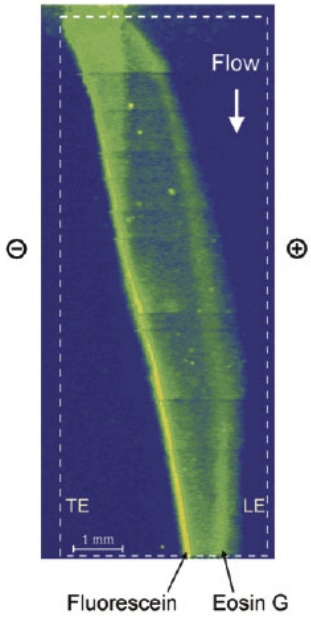


Fig. 2.16 FFITP separation and concentration of fluorescein, ASS, and eosin G displayed as an assembly of single micrographs over the whole chamber in false colors. (reproduced with permission from [47], copyright American Chemical Society)

### 2.5.4 Free-Flow Field Step Electrophoresis

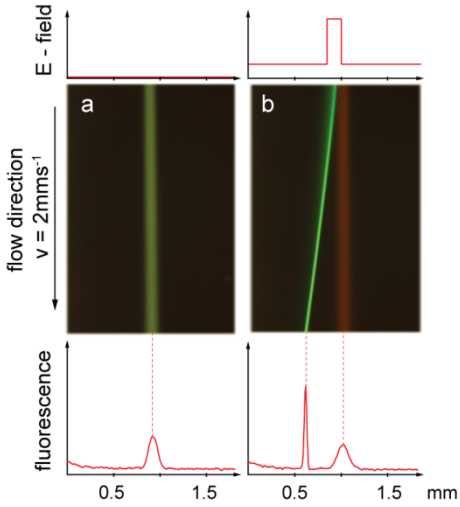


Fig. 2.17 Free-flow field step electrophoresis demonstrated in a microfluidic device of the authors. a) Mixture of Rhodamine B and fluorescein continuously flowing with no voltage applied. b) When 150 V were applied the negatively charged fluorescein migrated and focused due to the sudden decrease in electrical field strength.

To our knowledge, no results on microfluidic FFFSE have been published until now. To demonstrate the principle of FFFSE the authors separated a mixture of rhodamine B and fluorescein using their µ-FFE device. For this purpose the sample stream was hydrodynamicly focused in-between two sheath flow streams of lower electrical conductivity. As shown in Fig. 2.17, this resulted in an electrical field step when 150 V were applied. The negatively charged fluorescein migrated towards the anode and eventually concentrated (app. 4 fold) at the field step due to a decrease in its mobility. The neutrally charged, non migrating Rhodamine B showed only a slight band broadening maintaining its centered position.

### 2.5.5 Separation Results - Concluding Remarks

As shown by various publications, the four know separation modes, FFZE, FFIEF, FFITP and FFFSE have successfully been demonstrated in microfluidic devices. A wide spectrum of analytes has been separated including cell fragments, organelles, proteins, amino acids, fluorescent dyes and markers. The results shown until now, which can be considered as proof-of principle experiments, are difficult to compare in

terms of resolution, band width and peak capacity, since too many parameters differ from experiment to experiment. Obviously, also predicted by scaling laws, separation times were drastically reduced by miniaturization, making it more interesting for online monitoring tools rather than conventional systems meant for sample preparation. Samples were fully separated within several second and below. Furthermore, sample flow rates of several microliters per minute and below were applied. Generally one can say that Joule heating, a major concern in conventional FFE systems seems to be less relevant on a microfluidic scale. Due to the lack of lateral separation length higher electrical field strengths have to be applied in order to achieve comparable separation resolution and peak capacity as on the large scale. This is possible, because due to the lower electrical currents involved (typically in the μA range) less heat is generated, and because of the higher surface to volume ratios that favor fast heat dissipation. It would be beneficial for the field to investigate in more detail scaling effects by matching experiments performed on the micro and macro scale. Optical detection methods, usually involving large fluorescent microscopes and optical equipment, until now have been sufficient for first characterizations. However, as proposed already by Raymond et al. [33] the major advantage of a μ-FFE device is the possibility to integrate it more easily in a complex analysis system. Such an integration for online monitoring applications of separated analytes is not a straightforward task, as will be discussed in the following section.

## 2.6 Detection and Hyphenation

Size-reduced conventional mini-FFE devices have already been implemented into hyphenated analytical systems. Such systems can guide developers of integrated μ-FFE systems, and we therefore mention a few examples.

Chartogne et al. [20] coupled a FFE device to capillary isoelectric focusing (CIEF) as a cleaning step to remove interfering ampholyte substances prior to electrospray ionization into mass spectrometry (ESI-MS) to improve the MS sensitivity. This CIEF-FFE-ESI-MS system was successfully realized for three model proteins (myoglobin, carbonic anhydrase I and β-lactoglobulin B). Furthermore, Mazereeuw et al. [19] realized a system in which FFE was used as an online separation step of fluorescent compounds in a biochemical detection system. This system was based on the interaction of the affinity protein streptavidin with biotin, in which biotin acted as an

analyte. This FFE detection system was coupled to HPLC for the bioanalysis of biotin in human urine.

In the field of microfluidic FFE systems not much progress has been shown on the implementation of FFE with other separation or detection systems into so called micro total analysis systems (μ-TAS) or lab-on-a-chip devices (LOC) [21, 22, 61, 62]. In fact, until now only propositions for more integrated systems have been published.

Zhang et al. [45] concluded from their investigations, that microfluidic FFE presents a potentially powerful tool in proteomics studies. They proposed coupling μ-FFE with electrospray mass spectrometry as an on-line automated analytical tool in proteomics studies. By moving the chip perpendicular to the outlets separated components spray from respective channels and analyte streams are then received by the MS in scanning mode. Although they found that only little modifications are necessary for this detection approach, to our knowledge no results have been published until now. Instead of scanning the entire chip, the capability to steer the analyte by hydrodynamic focusing during FFZE separation, as shown by Kohlheyer et al. [34], might offer an interesting alternative to scan separated components through a single chip outlet connected to an ESI-MS system. A step towards this approach, was the coupling of a glass microchip for capillary electrophoresis to ESI-MS as e.g. successfully demonstrated by Hoffman et al. [63] and others [10]. Furthermore, Zhang et al. [45] proposed the use of μ-FFE combined with a microreactor, for on chip synthesis and separation of products. Using microchip capillary electrophoresis, on chip synthesis and separation of products was shown by Belder et al. [64]. In this initial study the device was successfully applied for testing biocatalysts created by directed evolution of enzymes. The use of μ-FFE instead of microchip capillary electrophoresis could enable high throughput and continuous screening of this reaction rather than the analysis of discrete plugs achieved by microchip capillary electrophoresis.

An integrated system approach combining microfluidic free-flow electrophoresis and surface plasmon resonance (SPR) detection was proposed by Kohlheyer et al. [65]. As illustrated in Fig. 1.6, a thin gold detection area is integrated into the FFE separation chip, located after the separation chamber. A monochromatic p-polarized light beam is coupled into the chip device and reflected under total internal reflection at the gold surface. Refractive index changes, near the gold surface e.g. caused by immobilization of molecules on the gold surface lead to local changes in the reflected light intensity.

These light intensity changes can be monitored for the whole detection region simultaneously by a CCD camera. For more information about SPR and its theoretical background one is referred to the review of Homola [66]. For experiments the proposed chip is placed inside a SPR imaging instrument (IBIS Technologies, The Netherlands) to monitor immobilization of separated fractions. Eventually this generated fraction pattern is used in a second step to study biomolecular interactions in the search for specific biomarkers present in e.g. patients sample. Collected fractions of immobilized lanes, which positively react with specific antibodies, will be analyzed off line by mass spectrometry for identification purpose. However, until now only preliminary results were presented and more work is currently performed.

## 2.7 Conclusions

In free-flow electrophoresis an electrical field is applied perpendicular to the flow direction and charged molecules are deflected from the carrier electrolyte flow direction, in a way that is controlled by the electrophoretic mobility, the flow velocity, and the electrical field strength. The research field of microfluidic free-flow electrophoresis methods is rather small, as evident from the numbers of papers reviewed. However, it carries large promise due to the continuous flow of separated sample enabling integration and continuous monitoring in miniaturized analysis systems. In this paper we showed that steady innovation is occurring in this research field. The results shown so far indicated that with μ-FFE systems one can achieve high separation resolutions which are comparable to or even better than those reached in their larger counterparts. The microfluidic devices furthermore accomplish this separation in a fraction of the time the larger devices need, and consuming a fraction of the sample volume. A trend can be foreseen in which the integration of lab on a chip devices using one of the FFE principles as reviewed in this chapter will further be developed for new applications in life sciences. Broadening the options of parallelization and assay implementation, including sample treatment on-a-chip will certainly contribute to an increased number of publications in the near future. Definitely a total analysis system approach instead of a device-based approach will lead to a growth of the field of microfluidic free-flow electrophoresis.

# 3 A Microfabricated Free-Flow Electrophoresis Device

*Based on a quick literature survey performed fall 2004, a new FFE chip design was made. The first successfully fabricated chips were experimentally characterized in spring 2005. The outcome of this project was published in LOC 2006; this chapter is based on this article. The new acrylamide membranes turned out to be an efficient method in FFE chips. This chapter describes the technological approach of implementing permeable membranes into FFE chips and two separation methods are shown.*

## 3.1 Abstract

This paper describes a microfabricated free-flow electrophoresis device with integrated ion permeable membranes. In order to obtain continuous lanes of separated components an electrical field is applied perpendicular to the sample flow direction. This sample stream is sandwiched between two sheath flow streams by hydrodynamic focusing. The separation chamber has two open side beds with inserted electrodes to allow ventilation of gas generated during electrolysis. To hydrodynamically isolate the separation compartment from the side electrodes, a photo-polymerizable monomer solution is exposed by UV light through a slit mask for in situ membrane formation. These so-called salt-bridges resist the pressure driven fluid, but allow ion transport to enable electrical connection. In earlier devices the same was achieved by using open side channel arrays. However, only a small fraction of the applied voltage was effectively utilized across the separation chamber during free-flow electrophoresis and free-flow isoelectric focusing. Furthermore, the spreading of the carrier ampholytes into the side channels resulted in a very restricted pH gradient inside the separation chamber. The chip presented here allows at least 10 times more efficient use of the applied potential and a nearly linear pH gradient from

pH 3 to 10 during free-flow isoelectric focusing could be established. Furthermore, the application of hydrodynamic focusing in combination with free-flow electrophoresis can be used for guiding the separated components to specific chip outlets. As a demonstration, several standard fluorescent markers were separated and focused by free-flow zone electrophoresis and by free-flow isoelectric focusing employing a transversal voltage of up to 150V across the separation chamber.

## 3.2 Introduction

Low sample capacity is a common problem in miniaturized separation systems, such as microchip-based capillary electrophoresis (CE), yielding discrete plugs of separated components on the nanoliter range [67]. The small sample volumes together with the often low concentrations of relevant bioactive compounds, put high demands on the detection system [68]. Free-flow electrophoresis (FFE) is a continuous separation method, providing bands along the separation chamber and thus a continuous supply of separated components. In FFE, charged particles are injected into a thin carrier flow with an electrical field applied perpendicular to the flow. The charged particles are deflected from the general flow direction at an angle determined by the flow velocity, electrophoretic mobility and electrical field strength. Components with different electrophoretic mobility have different deflection and can be collected separately at the end of the separation area [16]. Since the principle of FFE was described [69, 70], this technique has found application in chemistry and biochemistry mainly for the separation of proteins, enzymes, membrane particles, organelles and even cells [27, 71-75]. The most relevant modes of FFE include free-flow zone electrophoresis (FFZE), where the separation of particles is based on their charge to size ratio, and free-flow isoelectric focusing (FFIEF), where the separation and focusing of particles takes place according to their isoelectric point (pI). The fact that FFE separates with a continuous sample feed made it interesting for microchip based real-time separation and detection.

The first miniaturized version of FFE (μ-FFE) was introduced by Raymond and Manz in 1994 [31]. The chip, fabricated by etching the channels into silicon and anodic bonding with a glass cover, was successfully used for the separation of three rhodamine B isothiocyanate labeled amino acids in FFZE mode. A similar device was also used for the separation of high molecular weight compounds where band broadening effects were studied [33]. Joule heating, a major problem in conventional-

size FFE systems [76], plays no significant role in the chip based FFE since the high surface to volume ratio allows efficient heat dissipation. In conventional-size FFE systems the separation chamber is isolated from the electrode compartments by ion permeable membrane spacers [16]. In such a closed compartment electroosmotic flow (EOF) perpendicular to the general flow direction can cause electrodynamic band broadening effects [33]. Instead of membranes, Raymond et al. used dense transversal channel arrays with a high hydrodynamic resistance to functionally isolate the electrode compartments and the separation chamber [31, 33]. In such a more open system no electrodynamic circulation effects caused by EOF were observed. However, convection from the electrode beds into the chamber, or vice versa, influenced the separation efficiency. Kobayashi et al. [77] developed an FFE device from Pyrex glass, which was suited for higher voltages and thus provided increased separation efficiency. The device was used for the separation of cytochrome c and myoglobin. With the same principle of incorporating side channel arrays Zhang et al. presented a FFE chip fabricated from PDMS [45]. It allowed even higher electric fields strengths, flow velocities, separation efficiency and throughput. However, only 5% of the applied potential was used for separation since the high resistance channel arrays contributed to the potential loss. In an attempt to increase efficiency, Fonslow et al. [49] fabricated a μ-FFE device by etching of glass and anodic bonding with an intermediate layer of silicon. In this device the gas produced at the electrodes during operation at higher voltages proved to be the limiting factor. Xu et al. [46] introduced free-flow isoelectric focusing using an ampholyte mixture to establish a pH gradient. Focusing and separation was demonstrated with angiotensin I and II, and a 400-fold concentration of the solutes was achieved. However, due to the high electrical resistance, the side channel arrays contributed with 95% to the electrical potential loss. Furthermore, the major part of the ampholyte based pH gradient established inside these side channels arrays instead of inside the separation chamber. Lu et al. [52] fabricated a μ-FFIEF device with vertical gold electrodes, integrated into the separation chamber, by electroplating for the isoelectric focusing of sub cellular organelles. This device was used at very low voltages and therefore long residence times up to several minutes were required. Mitochondria were successfully separated from intact cells and focused at their isoelectric point.

### 3.2.1 Principle and Design

Here an improved µ-FFE device, as shown in Fig. 3.1, is presented, consisting of two thermally bonded glass plates with a microfabricated flow structure. The chip has a separation chamber, three inlets, three outlets and two parallel slits for the electrodes. Two integrated photo-patterned ion permeable salt-bridges isolate the separation chamber from the electrode compartments. These salt-bridges act as physical barriers towards the pressure driven flow but allow ions to pass in order to ensure electrical connection [55, 78].

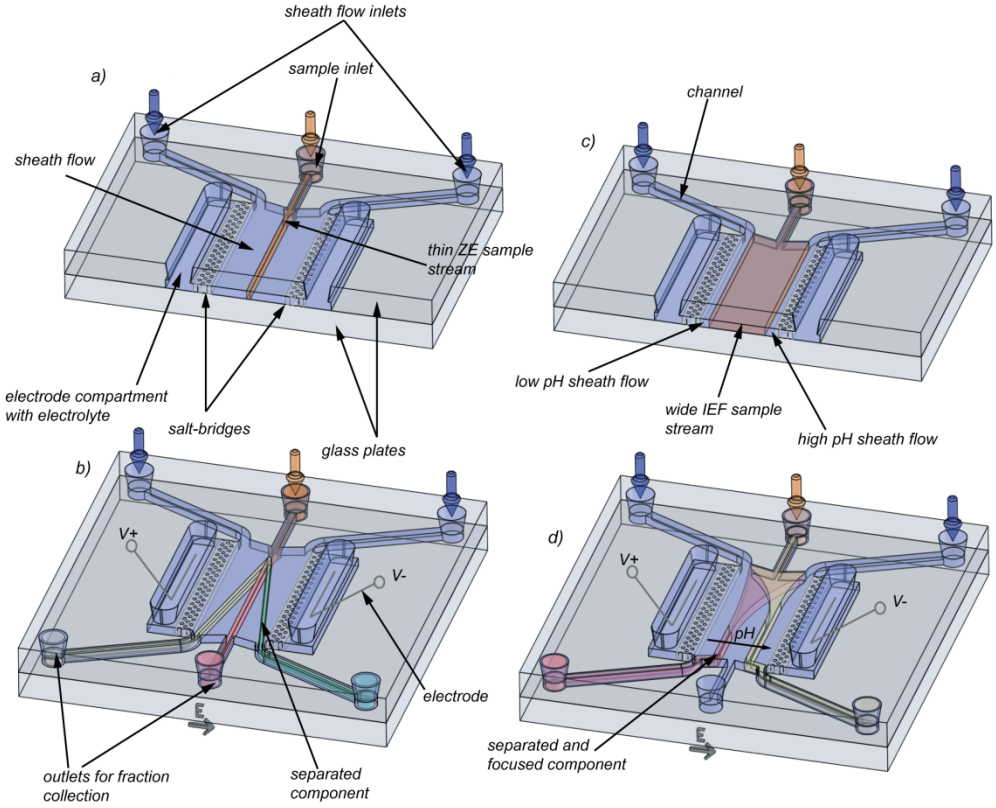


Fig. 3.1 Illustration of the µ-FFE device and applied separation methods: (a), (b) application of free-flow zone electrophoresis: (a) The sample mixture is hydrodynamically focused by two sheath flow streams containing buffer only and no voltage is applied. (b) Voltage is applied and different components separate due to their size to charge ratio. (c),(d) application of free-flow isoelectric focusing; (c), a wide sample mixture and ampholytes are sandwiched between two thin sheath flow streams of high and low pH; (d), In the presence of an electrical field the ampholytes build up and buffer a linear pH gradient. Components move towards and focus at their isoelectric points.

The device was used for efficient free-flow zone electrophoresis and isoelectric focusing. Furthermore, it is also suited for hydrodynamic focusing [79, 80], allowing full control over position and width of the sample stream sandwiched between two sheath flow streams (Fig. 3.1.a Bands of separated components can be guided to the desired outlet by adjusting the flow ratio of the sheath flow streams.

During FFZE operation, the electrode compartments are both filled with an aqueous buffer of same pH as compared to that of sample and sheath flow streams. If the electrical field is applied (Fig. 3.1b), the charged sample components are separated according to their charge to size ratio, showing a deflection behavior under a constant angle. Separated fractions can finally be collected at the chip outlets. For FFIEF, carrier ampholytes are added to the sample to establish a stable and linear pH gradient across the separation chamber. The wider sample is sandwiched between two thin sheath flow streams of low and high pH value, respectively (Fig. 3.1c). The electrode compartments are filled with an acidic and basic solution, respectively. In contrast to the thin sample stream during FFZE, a broader sample is established during isoelectric focusing to achieve higher focusing rates. In the presence of an electrical field and the natural pH gradient the ampholytes establish and maintain the required pH gradient. Components separate and focus according to their isoelectric point (pI) (Fig. 3.1d). At their respective pI the components become neutral and transversal migration stops. The separation will therefore result in parallel lanes.

## 3.3 Experimental

### 3.3.1 Materials and Reagents

Rhodamine B, fluorescein, fluorescent IEF markers, high resolution ampholytes (pH 3-10), Tween 20, hydroxpropylmethylcellulose (HPMC), HEPES, $H_3PO_4$, NaOH, acrylamide, N,N methylenebisacrylamide, 2,2-dimethoxy-2-phenylacetophenone, trimethoxysilyl–propylmethacrylate, and isopropanol (IPA) were purchased from Sigma-Aldrich-Fluka (The Netherlands). Chemicals for standard cleanroom fabrication techniques are not explicitly mentioned. Stock solutions of 10 mg $mL^{-1}$ rhodamine and 6 mg $mL^{-1}$ fluorescein were prepared in demineralized water. Stock solutions of fluorescent IEF markers (pI 4.5, 5.5, 7.6, 8.7) of 1 mg $mL^{-1}$ were prepared in 10% IPA in demineralized water. Working solutions were freshly prepared before each

experiment by diluting from the stocks (for final concentrations see results and discussion). All solutions were degassed in vacuum for 30 minutes to minimize air bubbles during flow operations.

### 3.3.2 Chip Fabrication

The microfluidic chips were fabricated at the MESA+ cleanroom facilities (Enschede, The Netherlands). Each chip consists of two 1.1 mm glass plates; the top plate contains the channels, separation chamber, fluidic inlets and outlets and the electrode openings, while the bottom plate is unprocessed. Processing of the top plate was done as follows (illustrated in Fig. 3.2 with a single chip): 1.1 mm thick Borofloat-glass was coated with a 140nm chromium-gold layer by metal sputtering. A photolithography step was performed prior to the patterning of the Cr-Au layer in a Cr-Au etch bath. This Cr-Au layer served as a mask during the following wet etching process in hydrofluoric acid to generate the channels and separation chamber in the underlying glass wafer. The etch depth was 15 µm. For the inlet and outlet reservoirs a second photolithography step was carried out on the back side, using a 100 µm polymer resist foil. This foil was exposed to a UV light source and was developed in a sodium carbonate solution. After that, powder blasting was performed with $Al_2O_3$ particles to create the inlet and outlet holes as well as the electrode openings. After ultrasonic cleaning in acetone and the removal of the Cr-Au layer, the wafer was thermally bonded to another Borofloat glass wafer. The bonded wafers were finally diced into several microfluidic chips. A more detailed glass-chip fabrication process can be found elsewhere [81].

A silanization step [82] was performed to achieve a chemical bond between the salt-bridges and the glass surface to increase the mechanical stability. Each chip was carefully flushed with 0.1 M NaOH and treated ultrasonically in 0.1 M NaOH for 30 minutes. After the cleaning, the chips were flushed with demineralized water to remove the NaOH. Next, the chips were placed in a trimethoxysilylpropylmethacrylate solution (0.5% in 50 mM NaAc, pH 4) for at least 60 minutes. The chips were flushed every 10 minutes to ensure fresh solution inside the chip. Finally, the chips were flushed with water and acetone and dried at 110 °C for 7 minutes.

An acrylamide solution of 18% acrylamide (monomer), 3% N,N-methylenebisacrylamide (crosslinker) and 3% 2,2-dimethoxy-2-phenylacetophenone (photoinitiator) was prepared in IPA [55]. The silanized chips were filled with the

monomer solution in the dark and placed in an in-house fabricated mask aligner. Exposure was performed with a mercury burner (Olympus U-LH100HG, light intensity I = 110 mW $cm^{-2}$) for 4 seconds through a slit mask in contact mode. Only the exposed areas solidified, and the remaining monomer was removed by flushing with IPA. Chips were stored in IPA for several hours. Afterwards, they were transferred to demineralized water and kept there overnight at room temperature.

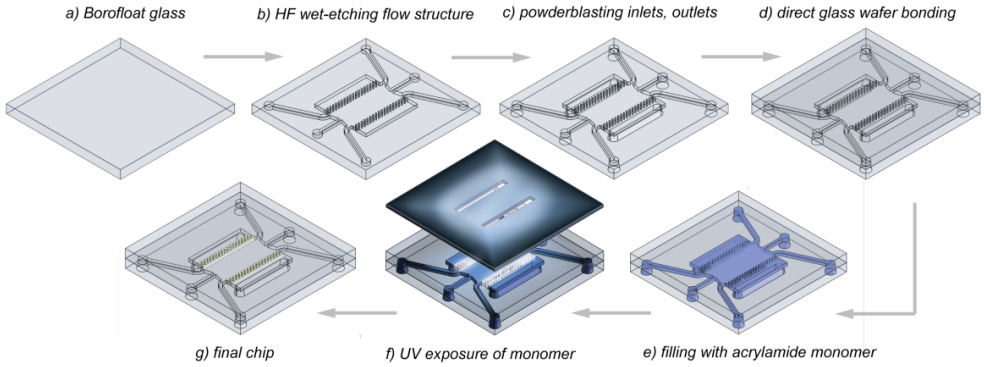


Fig. 3.2 Main micro fabrication steps of the µ-FFE chip: (a) Borofloat glass was taken as substrate (b) Hydrofluoric wet etching (15 µm) of glass was performed with a Cr-Au etch-mask to create microfluidic structures (c) Inlets, outlets and electrode openings were made by powder blasting with $Al_2O_3$ particles (d) Processed device was thermally bonded to Borofloat glass at 620 °C for 1 hour (e) Diced chips were filled with acrylamide monomer solution and exposed with UV light through slit mask (f) Unexposed monomer solution was removed by flushing the chip with IPA.

Each chip is 20 mm x 20 mm in size and the thickness is 2.2 mm. The channel and chamber depth is 15 µm. The width of the sample channel is 50 µm and of the sheath flow inlet channels 200 µm. In our studies we used chips with a chamber width of 1.5 mm and 3 mm, and a chamber length of 10 mm long. The salt-bridges are 1 mm wide.

To investigate the structure and the porosity of the polymerized acrylamide membranes, SEM scans were performed. The chip was dried and a part of the upper glass plate was truncated and removed. Here, the silanization step was not performed in order to remove the glass more easily without damaging the salt-bridges. Prior to the SEM scans the chip was coated with 5 nm gold by sputtering.

### 3.3.3 Experimental Setup and Methods

The fabricated chips were placed in an in-house fabricated plastic holder, as illustrated in Fig. 3.3. Three syringe pumps (CMA/102 Microdialysis, Sweden) were

connected via glass capillaries (Aurora, The Netherlands) and Nanoport connectors (Upchurch Scientific, USA) with the chip holder. High precision microliter glass syringes (Hamilton, Switzerland) were connected with the capillaries with Nanotight fittings (Upchurch Scientific, USA). Two integrated platinum electrodes were mounted inside the electrode compartments and connected with a power supply (IBIS Technologies, The Netherlands). Power supply and syringe pumps were controlled real-time with a personal computer and the software LabView (National Instruments), employing a simple analytical model for flow-rate calculations imbedded into the software. Chip outlets were connected via plastic tubes in order to collect fractions. The holder was placed on a fluorescence microscope (Olympus IX51) equipped with mercury burner and fluorescent filter sets for Rhodamine, fluorescein (XF57, Omega Optical, USA) and for IEF markers (XF02-2, Omega Optical, USA). Microscopic images were captured with the digital colour camera ColorViewII (Soft Imaging Systems, Germany) and recorded with the software package AnalySIS 5 (Soft Imaging Systems, Germany). For overview images, single microscopic images were combined to one overlay image.

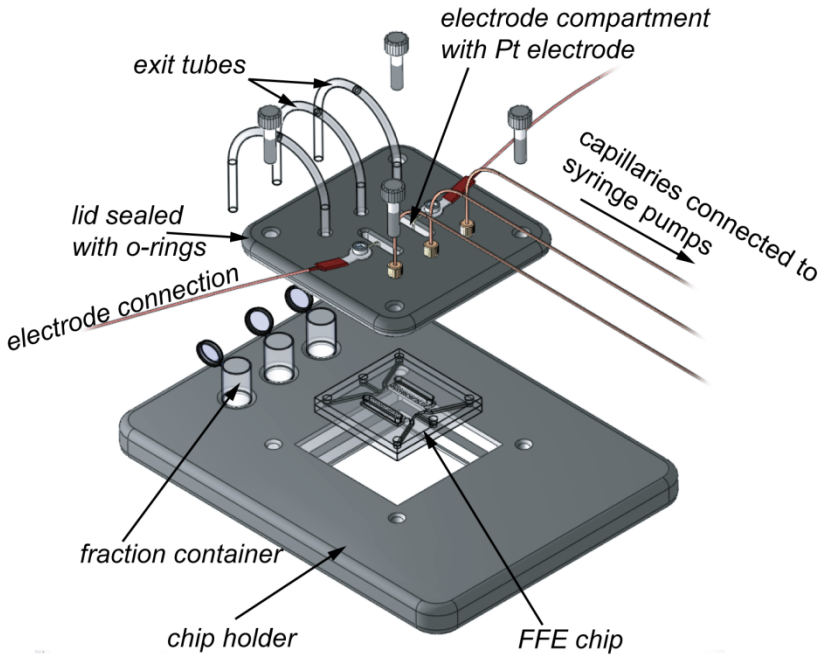


Fig. 3.3 Illustration of the in-house fabricated chip holder (partly disassembled) including all main components. The holder was placed on an inverted microscope for fluorescence observation during separation.

In case of FFZE, both electrode compartments were filled with 50 mM Hepes (pH 7.4). The sample mixture was 2 mg $mL^{-1}$ rhodamine and 2mg $mL^{-1}$ fluorescein in a solution of 10 mM Hepes (pH 7.4), 0.2% HPMC and 0.1% Tween 20 in demineralized water. This sample was hydrodynamically focused inside the chip in-between two sheath flow streams containing 10 mM Hepes (pH 7.4), 0.2% HPMC and 0.1% Tween 20 in demineralized water. Stream widths and flow velocities were adjusted by controlling the flow rates of the three syringe pumps.

For FFIEF, a pH gradient had to be formed perpendicular to the flow. Therefore, the electrode compartments were filled with an anodic electrolyte of 20 mM $H_3PO_4$ and a cathodic electrolyte of 40 mM NaOH. 2% ampholytes were added to the sample solution of 0.25 mg $mL^{-1}$ fluorescent IEF markers (pI 4.5 and 8.7 or 4.5, 5.5, 7.6 and 8.7) in 0.2% HPMC and 0.1% Tween 20. This sample was sandwiched by a side stream of 20 mM $H_3PO_4$ at the anodic side and a side stream of 40 mM NaOH at the cathodic side, both containing 0.2% HPMC and 0.1% Tween 20, respectively.

## 3.4 Results and discussion

### 3.4.1 Fabricated Chips

The composition of acrylamide monomer, crosslinker and photoinitiator was taken from Y. Takamura et al. [55] who describe high pressure EOF pumping with integrated salt-bridges. Therefore, it was assumed that the composition could also be used for the FFE chip. However, it turned out that the stability was poor in case of polymerization inside non-treated chips. When the chips were silanized before the formation with the acrylamide gel, the mechanical stability was higher. Treated chips could be used for FFZE for several days without major defects and deformation of the salt-bridges. Figure 4 shows a photograph of two chips before (Fig. 3.4.a, left) and after the salt-bridge fabrication (Fig. 3.4.a, right). A more detailed photograph can be seen in Fig. 3.4b showing the lower salt-bridge next to the electrode compartment. In this figure, one can see an array of 200 µm diameter glass pillars, which was included into the design to further increase the mechanical stability of the salt-bridges against the pressure driven fluid. As can be seen from the SEM scan in Fig. 3.4.c, the salt-bridge could be fabricated with homogenous porosity without defects. Since the salt-bridge was dried before the SEM, it shrunk and detached from the upper glass surface.

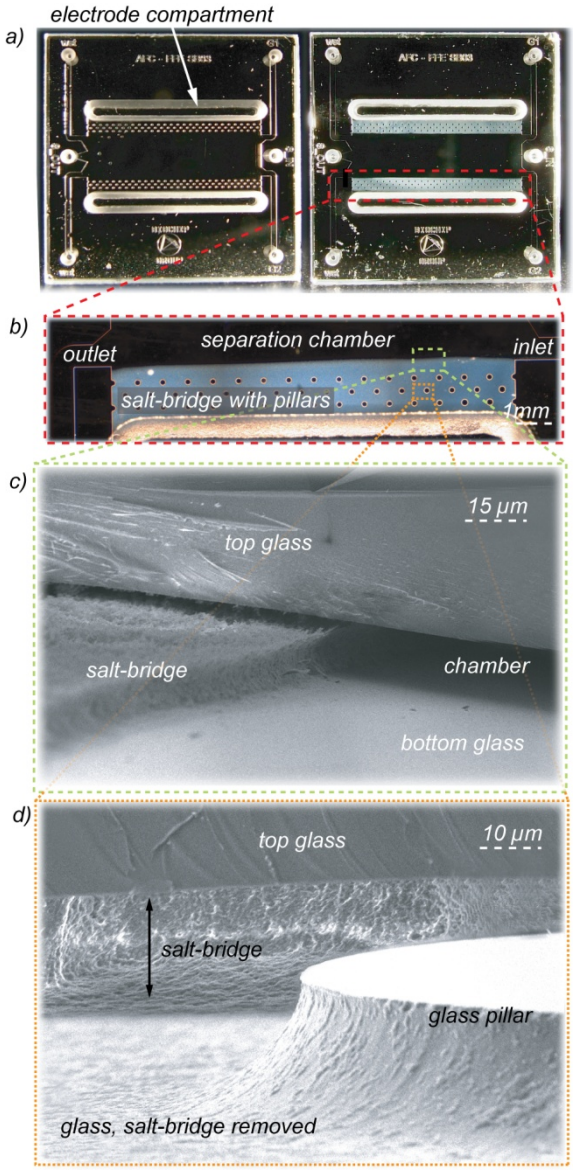


Fig. 3.4 Photographs of microfabricated FFE chips: (a), fabricated glass chips (in front of a black surface) without (left) and with (right) photo-polymerized salt-bridges; the chip size is 20 x 20 mm2, thickness 2.2 mm, the separation chamber is 3.5 mm x 12 mm and 15 µm high; (b), a microscopic photograph of a salt-bridge and surrounding parts is shown here; the mechanical stability of the salt-bridge is enhanced by an array of glass pillars; (c), photograph shows a SEM scan of a halved chip with the dried salt-bridge in front; (d), SEM image of the salt-bridge with glass pillar in front.

### 3.4.2 Free-flow Zone Electrophoresis

Two fluorescent standard dyes were used to demonstrate free-flow zone electrophoresis. In Fig. 3.5.a one can see the sample stream, containing a mixture of rhodamine B and fluorescein injected into the separation chamber in the absence of the applied voltage. It can be observed that the flow position of the stream is not affected or bended since the salt-bridges define a functionally closed environment.

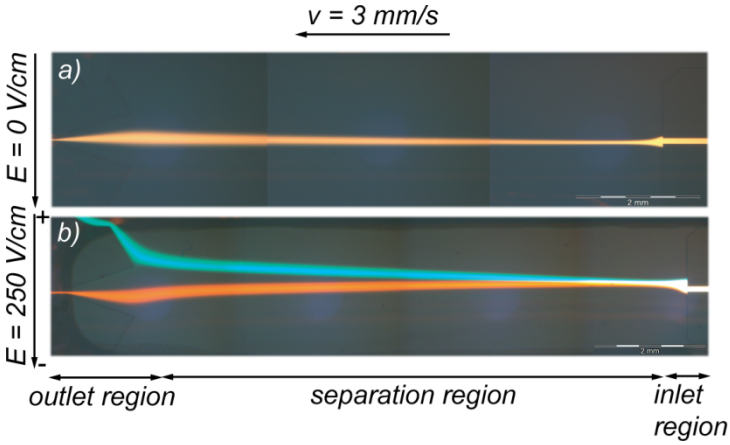


Fig. 3.5 Free-flow zone electrophoresis of 2 mg mL-1 fluorescein and 2 mg mL-1 Rhodamine B in 10 mM Hepes (pH 7.4), 0.1% Tween 20 and 0.2% HPMC. Buffer streams contained 10 mM Hepes, 0.1% Tween 20 and 0.2% HPMC. Electrode reservoirs were filled with 50 mM Hepes (pH 7.4). The chamber width was 3mm and flow velocity was app. 3 mm s-1. App. flow rates were: sample: 3 nl s-1 and sheath flows: 65 nl s-1. In these photographs the flow is from right to left. Several microscopic images were merged to one overview image. (a) 0 V; (b) 180 V (I = 50 µA), calculated electrical field strength of 250 V cm-1 across the separation area.

Until now, only side channel arrays were used to isolate the separation chamber in microfluidic FFE devices. In the case of a closed structure, as presented here, electroosmotic flow has to be suppressed efficiently since it can cause electrodynamic band broadening effects. Transversal electroosmotic flow was efficiently minimized by including HPMC in the solution as dynamic coating substance. The successful suppression of EOF in microfluidic channels with HPMC has recently been reported [83]. Fig. 3.5.b shows the separation result when 250 V $cm^{-1}$ (V = 180V, I = 30 µA) were applied. Fluorescein is negatively charged and was deflected under a constant angle towards the anode. The positively charged rhodamine B dye was slightly deflected towards the cathode. Comparable separation results were achieved in

previous devices with voltages up to 2 kV [45] where only 5% of this potential was present in the separation chamber. Since a membrane structure with a lower electrical resistance is used here, the applied potential was used at least 10 times more efficiently. In conventional large scale systems Joule heating plays an important role and has to be counteracted by sophisticated cooling systems. In µ-FFE systems, as reported here and earlier, Joule heating is not significantly affecting band broadening. This might also be due to the faster heat dissipation as higher surface to volume ratios are present. FFE typically involves higher electrical currents, which lead to gas formation at the electrodes due to electrolysis. This was reported to be the limiting factor in an earlier presented device, since bubbles can disrupt the fluid flow and electrical connection.[49] Here, no problems due to electrolysis could be observed, since the electrodes were located outside the separation chamber in open reservoirs, and $O_2$ and $H_2$ bubbles could not pass the membranes.

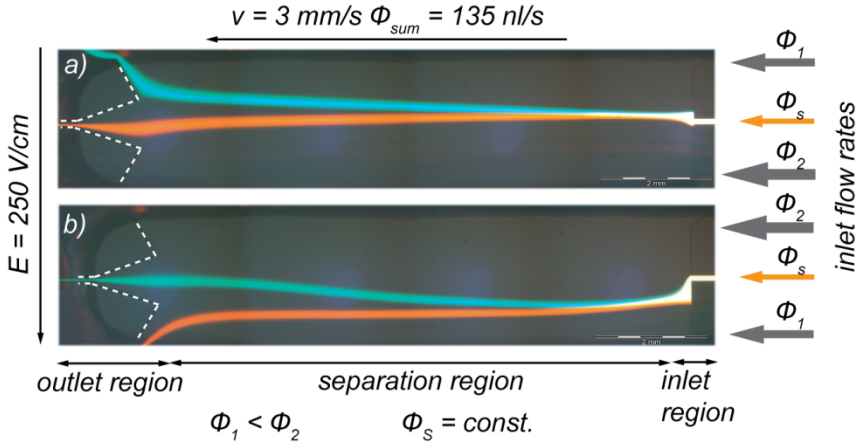


Fig. 3.6 Figure shows the steering of separated components during free-flow zone electrophoresis (the same concentrations as in figure 5). By hydrodynamic focusing of the sample streams in-between two buffer streams it was possible to steer the components to specific chip outlets by changing the inlet flow ratio of the two sheath flow streams. (a) The negatively charged fluorescein exits the chip at the upper outlet. (b) After flow rate changes now fluorescein exits the chip at the middle outlet.

Hydrodynamic focusing is used to control the position and width of the sample stream inside the separation chamber. This technique makes it possible to steer separated components to specific chip outlets, as shown in Fig. 3.6. In Fig. 3.6.a, the negatively charged fluorescein exits the chip at the upper outlet. By adjusting the flow ratio of the two sheath flow streams, it was possible to guide the fluorescein to the middle outlet,

as shown in Fig. 3.6.b. The steering was performed without changing the applied voltage and the flow velocity inside the separation chamber. Since the fluidic connectors and pumping systems were from rigid material and enclosed compressible air was removed, steering could be accomplished within seconds. This steering technique can be used in future devices to purify a sample mixture in such a way that only the separated component of interest is steered to a specific outlet. This specific outlet will be connected to further lab-ob-a-chip operation units. Furthermore, depending on the analytes charge, the steering can be used to adjust the injection position. A mixture of e.g. only negatively charged components would be injected near the negative cathode, in order to maximize the transversal migration distance and therefore the separation efficiency.

### 3.4.3 Free-flow Isoelectric Focusing

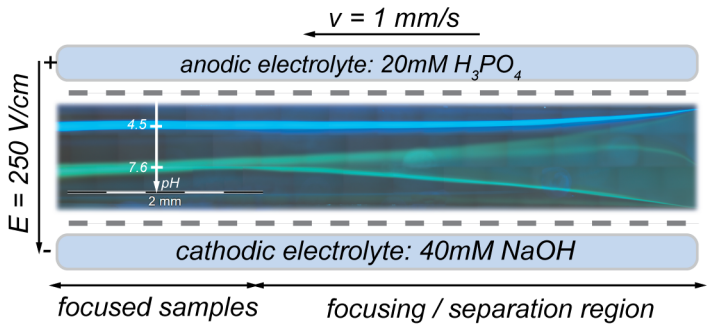


Fig. 3.7 Microscopic photograph showing free-flow isoelectric focusing of fluorescent IEF markers. The sample containing 0.2 mg mL-1 IEF markers (pI 4.5 and pI 7.6), 2% ampholytes, 0.2% HPMC, 0.1% Tween 20 was injected in-between a thin sheath flow stream of 20 mM H3PO4, 0.2% HPMC and 0.1% Tween 20 at the anodic side and a sheath flow stream of 40 mM NaOH, 0.2% HPMC and 0.1% Tween 20 at the cathodic side. The chamber width was 1.5 mm and flow velocity was app. 1 mm s-1. Typical flow rates were sample + ampholyte mixture: 20 nl s-1 and sheath flows: 1.5 nl s-1. When an electrical field was applied molecules focused at their isoelectric point.

Free-flow isoelectric focusing was performed with different fluorescent IEF markers having isoelectric points at pH 4.5, 5.5, 7.6 and 8.7. Carrier ampholytes (pH 3-10) were added to the sample to establish a linear pH gradient across the separation chamber. In the presence of a natural pH gradient (acidic and basic electrolytes) the ampholytes migrate until a stable pH gradient is established. As shown in Fig. 3.7, separation and focusing was observed. Within several seconds the analytes focused and transversal

migration stopped. This corresponded well with earlier published µ-FFE device [46]. However, as mentioned before, the side channels caused a potential drop of 95%. Due to spreading of the carrier ampholytes into the side channels, the larger part of the pH gradient formed inside the side channels and therefore, could not be used for separation. The here presented device makes it possible to use the full pH gradient, since the actual sample (+ ampholytes) is sandwiched between an acidic and basic electrolyte. Ampholytes and sample will never migrate into the sheath flow regions, since their movement will be counteracted as soon as their electrical charge changes. The usage of sheath flows ensures not only a stable pH gradient but also the manipulation of the width of the pH gradient and position. This makes it possible to steer components of interest, as mentioned above. Fig. 3.8 shows FFIEF with four fluorescent markers with isoelectric points between pH 4 to 9.

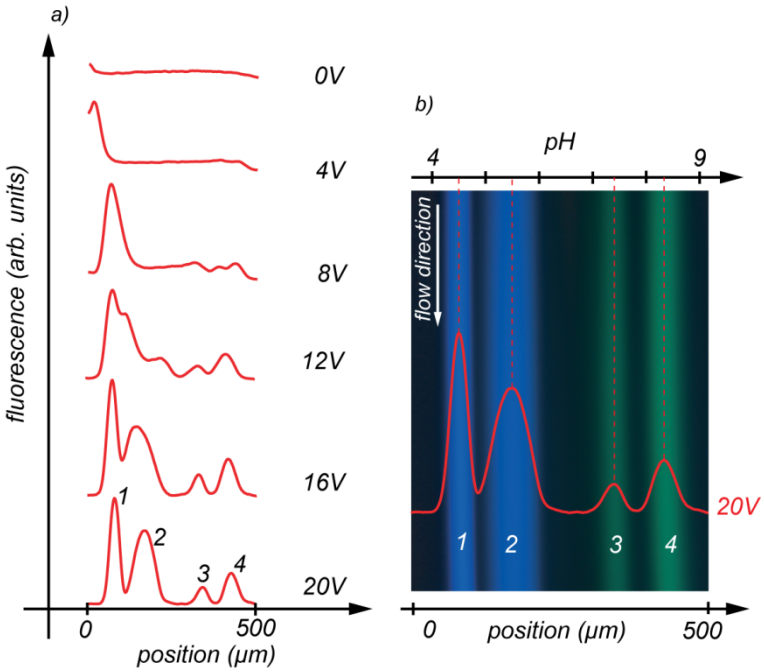


Fig. 3.8 Line profiles taken during free-flow isoelectric focusing: (a) fluorescent intensity line scans were taken 6 mm from the chip inlets with different voltages applied, the flow velocity was 2 mm $s^{-1}$ resulting in a residence time of 3 s at the point of measurement, (b) four different IEF markers (0.2 mg $mL^{-1}$, pI 4.5, 5.5, 7.6 and 8.7) focused at their isoelectric point when 20 V were applied, a nearly linear pH gradient was established using ampholytes (pH 3-10).

Fluorescent intensity profiles were taken at different voltage settings. It can be seen in Fig. 3.8.a that only 20 V was required to achieve a complete separation and focusing with a 600 μm wide pH gradient. Since the four IEF markers could not be excited at their fluorescence excitation maxima equally, emission intensities differ. In case of isoelectric focusing, the salt-bridges were stable for several hours but eventually broke apart and stopped the system from working. This is probably due to the fact that the silanization bond and acrylamide gel are not stable at extrem pH values.

## 3.5 Conclusions

A new microfluidic free-flow electrophoresis device has been fabricated and experimentally characterized. A new feature in the device is the inclusion of two photopolymerizable membranes that were fabricated inside the chip to isolate the microfabricated separation chamber from the electrodes. These membranes form a hydrodynamic barrier for the pressure driven fluid flow, yet allow electrical connection by its ion permeability. In earlier devices, mostly dense channel arrays with a high hydrodynamic and electrical resistance were used instead. The presented device is more laborious to fabricate but allows us to reduce the required voltage by at least a factor of 10 (factor of 100 in case of reduced separation zone by hydrodynamic focusing), and more important during free-flow isoelectric focusing, the full pH gradient (pH 3-10) was available for separation. At these high flow-rates of several mm/s this was not possible before. Furthermore, the combination of FFE and hydrodynamic focusing makes it possible to steer separated components to specific chip outlets. Compared with earlier devices, bubble generation during electrolysis did not limit the separation, since the electrodes were located in open compartments. Separation was successfully carried out in two modes: free-flow zone electrophoresis and free-flow isoelectric focusing. Several fluorescent dyes and IEF markers were separated. A stable and linear pH gradient was formed during free-flow isoelectric focusing. As proposed already in recent publications μ-FFE can be a promising technology especially in combination with sensors for real-time monitoring of separated components. This paper demonstrated the prove-of-principle to use acrylamide membranes in a μ-FFE device. More detailed experimental work is currently being performed.

# 4 Microfluidic Free-Flow Isoelectric Focusing

*After the successful realization of the first FFE chip generation, the design was further improved. Now, focus was laid on free-flow isoelectric focusing and increased chip performance. A new ampholyte system was applied and high resolution separation results of various markers and the protein HSA were obtained. These results demonstrate that microfluidic FFE systems can achieve higher separation results than their larger counterparts due to less technical problems involved. This chapter was published in Analytical Chemistry in 2007.*

## 4.1 Abstract

A microfluidic free-flow isoelectric focusing glass chip for separation of proteins is described. Free-flow isoelectric focusing is demonstrated with a set of fluorescent standards covering a wide range of isoelectric points from pH 3 to 10 as well as the protein HSA. With respect to an earlier developed device, an improved microfluidic FFE chip was developed. The improvements included the usage of multiple sheath flows and the introduction of pre-separated ampholytes. Pre-separated ampholytes are commonly used in large scale conventional free-flow isoelectric focusing instruments, but have not been used in micro machined devices yet. Furthermore, the channel depth was further decreased. These adaptations led to a higher separation resolution and peak capacity, which were not achieved with previously published free-flow isoelectric focusing chips. An almost linear pH gradient ranging from pH 2.5 to 11.5 between 1.2 and 2 mm wide was generated. 7 isoelectric focusing markers were successfully and clearly separated within a residence time of 2.5 seconds and an electrical field of 20 $Vmm^{-1}$. Experiments with pI markers proved that the device is fully capable of separating analytes with a minimum difference in isoelectric point of $\Delta(pI) = 0.4$. Furthermore, the results indicate that even a better resolution can be

achieved. The theoretical minimum difference in isoelectric point is Δ(pI) = 0.23 resulting in a peak capacity of 29 peaks within 1.8 mm. This is an 8 fold increase in peak capacity to previously published results. The focusing of pI markers led to an increase in concentration by factor 20 and higher. Further improvement in terms of resolution seems possible, for which we envisage that the influence of electroosmotic flow has to be further reduced. The performance of the microfluidic free-flow isoelectric focusing device will enable new applications, as this device might be used in clinical analysis where often low sample volumes are available and fast separation times are essential.

## 4.2 Introduction

In proteomics analysis protein separation is often achieved by two-dimensional gel electrophoresis (2D GE). To decrease the high sample complexity of proteins present in blood sera or cell extracts prior to a 2D GE separation, free-flow electrophoresis (FFE) has found its place as a pre-analytical pre-fractioning tool [71, 74, 75]. Free-flow electrophoresis allows the fractioning of particles, cells, organelles and macromolecules based on their electrophoretic mobility transverse to a hydrodynamic carrier flow [27].

One mode of FFE is free-flow isoelectric focusing (FFIEF), in which a pH gradient is established perpendicular to the carrier flow. This pH gradient is achieved and buffered by adding ampholytes to the solution. These ampholytes have specific isoelectric points and re-arrange by migration when an electrical field is applied [84]. Proteins migrate due to the applied external field along the pH gradient and get eventually focused where the local pH value is equal to their pI value, at which point their net charge is zero [17, 85]. The main disadvantage of applying large-scale FFE and FFIEF is the requirement for high sample volumes, typically ranging from a few milliliters to a few tens of milliliters. Especially in clinical analysis with often low amounts of patients sample available, miniaturization of FFE is therefore promising [22, 62]. Miniaturized microfluidic FFE systems allow easier control of laminar flow, as well as the possibility to apply higher separation voltages without Joule heating problems [86]. These advantages were already recognized by Raymond et al. in 1994 who presented the first microfluidic FFE device (μ-FFE) [31]. In the past years several μ-FFE systems, including microfluidic versions of FFIEF, were developed and the separation efficiency further improved [33, 45, 46, 49, 51, 52, 87, 88]. The particular

interest in μ-FFE systems is growing rapidly indicated by the relatively high number of publications in 2006 [34, 35, 37, 47, 48, 50, 54, 89]. Although the system performance of microfluidic FFE and FFIEF was steadily improved, resulting in faster separation, higher voltage efficiency and increased resolution, the published results so far are not sufficient compared to large scale conventional FFE systems. Besides the presentation of a new FFIEF chip, one of the aims of this paper was to study more intensively the performance-limiting factors in μ-FFIEF systems and how to further increase the separation performance.

Here we report on an improved microfluidic FFIEF chip, developed by learning from the large scale FFE instruments currently available and miniaturizing certain aspects, namely multiple sheath flows and pre-separated ampholytes [18]. This microfluidic chip device was characterized with a set of fluorescent IEF standards covering isoelectric points ranging from pH 3 to 11. In terms of separation peak capacity and resolution, the results surpass all thus far published devices.

### 4.2.1 Principle

The FFIEF chip presented here, is a further development of an earlier published version and for some details the reader is referred to this paper [34]. As illustrated in Fig. 4.1, the μ-FFIEF chip consists of a bottom glass plate (1) which is left unprocessed and a top glass plate (2) which incorporates a network of microfluidic channels (3) and the separation chamber (4). The bottom glass plate was bonded to the upper plate in order to seal the microfluidic network. Inlets and outlets (5) through the top plate provide access for fluidic connections. The separation chamber is connected to five inlet channels used to fill the chamber with different flow streams. Each stream serves a different purpose. The two outer inlet channels (6, 7) are used to infuse the separation chamber sides with a sheath flow of low pH and of high pH respectively to confine the limits of the applied pH gradient. The three inner inlet channels (8, 9 and 10) are used to fill the chamber with the required ampholytes to buffer the pH gradient. A detailed explanation is found along with Fig. 4.2. The center inlet channel (9) is also used to bring in the sample mixture. To couple the electrical field in, the chip has two parallel open electrode compartments (11) filled with an electrolyte solution into which two external platinum wires are placed. Two ion-permeable hydrogel membranes (12) at the sides of the separation chamber (4) form an electrically conducting, but fluid-leakage minimized bridge between the electrode

compartments and the separation region. In this way a stable electrical field can be applied and gas formation at the electrodes due to electrolysis will not disturb the separation. Fig. 4.1.a illustrates the device when no voltage is applied and the sample mixture exits the device unseparated (13). When an electrical field is applied across the separation region (Fig. 4.1b) the continuously flowing ampholytes re-arrange by migration to form the pH-gradient and the sample components (14) migrate towards and focus at their isoelectric points. The fractions can be collected separately (15). The number of chip outlets was limited to five for practical reasons, and does not correspond to the number of separated analytes.

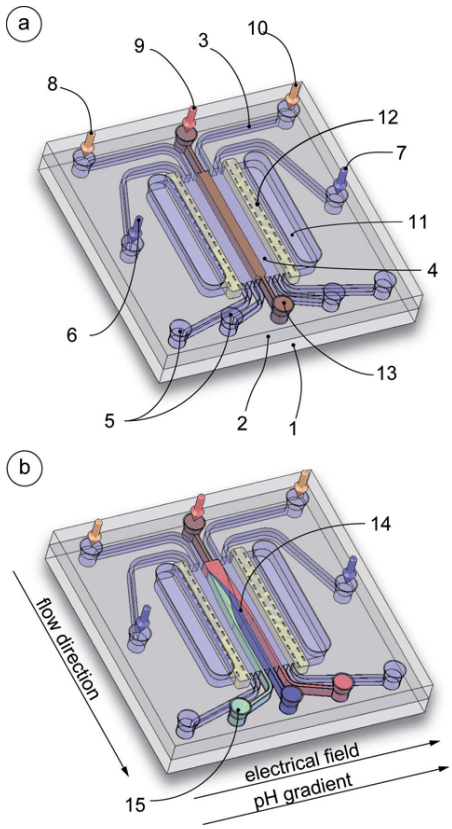


Fig. 4.1 μ-FFIEF chip layout and working principle: (a) No voltage applied, no separation; (b) Voltage applied, IEF of three components; (1, bottom chip plate; 2, top chip plate; 3, microfluidic channel; 4, separation chamber; 5, outlets; 6, low pH sheath flow inlet; 7, high pH sheath flow inlet; 8, ampholytes 1 inlet; 9, ampholytes 2 + sample inlet; 10, ampholytes 3 inlet; 11, electrode compartment; 12, conductive membrane; 13, not separated sample; 14, focused sample; 15, collected sample)

Conventional large scale FFE systems, such as introduced to the market by BD-Biosciences, use several inlets to fill the separation chamber with pre-separated ampholytes. The usage of these pre-separated ampholytes results in a lower electrical current and faster separation times, since the amphoteric substances need less time to reach their respective pI values. BD provides their standard ampholytes covering a pH range from 2.5 to 11.5. Here we refer to these pre-separated ampholyte reagents as Prolytes1, Prolytes2 and Prolytes3.

In Fig. 4.2, the application of pre-separated ampholytes is illustrated in more detail. The illustration shows three cross sections (Fig. 4.2.a, b and c) of the chip separation chamber. Each cross section corresponds to a different x-coordinate ($x_a$, $x_b$, $x_c$) along the chamber. Since it is a continuously flowing system, each position directly corresponds to a specific residence time depending on the flow velocity. To clarify the formation of the pH-gradient, diagrams of the expected pH-gradient are shown. Observing the cross section directly at the separation chamber entrance (Fig. 4.2.a), one can see that the chamber is infused with five adjacent fluid streams. With no electrical field applied, these streams would only mix by diffusion. The positive anode (1) is placed in an acidic solution of pH 2 while the cathode (2) is inserted into a basic solution of pH 12. The separation chamber is shielded by two ion permeable membranes (3). Next to the membranes two sheath flow streams of pH 2 (4) and pH 12 (5) confine the outer limits of the applied pH gradient. Depending on the ampholytes reagents used, the electrolyte and sheath flow pH values might differ. However, here only a wide pH range gradient (pH 2.5 – 11.5) was used. The inner three streams contain the ampholytes Prolytes1 (6), Prolytes2 (7) and Prolytes3 (8). Furthermore, the center stream (7) also contains the sample mixture. In this manner, a stepped pH gradient is generated. With increasing residence time (Fig. 4.2.b) of the ampholytes in the electrical field a continuous pH gradient starts to form due to migration of the ampholytes towards their pI. Past a certain position which depends on the flow rate and applied voltage, a linear pH gradient (Fig. 4.2.c) has fully developed and all sample components focus (9) at their isoelectric point.

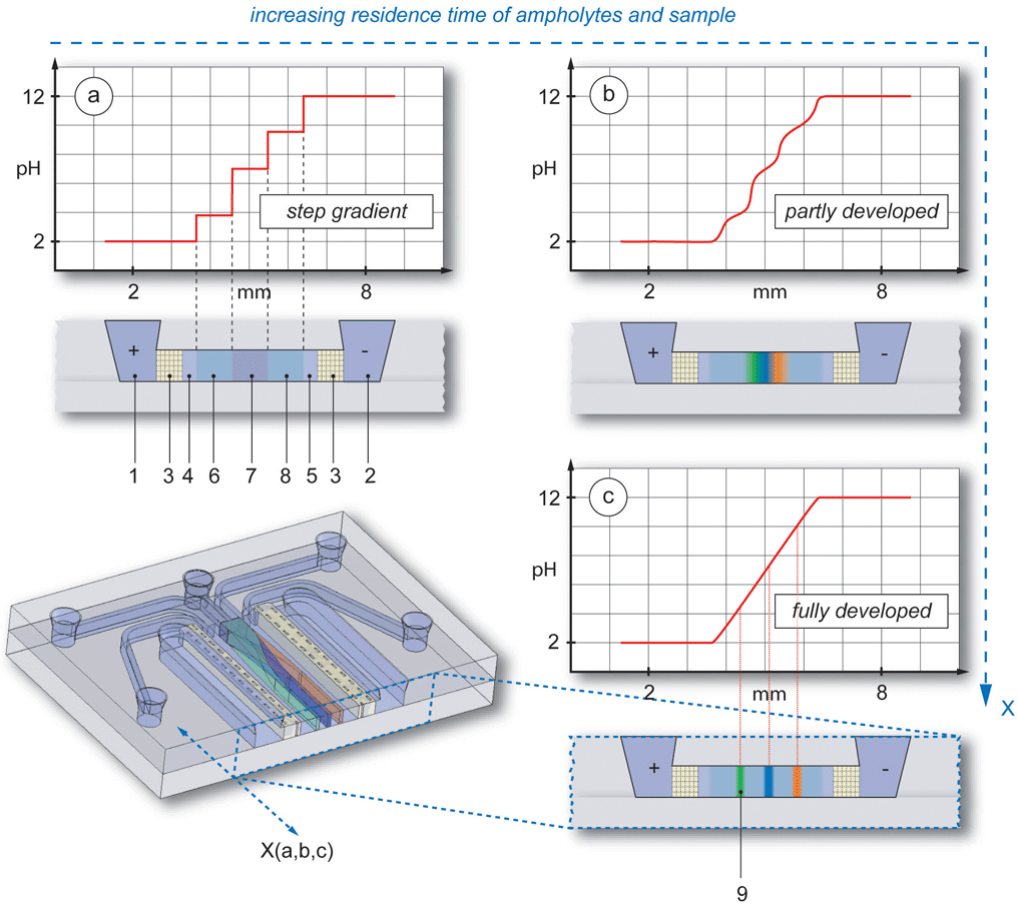


Fig. 4.2 pH gradient formation using pre-separated ampholytes: Figures a, b and c show cross section of the separation chamber at different position x and the corresponding pH gradient. With the increasing residence time, the pH gradient is further developing. (1, anodic electrolyte; 2, cathodic electrolyte; 3, membrane; 4, acidic sheath flow; 5, basic sheath flow; 6, Prolyte1; 7, Prolyte2 + sample; 8, Prolyte3; 9, fully focused sample component)

## 4.3 Experimental

### 4.3.1 Materials and Reagents

Fluorescent IEF standards and proteins were purchased from Sigma-Aldrich-Fluka (The Netherlands). Proteins were labeled by Active Motif Chromeon (Germany) using the CE-540 fluorescent dye. Ampholyte solutions Prolytes 1, 2 and 3 were obtained from BD Diagnostics (Germany). All other chemicals were obtained from Sigma-Aldrich-Fluka (The Netherlands). All solutions were degassed in vacuum for 10 minutes to minimize air bubbles during flow operations.

### 4.3.2 Chip Fabrication

Each chip consists of two thermally bonded Borofloat 33 glass plates (Schott Jenaer Glas, Germany); the top plate contains the channels, separation chamber, fluidic inlets and outlets and the electrode openings, while the bottom plate is unprocessed. Hydrofluoric acid was used to etch the channels and separation chamber while a chromium-gold layer protected the regions not to be etched. The etch depth was 10 µm. A powder blasting step was performed with $Al_2O_3$ particles to create the inlet and outlet holes, as well as the electrode openings. The processed glass wafer was thermally bonded to another Borofloat glass wafer. The bonded wafers were finally diced into several microfluidic chips. A silanization step with trimethoxysilylpropylmethacrylate was performed to achieve a chemical bond between the acrylamide membranes and the glass surface to increase the stability. An acrylamide solution, including a cross linker and photo initiator was used to fill the chip and was exposed through a slit mask using a UV light source. The photo polymerized acrylamide regions form the desired membranes. Finally the chips were filled with a solution of 1% polyvinylalcohol (PVA) in DI water and incubated overnight, to coat the channel surface to minimize electroosmotic flow (EOF) as well as protein absorption.

### 4.3.3 Experimental Setup and Methods

The fabricated chips were placed in an in-house fabricated holder. Syringe pumps (CMA/102, Microdialysis, Sweden) were used to control the flow rates. 1 mL glass syringes (Microdialysis, Sweden) were filled with the required solutions and

connected via glass capillaries (Aurora, The Netherlands) and Nanoport connectors (Upchurch Scientific, USA) with the chip holder. Two integrated platinum electrodes were mounted inside the electrode compartments and connected to a power supply (Labsmith, USA). Power supply and syringe pumps were controlled in real-time with a personal computer and the software LabView (National Instruments). Both electrolyte reservoirs were connected via polymer tubes to a peristaltic pump (Ismatec, Zwitzerland) to ensure a continuous refreshment of the solutions. The holder was placed on a fluorescence microscope (Olympus IX51) equipped with mercury burner and fluorescent filter set (XF02-2, Omega Optical, USA). Images were captured with the digital color camera ColorViewII (Soft Imaging Systems, Germany) and recorded with the software package AnalySIS 5 (Soft Imaging Systems, Germany).

For most of the FFIEF experiments the following conditions were used: The anodic electrolyte reservoir was filled with 20 mM $H_2SO_4$ and the cathodic electrolyte reservoir with 20 mM NaOH. All inner fluid streams (Fig. 4.2.a, streams 4-8) contained 0.1% Hydroxypropylmethylcellulose (HPMC) to reduce EOF and 0.1% Tween-20 to increase solubility of sample components, but more importantly to reduce the solution surface tension allowing air bubbles trapped in the channels to be removed more quickly. The acidic sheath flow (stream 4, stream numbers correspond with the numbers given in Fig. 4.2.a) contained 20 mM $H_2SO_4$ while the alkaline sheath (stream 5) contained 20 mM NaOH. The ampholyte streams (stream 6, 7 and 8) contained 20% of Polytes1, Prolytes2 and Prolytes3 respectively. The sample stream (stream 7) contained additionally a mixture of fluorescent IEF markers and proteins. All experiments were conducted at a flow velocity of 2 mm $s^{-1}$.

## 4.4 Results and Discussion

### 4.4.1 Fabricated Chips

A fabricated chip can be seen in Fig. 4.3.a. The glass chip is 20 mm x 20 mm in size and has a thickness of 2.2 mm. The etched channel depth is 10 µm. The five inlet channels and outlet channels are 300 µm in width. The size of the separation chamber is 10 mm in length and 3.5 mm in width, resulting in a volume of 350 nL. However, in practice only 30 to 60% of the total width is used for separation. The practical width of the separation region can easily be varied by adjusting the width of the outer sheath flows

(streams 4 and 5 in Fig. 4.2). While maintaining the total flow-rate, a wider low-pH and high-pH sheath flow stream (confining the limits of the used pH gradient) results in less space for the actual pH gradient. Width adjustments are performed by controlling the flow-rates of the appropriate syringe pumps. As shown in the dark-field microscopy image (Fig. 4.3.b), the width of the membranes between electrode opening and separation chamber is approximately 1 mm. To enhance the mechanical strength of the membranes and to withstand the pressure driven fluid inside the chamber, several glass pillars were included.

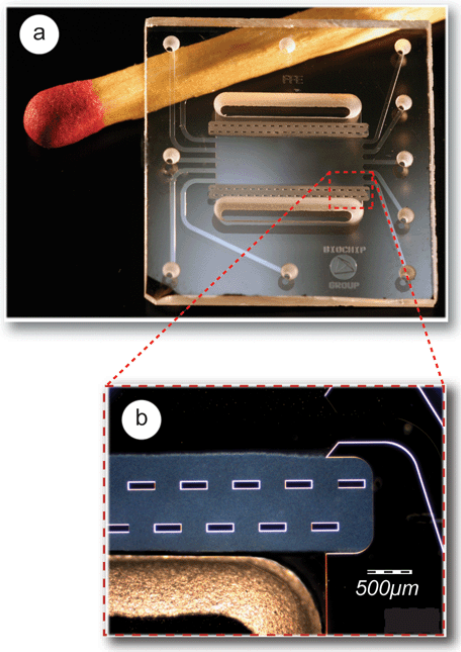


Fig. 4.3 Photographs of a fabricated µ-FFIEF chip: (a) The chip size is 20 mm x 20 mm with a thickness of 2.2 mm. The separation chamber has a volume of 350 nL (H x W x L: 10 µm x 3.5 mm x 10 mm). (b) Close-up on one of the membranes. The membranes are supported by glass structures to increase mechanical stability.

### 4.4.2 FFIEF of Fluorescent Low MW IEF Markers

#### 4.4.2.1 pH Gradient Quality

The usage of low molecular weight fluorescent isoelectric focusing markers has proven to be an accurate method to characterize IEF systems. In contrast to protein standards they show a lower tendency to precipitate at their pI due to a better solubility [84]. To cover a broad range of pH values the following fluorescent IEF markers were selected: pIs 4, 5.1, 5.5, 6.2, 7.2, 7.6, 8.1, 9 and 10.3.

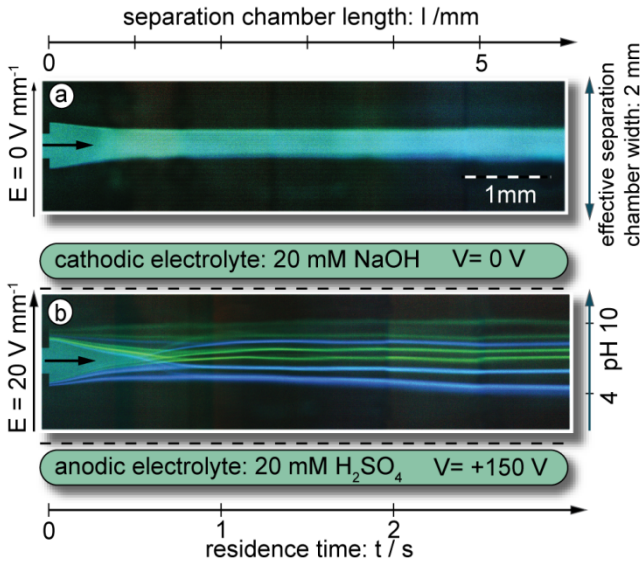


Fig. 4.4 Free-Flow Isoelectric focusing of 7 fluorescent IEF markers: (a) Photograph shows the device, when no voltage was applied. (b) When 150 V (I = 50 µA) was applied, the markers (pIs 4, 5.1, 6.2, 7.2, 8.1, 9 and 10.3) fully separated within less than two seconds. The sample flow rate was 0.4 µL $min^{-1}$ (2 mm $s^{-1}$) The apparent kinks in the fluorescent tracer paths are caused by merging multiple photographs.

Fig. 4.4 shows two photographs taken during FFIEF experimental work to clarify the working principle. The images show a 6-mm-long part of the separation chamber with the flow being from left to right. The total flow velocity inside the chamber was set to 2 mm $s^{-1}$. As long as no voltage was applied the adjacent streams did not mix except by diffusion (Fig 4.a). When an electrical field of 20 V $mm^{-1}$ was applied (voltage V = 150 V, current I = 50 µA) separation and focusing of all IEF standards was observed. After a residence time of less than two seconds all seven IEF markers were separated and after three seconds the focusing was completed (Fig 4.b).

The applied ampholyte system uses amphoteric substances with equal differences in isoelectric points over the whole pH range resulting in a linear pH gradient. Assuming all IEF markers focus exactly at their isoelectric points, one could derive the pH gradient which is actually achieved. Therefore, a fluorescence intensity plot was generated (Fig. 4.5.b) from a FFIEF experiment using 7 IEF markers (Fig. 4.5.a). Based on the peak positions, the experimentally interpolated pH gradient was derived as shown in Fig. 4.5.c. It can be seen that the pH gradient was fully developed and furthermore that the gradient linearity was close to ideal.

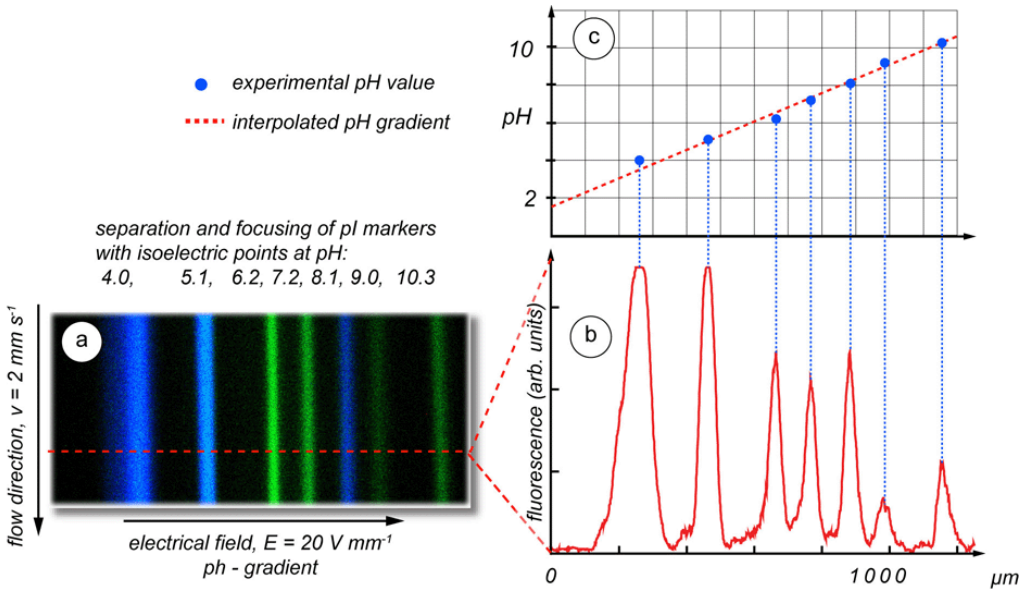


Fig. 4.5 Analysis of the established pH gradient from various IEF markers: (a) 7 IEF markers were focused during IEF and (b) an electropherogram generated. The experimental pH gradient was derived from the peaks positions (c). The focusing time was 2.5 seconds. (100 µg $mL^{-1}$ of pI markers 4, 5.1, and 6.2 and 20 µg $mL^{-1}$ of pI markers 7.2, 8.1, 9, 10.3).

#### 4.4.2.2 Peak Width

According to Giddings, a useful parameter system to express the quality of an equilibrium gradient separation system, such as isoelectric focusing includes the standard deviation of the peak width ($\sigma$), minimum pI value ($\Delta(pI)_{min}$) and peak capacity ($n$) [90]. Assuming a Gaussian concentration distribution, the standard deviation for a peak generated in IEF is given by

$$\sigma = \sqrt{\frac{D}{pE}} \tag{3.1}$$

where *D* is the diffusion coefficient, *E* the electrical field strength, and

$$p = -\frac{d\mu}{d(pH)} \cdot \frac{d(pH)}{dx} \tag{3.2}$$

Here *d(pH) / dx* is the pH gradient slope and *dμ / d(pH)* the mobility slope of the analyte [38]. For the separation results shown in Fig. 4.5 we derived the peak standard deviations. The results are given in table 1 and result in an average σ = 19 μm.

| **IEF marker (pI)** | **4.0** | **5.1** | **6.2** | **7.2** | **8.1** | **9.0** | **10.3** |
|---|---|---|---|---|---|---|---|
| peak position x (μm) | 245 | 456 | 646 | 756 | 857 | 953 | 1119 |
| peak width between inflection points w (μm) | 65 | 47 | 30 | 30 | 28 | 39 | 28 |
| standard deviation σ (μm) | 32.5 | 23.5 | 15 | 15 | 14 | 19.5 | 14 |

Tab. 4.1 Peak standard deviations for the experimental results shown in Fig. 4.5. The average deviation is $\sigma_{avg}$= 19 μm.

Of the variables in eq. (4.1), the diffusion coefficient and mobility slope are intrinsic properties of the analytes, so that only the electrical field and the pH gradient can be varied experimentally to reduce the peak width. Obviously, a shallower pH gradient would lead to higher resolving power but within a more limited pH range. The present device was designed for a constant wide range pH gradient (pH 2.5 – 11.5). Therefore, only the electrical field was varied during experiments. Eq. (4.1) predicts that a high electrical field decreases the peak width. To investigate the influence of the electrical field, the average standard deviation $\sigma_{avg}$ was determined for various electrical field settings and the results are shown in Fig. 4.6.

As shown in Fig. 4.6, for electrical field strengths below 10 V mm$^{-1}$ we observed an approximately linear decrease of σ. We concluded from the current / voltage curves to be shown in Fig. 4.7 and discussed there, that this improvement in peak width is directly related to the pH gradient formation and that a minimum electrical field of 10 V mm$^{-1}$ is required to reach a fully developed and steady state pH gradient at the flow velocity of v = 2 mm s$^{-1}$. In contrast to the theory given by eq. (4.1), an increasing

electrical field did not reduce the peak width any further, but between 10 and 40 V $mm^{-1}$ the average standard deviation reached a constant value of around 18 µm. Furthermore, fields above E = 50 V $mm^{-1}$ caused increasing band broadening and eventually destabilization of the separation (data not shown here, see also Fig. 4.8). Possible reasons which might explain the lack of a further decrease in peak width above E = 10 V $mm^{-1}$, can be Joule heating and electroosmotic flow. Both parameters are well known from free-flow electrophoresis leading to band broadening in the form of a crescent-shaped deformation of the sample [16]. We will first consider the influence of Joule heating which has been widely discussed and investigated in capillary electrophoresis.

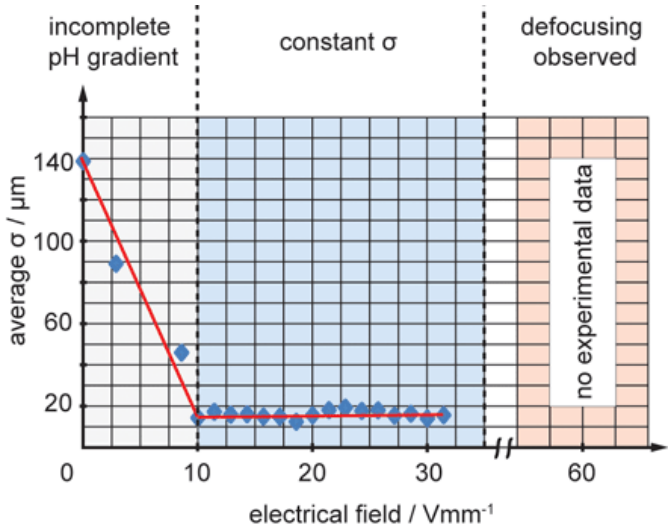


Fig. 4.6 Electrical field increase during FFIEF and average σ of 7 IEF markers ($\Phi_{sample}$ = 0.4 µL $min^{-1}$, v = 2 $mms^{-1}$) determined. The plot indicates that after an initial phase where an increasing electrical field strength decreases the peak width, the peak width does not decrease further, but tends to reach a constant value.

#### 4.4.2.3 Joule Heating

An analytical Joule heating model for electrophoresis in rectangular channels, which is a good approximation to our FFIEF chip, was applied by Cifuentes et al. [91]. Considering that the temperature gradient between the top and the bottom of the flow chamber is negligible because of the 10 µm height of the chamber, the results of Cifuentes et al. can be simplified to

$$T_I = T_m + W_v \left[ \frac{abd}{2(a+b)k_2} \right] \tag{3.3}$$

where $T_I$ is the temperature inside the separation chamber, $T_m$ is the measured temperature at the outside glass wall, a the channel height, b the channel width, d the glass wall thickness, $k_2$ the thermal conductivity of the wall material and $W_v$ the power dissipation per unit volume. $W_v$ can be calculated from the applied voltage times the electrical current divided by the separation chamber volume. In order to obtain values for $T_m$, the chip outside temperature was measured using a thermocouple probe attached to the glass surface. The calculated fluid temperature and also the measured electrical current are shown in Fig. 4.7.

At electrical field strengths below 15 V mm$^{-1}$ a steep linear increase in current can be observed, which corresponds to the decrease in peak width in Fig. 4.6. We explain this rapid increase by the contribution of an increasing sorting of the ampholytes during their residence time in the device. At a flow velocity of 2 mm s$^{-1}$, a residence time of 5 seconds seems insufficient to reach a full separation of the ampholytes and thus a linear pH gradient before E = 15 V mm$^{-1}$ (see also Fig. 4.2.b). Around 15 V mm$^{-1}$ the ampholytes become totally sorted within the residence time of 5 s. Above this field strength the further increase of electrical current with electrical field will only represent the carrier solution conductivity plus a contribution to rectify the position of diffusing ampholytes.

Between 20 and 60 V mm$^{-1}$ the current increases linearly, while the fluid temperature remains stable and equal to room temperature. This region corresponds to the constant peak width ($\sigma_{avg}$) as shown in Fig. 4.6 We can conclude that the device is operational up to electrical field strengths around 60 V mm$^{-1}$ and an electrical current of 70 µA without the influence of Joule heating. Therefore, Joule heating cannot explain the lack of peak width decrease with a increasing electrical field, which was contrary to theoretical predictions.

As shown in Fig. 4.7, electrical fields above 60 V mm$^{-1}$ led to Joule heating. During experiments we observed significant band broadening and eventually defocusing of the sample in this region (see also Fig. 4.8). Both diffusion and fluid viscosity are highly temperature dependent. An increase in diffusion would result in band broadening, as can be seen by eq. (4.1). Furthermore, a decreasing viscosity would increase the electroosmotic flow. Probably the combination of viscosity change and

EOF destabilizes the isoelectric focusing at elevated electrical field strengths. An integrated cooling system as investigated by Albrecht et al. can reduce the influence of Joule heating and might allow the application of electrical fields in this region [37].

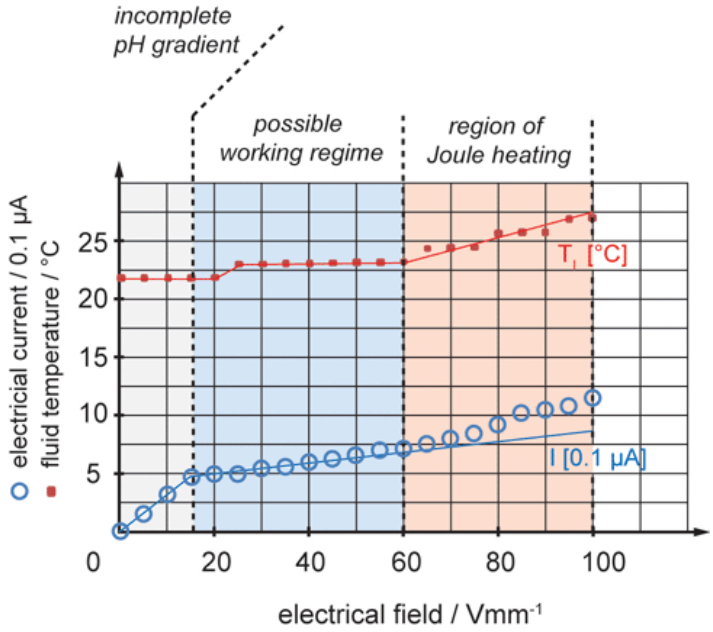


Fig. 4.7 As a function of electrical field three current regions can be distinguished. Joule heating occurs at high field strengths.

#### 4.4.2.4 Electroosmotic Flow

Since Joule heating seems to be negligible below 60 V $mm^{-1}$, it cannot explain the observed lack of peak width decrease. We assume that most likely EOF is hindering a further increase in resolution between 15 and 60 V $mm^{-1}$. Electroosmotic flow is directly proportional to the applied electrical field strength, thus an attempt to improve the resolution by increasing the voltage, increases EOF as well. Although the chip surface has been PVA coated (minimizing zeta potential) and HPMC was added (increasing viscosity) to the solutions, it is uncertain to what extent EOF was suppressed. In closed channel systems, such as in our FFIEF device, electroosmotic flow near the walls will cause a hydrodynamic counter flow in the channel center [16, 92]. This recirculation can obviously cause band broadening. However, it is unclear how the EOF flow profile in case of FFIEF devices will look like, since the zeta potential and therefore the EOF are highly pH dependent. Possibly, regions of high and

low EOF would exist causing localized recirculation effects and heterogeneous band broadening, working against the focusing and limiting the device in terms of resolution. In microfluidic FFE devices the reduced channel height is already advantageous over conventional FFE systems where channel heights of several hundred micrometers are used, since the band broadening caused by EOF is counteracted by lateral diffusion more efficiently. The influence of a parabolic flow profile can be quantified by defining an effective diffusion coefficient $D_T$ which represents the sum of both thermal diffusion and the convective dispersion [93].

$$D_T = D + \frac{u^2 d^2}{210 D} \tag{3.4}$$

where $u^2d^2D^{-1}$ represents the dispersion caused by a pressure driven flow with the velocity u in an indefinite wide channel with the height d. In our situation, this flow will be proportional to the EOF, and thus $u$ can be replaced by $u_{EOF} = \mu_{EOF}E$. Furthermore, replacing the diffusion constant D in eq. (4.1) with the effective diffusion constant $D_T$ from eq. (4.4) results in

$$\sigma_{EOF} = \sqrt{\frac{1}{p}} \sqrt{\frac{D}{E} + \frac{E d^2}{210 D} \mu_{EOF}^2} \ . \tag{3.5}$$

Eq. (4.5) shows the band width dependence on the electrical field when EOF is taken into account. With increasing E, the first summand does decrease σ while the second summand increases σ and compensates for this enhancement. This could explain the stabilized band width observed for electrical field strengths between 20 and 60 $Vmm^{-1}$. Substituting reasonable values for D and $\mu_{EOF}$, indeed hardly any change of σ is predicted from E = 20 and 60 $Vmm^{-1}$. If these considerations are correct, the further suppression of EOF ($\mu_{EOF} \rightarrow 0$) has to be the major issue to overcome current limitations in terms of resolution. Different wall coatings reducing the zeta potential or different chip materials for example could be investigated.

#### 4.4.2.5 System Performance

A way to express the separation quality in IEF systems in terms of system properties is the minimum pI difference required for two species to be separated. It is generally expressed by:

$$\Delta(pI)_{\min} = \frac{d(pH)}{dx} 3\bar{\sigma} \ , \tag{3.6}$$

which assumes a minimum distance between two separated peaks of 3 times σ. Another important characteristic quality parameter is the peak capacity n given by

$$n = \frac{L}{4\bar{\sigma}} \tag{3.7}$$

where L is the total length of the pH gradient [38].

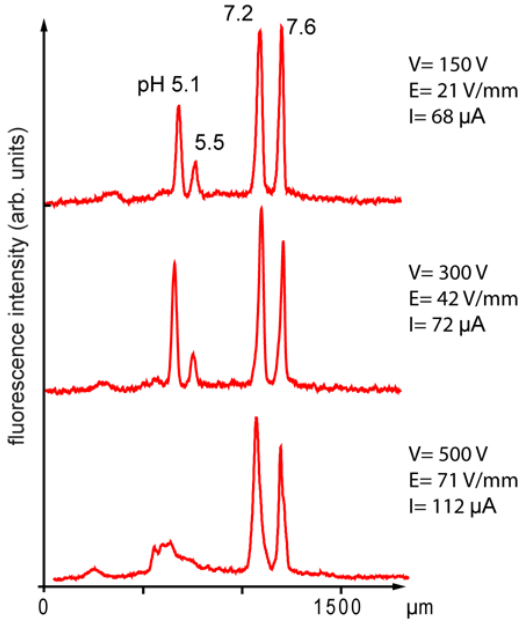


Fig. 4.8 Three electropherograms showing the separation of 4 IEF markers. The device is capable of separating with a minimum pH difference of $\Delta(pH)_{min}$= 0.4. Best separation was achieved with 150 V (21 V mm$^{-1}$). Flow velocity was 2 mm s$^{-1}$ and the residence time $t_R$= 2.5 s. (40 µg mL$^{-1}$ of IEF marker 5.1, 5.5, 7.2 and 7.6)

In order to obtain experimental values for $\Delta(pI)_{min}$ and n, which are typical for analyte separations we separated analytes with small differences in pI, namely four fluorescent IEF markers with pI = 5.1, 5.5, 7.2 and 7.6. The experimental conditions were the same as before, except for the total width of the pH gradient, which was increased from 1.5 mm to 1.8 mm by adjusting the width of the outer sheath flows. The separation results are shown in Fig. 4.8. It can be seen, that all markers were clearly separated and focused. As can be seen in Fig. 4.8, an increase in electrical field strength did not lead to a further improved separation. In contrast, de-focusing was observed at field strengths higher than E ≈ 70 V mm$^{-1}$, which corresponds to the theoretical considerations discussed before. Applying eq. 6 and 7 we calculated (pH

2.5 – 11.5 and L = 1800 µm) a minimum pI value $\Delta(pI)_{min}$ = 0.23 and a theoretical peak capacity of n = 29 peaks. In our previous device [34] we were only able to reach a peak capacity of 7 peaks and a minimum $\Delta(pI)_{min}$ = 0.7, indicating that the present device represents an important improvement. In terms of focusing, we furthermore reached a 20 fold increase in sample concentration. Rough comparisons between the FFIEF results published by Albrecht et al. [37] and our achievements indicate an 8 fold increase in peak capacity, a 4.3 fold decrease in minimum ΔpI and a 2.6 fold reduction of the applied voltage in our device. To be fair it must be realized, however, that Albrecht et al. optimized their device with respect to a higher throughput. Furthermore, comparisons should be considered with care, since many parameters have to be taken into account. In FFIEF devices the flow rate and related to that the residence time are important parameters as well. As shown by Fonslow et al. using a µ-FFE system, flow rate, electric field, and migration distance must all be considered in free flow systems to optimize bandwidth and resolution [35]. Here we investigated only the influence of the electrical field on the performance with a fixed flow-rate, since in our device, especially the stability of the acrylamide membranes turned out to be the limiting factor in terms of flow rates. Velocities higher than approximately 4 mm $s^{-1}$ caused breakage of the membranes often within minutes. Therefore, all experiments were carried out with a constant velocity of 2 mm $s^{-1}$.

To investigate the benefit of pre-separating the ampholytes by introducing them in different inlets an additional experiment was performed. The ampholytes Prolytes 1, 2 and 3 were mixed so that no stepped pH gradient was applied. Experimental results confirmed that in this case with an electrical field strength of 20 V $mm^{-1}$ no separation was achieved within the present separation chamber length (data not shown here). Even when increasing the separation voltage and electrical field, a complete separation was not observed. This indicates the advantage of using pre-separated ampholytes over common non-separated ampholytes in microfluidic FFIEF systems, since it leads to faster separation times and therefore better resolution also observed in large scale conventional FFIEF systems[18].

### 4.4.3 FFIEF of Human Serum Albumin

The separation of low MW IEF markers, as demonstrated, is a practicable model system. However for clinical analysis one would like to know about protein separation. Often described in literature is a decreased separation resolution of

fluorescently labeled proteins due to heterogeneous labeling. Recently, a new type of fluorescent label has been introduced which is not altering the native charge of the protein and thus minimizes band broadening [94]. We decided to investigate these labels in our system. We chose human serum albumin (HSA, pI ≈ 4.8, MW 67 kDA) as a test protein. According to eq. (4.1), one would expect that proteins which have a higher MW than the low MW IEF markers (estimated MW ≈ 500), and therefore a lower diffusion coefficient, which would result in better separation resolution and sharper peaks. This was indeed confirmed in an experiment using two fluorescent pI markers, pH = 4 and 9 and the protein HSA. The results are shown in Fig. 4.9. All components were fully separated (Fig. 4.9a) and as expected a narrower HSA peak was observed (Fig. 4.9b). The width of the HSA peak (full width half maximum) is approximately 2 times smaller than of the IEF markers. Using the two markers as a reference, the derived pI value for HSA is 4.4 which is acceptable.

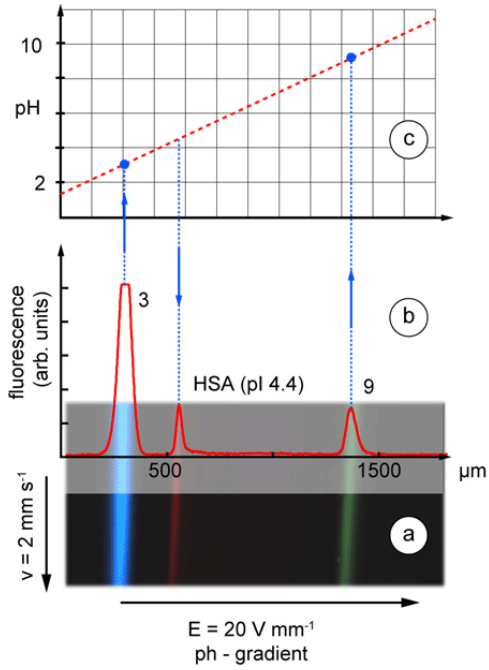


Fig. 4.9 FFIEF of two fluorescent IEF markers (pI = 3 and 9) and HSA. The focusing of the low molecular weight standards results in wider bands compared to HSA. HSA focused at pH 4.4. Concentrations were: 330 µg $mL^{-1}$ HSA, 80 µg $mL^{-1}$ of IEF markers pH 3 und 9. The focusing residence time was 2.5 s.

## 4.5 Conclusions

Microfluidic free-flow isoelectric focusing was successfully demonstrated using a glass chip in which pre-separated ampholytes were infused into a 350 nl separation chamber, which resulted in a more efficient generation of a linear wide range pH gradient in terms of electrical current and formation time, than without preseparation. This method led to a highly improved separation resolution. We determined, that the device is capable of separating analytes with a minimum difference in isoelectric point of Δ(pH) = 0.23. This results in a theoretical peak capacity of 29 peaks within 1.8 mm for a pH gradient pH 2.5 – 11.5. Furthermore, linearity of the pH gradient was demonstrated by the separation of 7 IEF markers ranging from pI 4 to 10. All components were separated transverse to the carrier flow within 1.2 millimeters, and complete focusing (20 fold concentration increase) was realized in only 2.5 seconds. From theoretical considerations and experimental results, we concluded that band broadening caused by EOF and eventually Joule heating probably limits the separation resolution at elevated electrical field strengths. Further minimizing the EOF and integrating a cooling system might therefore lead to still higher resolution. The device was also used to focus HSA showing that with high MW molecules even narrower peaks can be realized. The resolution achieved was superior to all microfluidic FFIEF chips until now. This device might be applicable in clinical analysis as a pre analytical fractioning method, when only low sample volumes are available and fast separation times are necessary.

# 5 Bubble-Free FFE Chip with Integrated Platinum Electrodes

*Although the implementation and usage of permeable membranes, as described in previous chapters, turned out to be an efficient and reliable method in FFE chips, alternative ideas were investigated. Instead of integrated membranes electrodes were placed inside the separation region and electrolysis was suppressed chemically. The results of this investigation were published in Analytical Chemistry in 2008.*

## 5.1 Abstract

In order to ensure a stable and efficient separation in microfluidic free-flow electrophoresis (FFE) devices various methods and chips have been presented until now. A major concern hereby is the generation of gas bubbles caused by electrolysis and the resulting disturbances in the position of the separated analyte lanes. Instable lane positions would lead to a decreased resolution in sample collection over time which certainly would be problematic when incorporating a stationary detector system. In contrast to our previous publications, in which we implemented laborious semi-permeable membranes to keep bubbles outside the separation region, here we describe an electrochemical approach to suppress the electrolysis of water molecules and therefore bubble formation. This approach allowed a simpler and additionally a closed chip device with integrated platinum electrodes. Using this chip the successful separation of three fluorescent compounds was demonstrated. Quinhydrone, which is a complex of hydroquinone and p-benzoquinone, was added only to the local flow streams along the electrodes, preventing mixing with the separation media and sample. The electrical current was generated via the oxidization and reduction of hydroquinone and p-benzoquinone up to a certain limit of the electrical current without gas formation. The separation stability was investigated for the chip with and without quinhydrone, and the results clearly indicated the improvement. In contrast to the device operating without quinhydrone, a 2.5 fold increase in resolution was

achieved. Furthermore, separation was demonstrated within tens of milliseconds. This chemical approach with its high miniaturization possibilities offers an interesting alternative, in particular for at low electrical current operating miniaturized FFE systems, in which large and open electrode reservoirs are not tolerable.

## 5.2 Introduction

Free-flow electrophoresis (FFE) is the continuous separation of charged analytes injected into a thin carrier medium flowing between two insulating plates with an electrical field applied perpendicular to the flow direction. Components with different electrophoretic mobility are deflected under different angles and are separated into various lanes which can be collected at the device outlet [16]. This separation method has found a permanent position in preparative methods in biochemistry and chemistry for the separation of e.g. cells, organelles, peptides, proteins, and inorganic and organic compounds. Mostly large scale preparative purpose systems have been developed and applied [15, 17, 27]. However, a steadily increasing number of publications on miniaturized FFE have shown that micro-FFE allows for high separation resolution with fewer problems, such as Joule heating, compared with their larger counterparts [34-37, 45, 46, 54, 60]. A known problem in FFE is the gas bubble generation at the electrodes due to electrolysis of water which might lead to a distorted separation or loss of the separation voltage. Several approaches have been presented to solve this problem. When bubbles are allowed to form, several technological approaches have been applied in µ-FFE devices to eliminate their influence, e.g. by introducing semi-permeable membranes or arrays of bubble-blocking micro channels between the electrode regions and the separation area. A device with integrated electrodes, as presented in this chapter, was applied by Lu et al. [52]. They demonstrated a free-flow electrophoresis chip with integrated gold electrodes. In particular they showed free-flow isoelectric focusing and to avoid bubble formation the applied voltage was below the electrolysis potential. However, due to the low electrical field strength this device could be used only for relatively large compounds and also separation times of several minutes were necessary. For more references and further details the reader is referred to the review on miniaturized free-flow electrophoresis devices by Kohlheyer et al. [95] or chapter 2 of this thesis. For a more broad overview of continuous flow microfluidic separation techniques in general the reader is referred to the recent review by Pamme [25]. In

the paper presented here, a new approach is demonstrated to overcome the problem of electrolysis in microfluidic free-flow electrophoresis chips. In this approach the generation of oxygen and hydrogen bubbles was suppressed by adding a redox-couple to the electrolyte flowing along the electrodes. As a first demonstration quinhydrone (QH), which is complex between hydroquinone ($H_2Q$) acting as an electron donor and p-benzoquinone (Q) acting as an electron acceptor, was added to the flow streams at the anode and the cathode. QH is known for its application in pH sensor and related devices [96]. Instead of water oxidation and reduction, generating oxygen and hydrogen, now $H_2Q$ is oxidized and Q reduced without the generation of bubbles. Although this method is only applicable with low electrical current densities due to the depletion of QH, it was successfully demonstrated with fluorescent components separated in free-flow zone electrophoresis, as described here. This approach allows for a simple chip design, where the electrodes can be located directly inside the separation chamber without the need for separating structures or membranes. Although the chip design was simplified, the setup was slightly more complex since additional sheath flows were used to isolate the redox species from the analyte solution as described in the following section in more detail.

### 5.2.1 Principle

The layout and device configuration is shown in Fig. 5.1. The device has five inlets, which are connected via capillaries to a set of syringe pumps, to allow multiple adjacent flows with different chemical composition and flow rate. Inlets 5 and 6 (see Fig. 5.1) are used for the anodic and cathodic electrolyte flow. Only these streams contain the redox-couple QH. The sample solution is introduced via inlet 8 and is hydrodynamically focused by two parallel sheath flow streams (inlets 7 and 9). Due to this stream configuration the sample stream is shielded from the QH containing electrolytes. Since QH is electrically neutral, cross contamination between the streams is based on diffusion only. Five outlets (18) can be used to collect the separated fractions. The number of outlets does not correlate with the number of analyte fractions and was just chosen for practical reasons to allow a simple chip design.

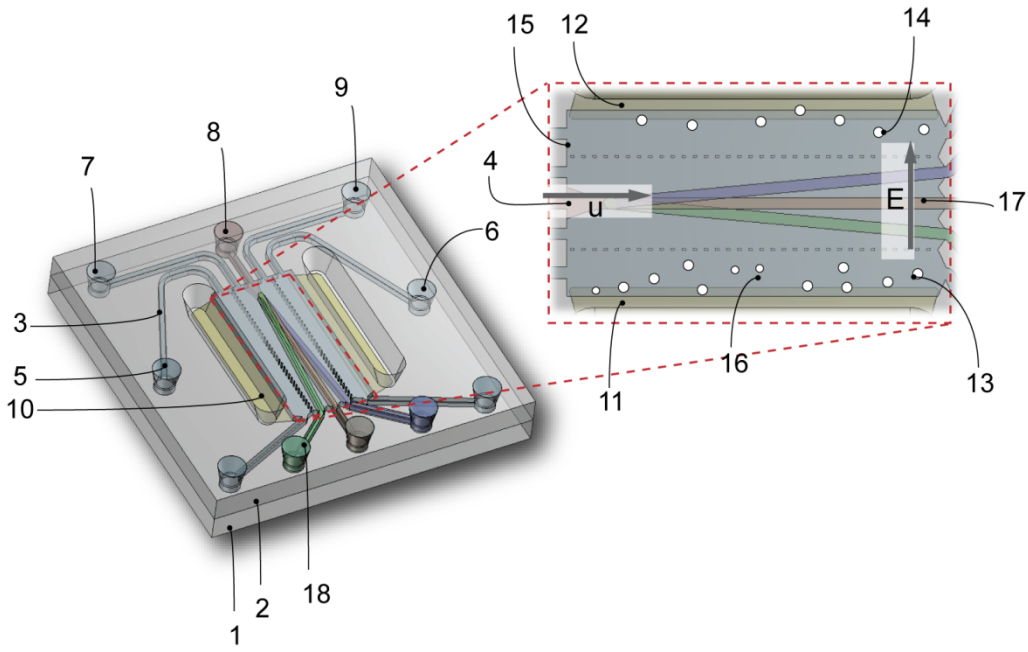


Fig. 5.1 Schematic illustration of the microfluidic free-flow electrophoresis chip with integrated platinum electrodes. Oxygen and hydrogen bubbles generated at the electrodes disturb the separation and flow pattern. Bubble generation can be suppressed by adding adequate chemical substitutes. (1, bottom chip plate; 2, top chip plate; 3, inlet channel; 4, hydrodynamicly focused sample stream; 5, inlet for anodic electrolyte; 6, inlet for cathodic electrolyte; 7,9, inlets for carrier electrolyte sheath flows; 8, sample inlet; 10, electrode contact pad; 11, anode; 12, cathode; 13, oxygen bubble; 14, hydrogen bubble; 15, cathodic electrolyte stream; 16, anodic electrolyte stream; 17, separated component;). The entire separation and electrode area has a depth of 10 μm. To distinguish between the electrode electrolyte regions and the separation chamber, and to allow easy chip alignment during microscopy, two rows of micropillars were implemented into the design. These pillars do not disturb or influence the device performance.

## 5.3 Experimental

### 5.3.1 Materials and Reagents

If not otherwise stated, all chemicals were obtained from Sigma-Aldrich-Fluka. Solutions were degassed in vacuum prior to application. The carrier medium solution contained 10 mM Hepes (adjusted with 2 M NaOH to pH 7), 0.1% Tween 20 and 0.1% HPMC (chip inlets 7 and 9, see Fig. 5.1), and was used for the hydrodynamic focusing.

All other solutions were of this basic composition plus additional compounds as described in the following. The sample solution contained 0.5 mg $mL^{-1}$ fluorescein, 0.5 mg $mL^{-1}$ rhodamine B and 0.5 mg $mL^{-1}$ rhodamine 6G (in total 1.5 mg $mL^{-1}$) (chip inlet 8). A sample solution without rhodamine 6G was prepared additionally (chip inlet 8). Furthermore, two solutions of 18 mM p-benzoquinone and 18 mM hydroquinone respectively were prepared (chip inlets 5 and 6). Since the QH complex degrades within hours, the two components were prepared and mixed in a 1:1 ratio just before the experiments.

### 5.3.2 Chip Fabrication

Each chip consists of two thermally bonded Borofloat 33 glass plates (Schott Jenaer Glas, Germany); the top plate contains the channels, separation chamber, fluidic inlets and outlets and the electrode openings, while the bottom plate contains the patterned platinum electrodes. On the top plate hydrofluoric acid was used to etch the channels and separation chamber while a chromium-gold layer protected the regions not to be etched. The etch depth was 10 µm. A powder blasting step was performed with 30 µm in diameter $Al_2O_3$ particles to create the inlet and outlet holes, as well as the electrode openings [97]. A photolithography step was carried out to transfer the pattern of the electrodes onto the surface of the bottom plate. The glass was exposed for 10 min to a BHF etch to obtain a recess of 200 nm depth at the areas where the platinum would be deposited. Subsequently a 10 nm chromium adhesion layer was sputtered on top of the wafer followed by a 190 nm platinum layer [98]. A lift-off in acetone was performed, leaving the surface of the platinum electrodes level with the surface of the glass plate, so that no steps were present on the surface. This allowed direct wafer bonding to the top plate. The top and bottom glass plates were aligned by stereomicroscope and thermally bonded at 600 °C for 1 hour, whereas heating-up and cooling down was carried out over 12 hours in total to avoid internal material stress. The bonded plates were finally diced into several microfluidic chips. For electrical connection two wires were soldered to the platinum connections pads, with the final chip shown in Fig. 5.2.

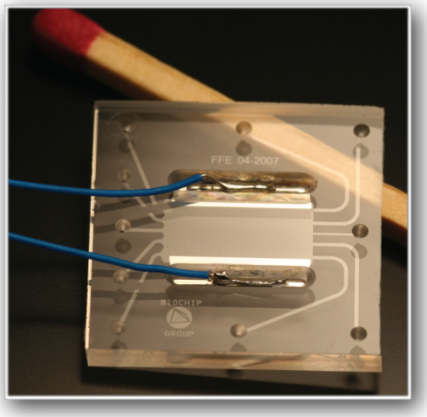


Fig. 5.2 Photograph of the microfabricated glass free-flow electrophoresis chip with integrated platinum electrodes and soldered electrical connections. The chip size is 20 mm x 20 mm with a thickness of 2.2 mm. (separation chamber: L x W x H: 10 mm x 6 mm x 10 µm, volume = 600 nl).

### 5.3.3 Experimental Setup and Methods

The fabricated chips were placed in an in-house fabricated plastic holder, similar to the holder used in chapter 3. Syringe pumps (CMA/102, Microdialysis, Sweden) were used to control the flow rates. 1 mL glass syringes (Microdialysis, Sweden) were filled with the required solutions and connected via glass capillaries (Aurora, The Netherlands) and Nanoport connectors (Upchurch Scientific, USA) to the in-house fabricated chip holder. The two integrated platinum electrodes were connected to a power supply (Labsmith, USA). Power supply and syringe pumps were controlled in real-time with a personal computer and Labview software (National Instruments). The holder was placed on an inverted microscope (Olympus IX51) equipped with mercury burner and fluorescent filter set (XF57, Omega Optical, USA) for fluorescence detection. Images were captured with the digital color camera ColorViewII (Olympus) and recorded with the software package AnalySIS 5 (Olympus). Intensity profiles were further analyzed using Origin (Microcal Software) to determine peak positions and standard deviations.

## 5.4 Results and Discussion

### 5.4.1 Bubble Free FFZE

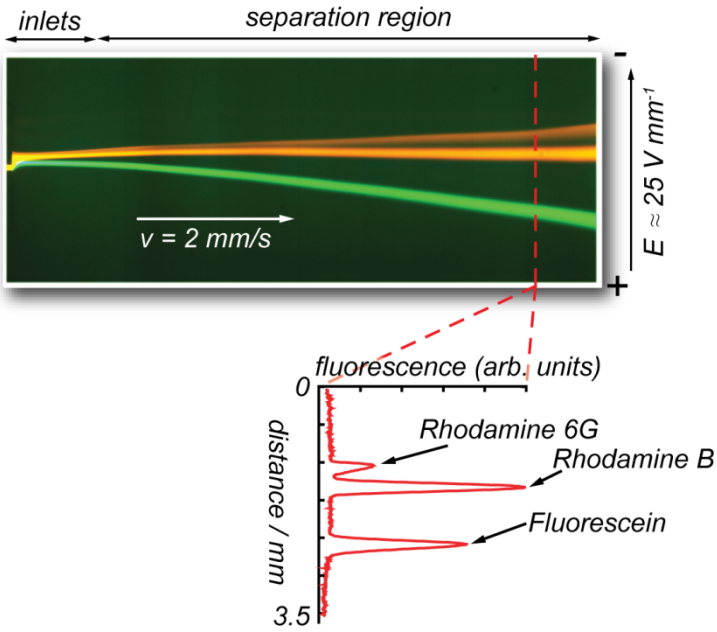


Fig. 5.3 Image showing free-flow zone electrophoresis of three fluorescent dyes. An intensity profile was generated to demonstrate separation performance. Here, the suppression of oxygen and hydrogen bubbles enabled a stable non distorted continuous separation. (Image contrast and colors were enhanced for better visualization)

The three fluorescent dyes namely fluorescein, rhodamine B and rhodamine 6G were chosen as a set of model components to demonstrate bubble-free FFZE using QH as redox couple. As shown in Fig. 5.3, all three components clearly separated and followed diverging lanes at an overall flow velocity of 2 mm $s^{-1}$, an applied voltage of 300 V (resulting in an app. electrical field of E ≈ 15 V $mm^{-1}$ across the separation region) and an average electrical current of I ≈ 20 µA. At pH 7 rhodamine B is neutral [99] and as expected showed no deflection, while fluorescein (charge -2) moved towards the anode and rhodamine 6G (charge +1) [99] was deflected towards the cathode. The deflection *d* in free-flow zone electrophoresis is be described by

$$d = \mu_p E t \tag{5.1}$$

where $\mu_p$ is the apparent electrophoretic mobility, $E$ is the electrical field strength and $t$ is the residence time of molecules in the separation chamber [33]. At a residence time of $t_r$ = 4 s, the lateral deflection of fluorescein was app. $d_{fluorescein} \approx$ -1 mm, and the deflection of rhodamine 6G app. $d_{rhodamine6G} \approx$ +0.4 mm.

### 5.4.2 Quinhydrone Redox-Couple

Although the position of the separated lanes was not fully stable, as discussed later, no gas bubbles appeared and distorted the separation. In the experiment shown in Fig. 5.3 and described above, a solution of 18 mM QH was used as electrolyte flowing along the electrodes. With a resulting electrical current of app. 20 µA, instead of electrolysis of water molecules at the electrodes, hydroquinone was undergoing oxidization (loosing electrons at the anode) and p-benzoquinone reduction (gaining electrons at the cathode) to enable electrical current flow. QH gets oxidized and reduced at lower potential than water molecules, and without gas formation. The QH electrode reactions are given by [96]:

anodic reaction

$$C_6H_4O_2H_2 \rightarrow C_6H_4O_2 + 2H^+ (aq) + 2e^- \quad (5.2)$$

and cathodic reaction

$$C_6H_4O_2 + 2H_2O + 2e^- \rightarrow C_6H_4O_2H_2 + 2OH^- \quad (5.3)$$

The addition of QH enabled a stable separation of the three components which would not be possible without. However, the transport of electrons via the oxidization and reduction of the redox active molecules hydroquinone and p-benzoquinone molecules is limited by their efficient mass transport towards the electrodes [100]. Since the QH complex is electrically neutral, the actual concentration of the redox-couple near the electrodes is dependent on the consumption, caused by oxidization and reduction, and diffusion away from the electrodes. The diffusion distance x defined by

$$x = \sqrt{2Dt} \quad (5.4)$$

and assuming a diffusion constant of hydroquinone of D = $1 \cdot 10^{-9}$ $m^2$ $s^{-1}$ and a maximum residence time inside the separation chamber of t = 5 s, the diffusion distance will be approximately 100 µm [101]. Since the diffusion distance is much larger than the electrode compartment height (10 µm) a uniform concentration can be

assumed above the electrodes. With an applied electrolyte-fluid stream width (containing the redox-couple) along the electrodes of 1 mm, covering the entire electrode surface (w = 500 µm, L = 10 mm) plus 500 µm additionally next to the electrode, it is clear that depletion of QH due to lateral diffusion can be excluded as the limiting factor. However, with an increasing electrical current the surface concentration of QH at the electrodes downstream in the electrode compartment will decrease and eventually becomes zero, and $H_2O$ molecules will started to be oxidized and reduced in addition to enable the higher electrical current to flow. This of course will lead to gas formation again. Here we observed this effect with an electrical current between 30 and 40 µA.

In the following section it is investigated if the current limitation was governed by the depletion of QH molecules near the electrodes. According to Faraday's law of electrolysis the amount of electrical charges transported is proportional to the amount of molecules produced at the electrodes. In our situation this would be e.g. the amount of hydroquinone oxidized by losing two electrons at the anode. The amount of molecules n consumed is given by

$$n = \frac{It}{zF} \tag{5.5}$$

where $I$ is the electrical current over a time period $t$, $z$ the number of electrons transferred per produced molecule and $F$ = 96485 C the Faraday constant [102]. With eq. (5.5) and an electrical current of app. $I_{max}$ = 40 µA, a total residence time of $t$ = 5 s (flow velocity $v$ = 2 mm $s^{-1}$) and $z$ = 2 (see eq. (5.2) and (5.3)) one can derive $n_{con\_5s}$ = $10.4 \cdot 10^{-10}$ mol. The concentration of the QH solution was 18 mM of hydroquinone and 18 mM p-benzoquinone. Assuming a flow-rate of the QH solution above the electrode of φ = 0.01 µL $s^{-1}$ a total fluid volume of V = 0.05 µL passes the electrode within the residence time of t = 5 s. This volume contains app. $n_{avaliable\_5s}$ = $9 \cdot 10^{-10}$ mol of hydroquinone and p-benzoquinone respectively. From these calculations it is obvious that if the amount of molecules required to transport a specific electrical current exceeds the present amount of redox molecules, water molecules are oxidized and reduced instead. Occurring bubbles were observed first near the end of the electrode which makes sense considering the above considerations, since the outlet is the most redox-couple depleted region. To increase the maximum current, consequently the concentration of QH was increased. However, filming and deposition of material was observed at the electrodes and surroundings. At lower QH concentrations, e.g. c(QH) =

18 mM no significant filming could be observed, even after several hours of experimental work. The given calculations though reflecting only a simplified system, can suggest possible beneficial alterations to the system. It seems plausible that in order to improve the maximum current (and hence the maximum applicable separation voltage) an increase of the electrode surface area which is in contact with the electrolyte and the required redox-couple would be beneficial. For the approach presented here, no detailed investigations on the electrical current density were performed.

### 5.4.3 Electrolysis of Water

Without QH added to the electrolyte solutions, electrolysis and gas bubble formation was observed when the electrical current exceeded app. I = 15 µA. It is assumed, that electrolysis still occurred below that value, but that the gas formed at the electrodes remained dissolved in the solution. Bubbles that appeared inside the outlet channels millimeters downstream of the electrodes at lower electrical currents support this assumption, as presumably the water became saturated with oxygen and hydrogen inside the smaller outlet channels. Gas formation was first observed at the cathode (hydrogen) and at higher electrical currents also at the anode (oxygen).

Fig. 5.4 visualizes the problem caused by bubble generation during FFE. Fig. 5.4.a shows the absence of bubbles at the cathode during the experiments with QH, and Fig. 5.4.b the appearance of hydrogen bubbles at the cathode in the absence of QH. These bubbles can significantly influence the separation since they deform the local laminar flow lines. This effect is shown in the disturbance of the lanes of fluorescein and rhodamine B in Fig. 5.4.c due to a bubble formed. Obviously this can disturb the lane pattern and would reduce the separation resolution over time, e.g., when collecting fractions or monitoring fractions with a stationary detector. Therefore, this influence is further analyzed in the following section.

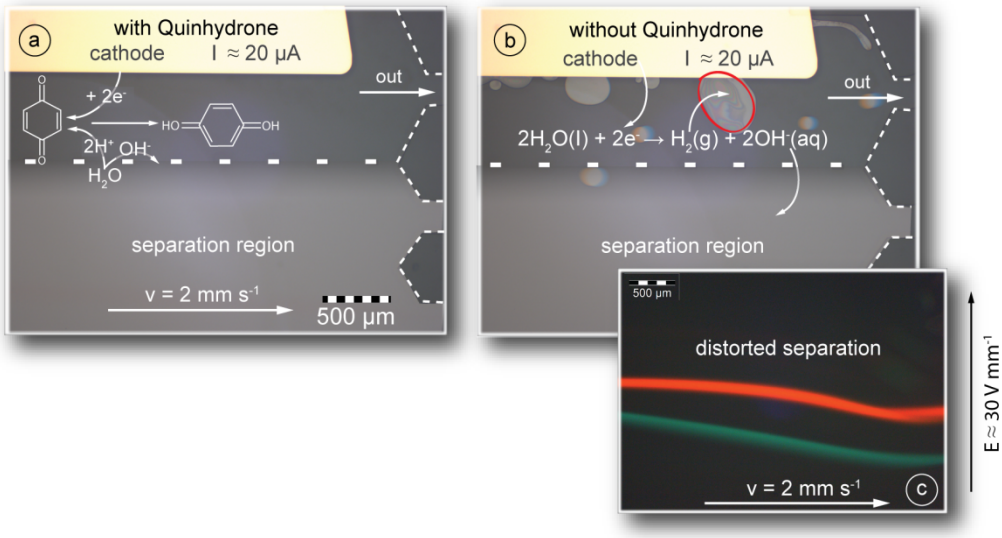


Fig. 5.4 (a) Microscopic photograph showing the cathode during free-flow electrophoresis operations. The quinhydrone complex present in the electrolyte flowing along the cathode (and anode, not shown here) allows for bubble free separations up to a certain electrical current. (b) When no QH is present, water molecules undergo electrolysis generating hydrogen gas bubbles at the cathode and therefore (c) disturbing the flow and separation (here separation of fluorescein and rhodamine B). For a clear visibility, the channel outlines are indicated by dotted lines and the separation region is slightly brightened.

### 5.4.4 Quantitative Bubble Influence

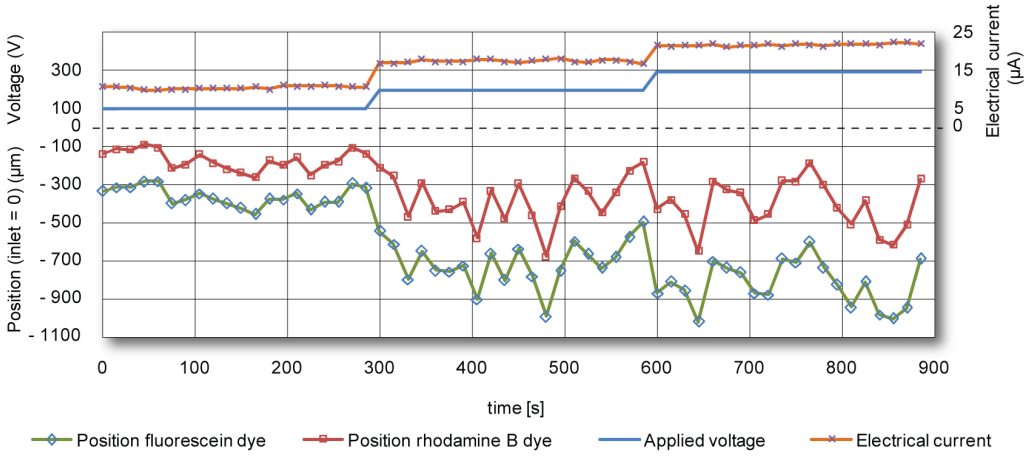


Fig. 5.5 Diagram showing the lane position measured after a residence time of 2 seconds in the separation chamber in the absence of QH. Images were taken every 15 seconds and peak center positions derived of the two separated components (fluorescein and rhodamine B) over a total measurement period of 15 minutes. The voltage was increased from 100 V to 200 V and to 300 V after 5 minutes respectively. The position of the lanes was measured relatively to the sample inlet (position = 0 um).The lane positions are strongly influenced by the gas bubbles generated at the electrodes.

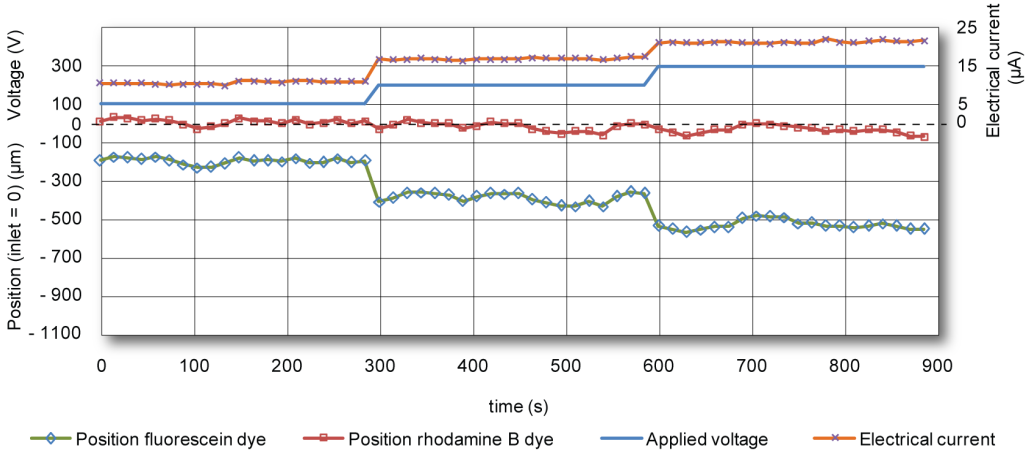


Fig. 5.6 Diagram showing the lane position measured after a residence time of 2 seconds in the separation chamber in the presence of QH. Since no gas bubbles were formed at the electrodes, the effect of QH on the separation quality is clearly evident. The remaining lane fluctuations were caused by the used pumping equipment. See Fig. 5.5 for more details

The influence of the formation of electrolytic gas bubbles on the separation performance was investigated in more detail, particularly the impact on the separation resolution.

Two experiments were set up, one with rhodamine B and fluorescein as tracing compounds: First without the redox-couple and second with QH added to the electrolyte. During separation microscopic images of the separated lanes of fluorescent dyes were taken and analyzed to determine the time dependent lane positions. For this, the lane center positions of the separated dyes after a residence time of $t_r$ = 2 s in the separation chamber were determined every 15 second over a period of 15 minutes. The voltage was set to 100 V and in five minute intervals increased to 200 V and 300 V. The results obtained are shown in Fig. 5.5 and Fig. 5.6 and further details given in Tab. 5.1. The positions were measured relatively to the sample inlet which is therefore x = 0 µm. Deflections towards the anode were defined as negative, to allow an easier illustration. When it is referred to specific values in Tab. 5.1, in order to guide the reader, corresponding lanes and columns are indicated in brackets.

When no QH was present, as shown in Fig. 5.5, both components fully separated. However, it is in evident that the lane positions were significantly influenced resulting in displacements as large as 500 µm, which is more than 5 times higher than the width of that lane. Furthermore, it can be seen that despite the short fluctuations, both lanes (including that of the neutral dye rhodamine B) were deflected towards the anode. From observations we concluded, that a certain amount of bubbles that remained attached to the electrodes led to a stagnant lane deflection (here between app. 150 and 400 µm derived from the electrically neutral dye rhodamine B, see Tab. 5.1 (6, a-c)). Since more hydrogen gas was formed during electrolysis than oxygen gas, most of the influence was caused by cathodic hydrogen bubbles leading here to a negative deflection. Bubbles at the anode did not tend to stick to the metal electrode and were of smaller size (up to app. 10 fold smaller). This stagnant lane deflection might explain the slightly reduced separation distance in contrast to the results obtained with QH, see Tab. 5.1 (7, a-f)). The stagnant layer of hydrogen bubbles furthermore led to an increased linear flow velocity thereby reducing the sample residence time and the migration distance (see eq. (5.1)). In addition to the stagnant distortion, bubbles released from the electrodes caused short term fluctuations of the lane positions, which can be quantified by their standard deviations given in Tab. 5.1 (8-10, a-c)).

These standard deviations were in the order of the lane widths Tab. 5.1 (11-12, a-c)) and higher. A common method to describe the separation efficiency for electrophoretic separation systems is the resolution *R* defined by

$$R = \frac{d_1 - d_2}{2(\sigma_{w1} + \sigma_{w2})} \tag{5.6}$$

where $d_1$ and $d_2$ are the center position of two adjacent peaks and $\sigma_{w1}$ and $\sigma_{w2}$ are the corresponding standard deviations of the peak widths which here correlate to the lane widths. Except for minor variances (see Tab. 5.1 (9-10, a-f)), both streams, fluorescein and rhodamine B, were equally displaced by appearing bubbles so that at a single moment in time the resolution was not affected, as shown in Tab. 5.1 (15, a-f). When signals or fractions would be collected over longer periods, however, resolution (as defined by eq. (5.6)) would be greatly compromised. This can be quantified with the total standard deviation $\sigma_{total}$, including the lane width standard deviation $\sigma_w$ and the standard deviation caused by the fluctuations $\sigma_p$. Adding the variances we obtain

$$\sigma_{total} = \sqrt{\sigma_w^2 + \sigma_p^2} \ . \tag{5.7}$$

At 100 V the derived resolution $Rs_{5min\_100V}$ for a sampling time of 5 minutes, indeed was app. 1.4 fold lower than $Rs_{\_100V}$ for a single moment in time (Tab. 5.1 (15-16, a)). With the application of 300 V the fluctuations increased significantly resulting in a 2.4 fold decrease in resolution over 5 minutes (Tab. 5.1 (15-16, c)). One can conclude that for practical separations and applications where e.g. a dense array of outlet channels is used to obtain pure fractions, such fluctuations in the order of the lane width and higher are not acceptable. It has to be pointed out, that fluctuations on shorter timescales than 15 seconds were not recorded. Since a certain number of bubbles moved with the applied flow velocity of app. 2 mm $s^{-1}$ spending less than 5 seconds in the detection window, the achieved results give only an indication of the low frequency fluctuations and the actual variations can still be worse.

| | | | | a | b | c | d | e | f |
|---|---|---|---|---|---|---|---|---|---|
| | | variable | unit | no QH | | | with QH | | |
| 1 | applied voltage | **U** | **V** | **100** | **200** | **300** | **100** | **200** | **300** |
| 2 | ø current | **I** | **µA** | 10.70 | 17.68 | 22.02 | 10.63 | 16.86 | 21.24 |
| 3 | E-field utilized for separation | **E** | **V mm$^{-1}$** | 7,54 | 12,45 | 15,51 | 7,49 | 11,87 | 14,96 |
| 4 | mobility of fluorescein | **$\mu_f$** | **cm$^2$ (Vs)$^{-1}$** | $1.42^{\pm0.1}\cdot10^{-4}$ | | | | | |
| 5 | fluorescein mean lane position | **$d_f$** | **µm** | -360 | -707 | -824 | -196 | -389 | -530 |
| 6 | rhodamine B mean lane position | **$d_r$** | **µm** | -168 | -375 | -407 | 9 | -17 | -35 |
| 7 | mean separation distance ($x_r - x_f$) | **$d_{rf}$** | **µm** | **192** | **332** | **417** | **205** | **372** | **495** |
| 8 | separation distance stdev. deviation | **$\sigma_{xrf}$** | **µm** | 9 | 16 | 20 | 4 | 8 | 10 |
| 9 | fluorescein stdev. lane position | **$\sigma_{pf}$** | **µm** | 51 | 121 | 119 | 17 | 26 | 24 |
| 10 | rhodamine B stdev. lane position | **$\sigma_{pr}$** | **µm** | 52 | 128 | 128 | 16 | 22 | 20 |
| 11 | fluorescein stdev. lane width | **$\sigma_{wf}$** | **µm** | 51 | 54 | 62 | 57 | 63 | 66 |
| 12 | rhodamine B stdev. lane width | **$\sigma_{wr}$** | **µm** | 50 | 48 | 52 | 55 | 54 | 55 |
| 13 | fluorescein total stdev. | **$\sigma_{pwf}$** | **µm** | 72 | 132 | 134 | 60 | 68 | 70 |
| 14 | rhodamine B total stdev. (eq. (5.7)) | **$\sigma_{pwr}$** | **µm** | 72 | 137 | 138 | 57 | 58 | 59 |
| 15 | resolution single moment | **Rs** | **-** | **$0,95^{\pm0.05}$** | **$1,63^{\pm0.08}$** | **$1,83^{\pm0.09}$** | **$0,92^{\pm0.02}$** | **$1,60^{\pm0.03}$** | **$2,05^{\pm0.04}$** |
| 16 | separation resolution over 5 min | **$Rs_{5min}$** | **-** | **$0,67^{\pm0.22}$** | **$0,62^{\pm0.22}$** | **$0,77^{\pm0.22}$** | **$0,88^{\pm0.07}$** | **$1,48^{\pm0.1}$** | **$1,92^{\pm0.09}$** |

Tab. 5.1 Separation pattern of fluorescein and rhodamine B analyzed over 15 minutes with and without QH. The measurements were obtained after a residence time of tr = 2 s. See chapter 3.5 for explanation

When QH was added to the electrolyte with the results shown in Fig. 5.6, it was observed that the fluctuations were significantly reduced and that no bubbles where observed. The standard deviations of the lane center positions were roughly half of the values compared to those determined without bubble suppression at 100V and app. 6 fold lower at 200V and 300V, as shown in Tab. 5.1 (9-10, d-f). The remaining variance of lane position was most likely caused by the used syringe pumps, since especially the pump for the sample solution was running with at the lower flow-rate limit for this pump (app. $\varphi$ = 0.1 µL $min^{-1}$). This assumption is supported by the fact that fluctuations seemed less independent on the applied voltage (Tab. 5.1 (9-10, d-f)). It is thus concluded, that this remaining source of variance can be reduced by using syringes with a smaller volume size and consequently allowing an increased piston speed. However, also the equipment-related lane fluctuations slightly influenced the resolution (see Tab. 5.1 (15-16, d-f)).

As discussed, the positive effect of QH on the separation quality is in evidence. The separation resolution over a measurement period of 5 minutes for the bubble-free FFE operation was 2.5 fold higher in comparison with the device operating without QH (Tab. 5.1 (16c;16f)).

### 5.4.5 Limitations and Possibilities

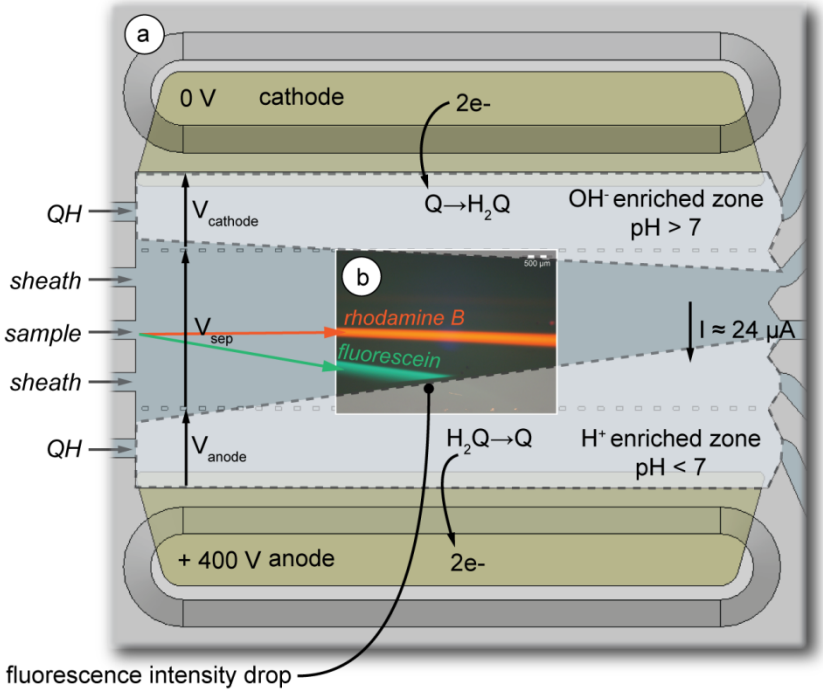


Fig. 5.7 (a) Top view illustration of the separation chamber with electrodes with inset (b) microscopic photograph (enhanced contrast) showing the separation of rhodamine B and fluorescein when Vtotal = 400 V were applied. Fluorescein migrated into the H+ enriched acidic zone which caused a sudden decrease in the fluorescence emission intensity.

An important aspect to be mentioned is the variation in pH value of the carrier medium near the electrodes. As shown by the reaction eqs. (5.2) and (5.3), QH oxidation and reduction just like water electrolysis involves the production or consumption of one proton per electron. In other FFE systems electrodes are placed in regions with higher volume flow rates and larger volumes and may be strongly pH buffered to ensure stable pH values. However, in the simple chip described here the volume of the electrode flow compartments is in the order of tens of nanoliters and consequently slight variations in the number of $H^+$ or $OH^-$ ions lead to rapid pH changes. Furthermore, due to the applied electrical field these ions migrate towards the cathode and anode respectively in addition to diffusion. The consequences of this process were observed when the fluorescein lane was deflected far enough to reach the $H^+$ enriched acidic electrode region. The sudden drop in pH value caused a sharp

decrease in the fluorescence emission intensity, as shown in Fig. 5.7. The pH dependent fluorescence of fluorescein is well known, with the fluorescence practically disappearing below pH = 6 [103]. Since the charge of many analytes (e.g. proteins) is highly dependent on the local pH, this would certainly affect the electromigration and thus the separation quality of these analytes. The region available for separation is therefore limited depending on flow velocity and applied voltage and buffer capacity of the QH solution. Here we found that with the application of 400 volt and a flow velocity of 2 mm $s^{-1}$, the fluorescein band reached the linearly increasing $H^+$ enriched region (pH < 6) after 5 mm, which is after 2.5 s residence time as illustrated in Fig. 5.7.b The region of pH < 6 expands into the separation chamber at a rate considered to be app. 400 µm $s^{-1}$ (V = 400 V) due to electromigration and diffusion and app. 300 µm $s^{-1}$ for V = 300 volts. Although not further investigated, the production of $OH^-$ ions at the cathode will conversely lead to an enrichment of $OH^-$ and a zone of high pH. The migration of this zone towards the separation region is assumed to be slower, due to the lower mobility and diffusion of $OH^-$. Despite this limitation, the device still performed well and a clear separation was achieved. As a concluding remark, it must be stated that the fabricated device with a separation chamber length of 10 mm is longer than necessary. If not necessary the separation length thus residence time should be kept as low as possible, also to minimize band broadening e.g. by diffusion [35]. In principle, separations can be performed within hundreds of milliseconds thus completely avoiding a contamination of the separation region by chemical side products from the electrode, as shown in Fig. 5.8, where three fluorescent dyes were separated within 320 ms. Here the separation started instantly at the sample inlet and eventually followed a linear deflection, as expected. This rapid separation demonstrates the capability of the device, and indicate high miniaturization potential, since ultra rapid separations can be performed within a surface area below 1 $mm^2$. To be fair, it should be mentioned, that the separation shown is not typical for biochemical separations since all three dyes have different charge states allowing easy electrophoretic separation.

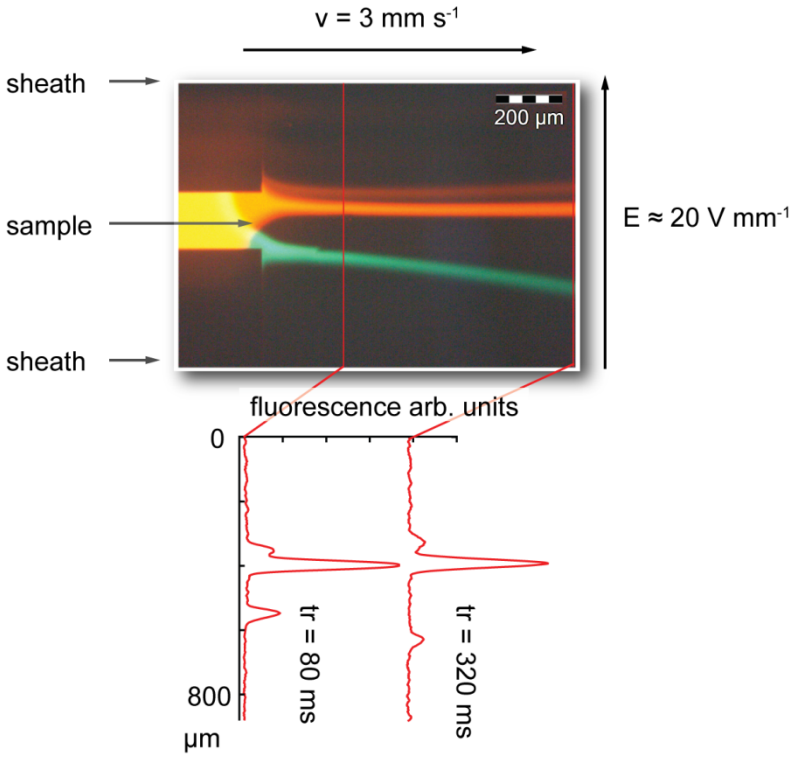


Fig. 5.8 Microphotograph showing the rapid separation of rhodamine B, rhodamine 6G and fluorescein below 320 ms residence time. The separation starts instantly at the sample inlet and analytes eventually follow a linear deflection as expected.

Another observation during experimental characterization was that the system did not behave like an Ohmic resistance with a linear electrical current to voltage behavior, like a stable electrolysis cell. In such a cell depletion of ions at the electrodes and resulting concentration polarization is prevented by adding sufficient current conducting background electrolyte. In our device only a 10 mM concentration of HEPES was present to limit the electrical current needed for operation at the required separation voltage. Hence, insufficient background electrolye was present to prevent concentration polarization and loss of separation voltage (see Fig. 5.7; $V_{sep}$). This correlates with the observation that with linearly increasing the applied voltage, the electrical current did not increase linearly, as can be seen in Fig. 5.9.

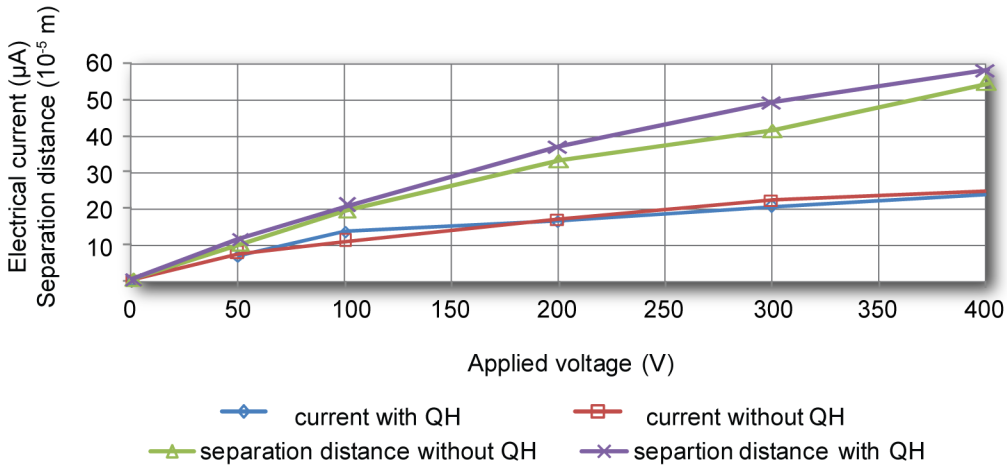


Fig. 5.9 Diagram showing the electrical current and separation distance behavior dependent on the applied voltage. The current follows a non-linear trend presumably due to concentration polarization at the electrodes thereby reducing the electrical field strength available for separation.

Assuming an Ohmic behavior of the local separation region (without electrode regions) and constant composition and conductivity of the electrolyte inside the separation chamber (sheath + sample), the electrical resistance of the separation chamber can be calculated by

$$R = \frac{l}{\sigma A} \tag{5.8}$$

where $l$ is the length (here the separation chamber width, $l$ = 4 mm), $\sigma$ the electrical conductivity ( $\sigma_{RT}$ = 140 µS cm$^{-1}$), and A the cross sectional area (height x separation chamber length, $A$ = 0.1 mm$^2$) [102]. With eq. (5.8), Ohms law, and the measured electrical currents one can derive the electrical field strength actually utilized across the separation chamber, with the results given in Tab. 5.1(3, a-f). More precise calculations of the electrical field strength across the separation region should include the conductivity changes near the sides, caused by the migrating zones of changing pH. However, as can be observed in Fig. 5.3 the linearity of the separation pattern was only negligibly distorted, for this reason and for simplicity a homogeneous electrical field strength along the separation chamber was assumed. With the above calculations, one can derive the mean electrophoretic mobility of fluorescein for the performed experiments applying eq. (5.1), which results in $\mu_f = 1.42^{\pm 0.1} \cdot 10^{-4}$ cm$^2$ (Vs)$^{-1}$. This value is lower than in previous CE related publications [104], however,

correspond to values obtained e.g. by Fonslow et al. with a µ-FFE device [35]. In terms of voltage efficiency [95], as defined by the ratio of the utilized voltage for separation and the total applied voltage, the system suffers from the potential loss across the electrode regions (compare chapter 2.4.1). Here we found a voltage efficiency between 30% and 20%.

## 5.5 Conclusions

In this chapter the bubble-free operation of a new microfluidic FFE chip with integrated platinum surface electrodes was presented. In contrast to earlier publications electrodes were placed directly in contact with the separation medium. To avoid electrolytic bubble formation that would distort the separation lane positions, QH, a complex of hydroquinone and p-benzoquinone was added to the fluid streams along the electrodes for electron transfer to the solution without gas formation. This method enabled a stabilized and clear separation applying free-flow zone electrophoresis, demonstrated with a set of fluorescent dyes. A maximum electrical current between 30 and 40 µA was found before electrolysis was observed presumably due to QH depletion at the electrode surface. This value is certainly acceptable for FFE applications with low electrical currents involved. It was found, that bubbles have significant influence on the separation performance as defined by the resolution. For the first time in µ-FFE devices a time based resolution was derived, which is of great importance for long-term signal or sample acquisition. The resolution obtained, when applying QH as bubble suppression was 2.5 fold higher that when electrolysis was involved. The migration of $H^+$ ions formed at the electrodes can negatively influence the actual available width of the separation region since the low fluid volume inside the chip (V = 600 nl) allows quick changes in the local pH. This will be a disadvantage when separating molecules which charge is dependent on the local pH. However, it was shown, that the device is capable of separating components within tens of milliseconds residence time and a surface region below 1 $mm^2$ thereby totally avoiding the pH unstable region. This demonstrates the capability for further miniaturization and integration into more complex LOC systems. This is of further interest, especially where the presence of open fluid reservoirs (common in miniaturized FFE systems) and reachable electrodes should be avoided.

# 6 Continuous-Flow Bio-Array Patterning

*A side aspect during the overall research project was how to immobilize bio-active ligands inside the microfluidic FFE chip available for bio-molecular interactions. Although, not further investigated due to limited time available, a new chip was developed which might be applicable in future microfluidic devices. The results of this project were published in Microfluidics & Nanofluidics in 2007.*

## 6.1 Abstract

This chapter describes a microfluidic chip in which two perpendicular laminar-flow streams can be operated to sequentially address the surface of a flow-chamber with semi-parallel sample streams. The sample streams can be controlled in position and width by the method of electrokinetic focusing. For this purpose, each of the two streams is sandwiched by two parallel sheath flow streams containing just a buffer solution. The streams are being electroosmotically pumped, allowing a simple chip design and a setup with no moving parts. Positioning of the streams was adjusted in real-time by controlling the applied voltages according to an analytical model. The perpendicular focusing gives rise to overlapping regions which, by combinatorial (bio)chemistry, might be used for generation of spot arrays of immobilized proteins and other biomolecules. Since the patterning procedure is done in a closed, liquid filled flow-structure, array spots will never be exposed to air and are prevented from drying. With this device configuration, it was possible to visualize an array of 49 spots on a surface area of 1 $mm^2$. This chapter describes the principle, fabrication, experimental results, analytical modeling and numerical simulations of the microfluidic chip.

## 6.2 Introduction

The research areas of lab-on-a-chip and micro-total-analysis systems have grown rapidly in the last years [21, 105]. Miniaturization of (bio)chemical analysis and synthesis systems has important advantages such as the small amount of reagents needed, improved reproducibility and speed of analysis [106-108]. As microfluidics operate at low Reynolds numbers (Re < 2000) [109], the position and the width of a laminar-flow stream can be varied by sandwiching the stream in-between two parallel flowing sheath flow streams. This technique, in case of pressure driven systems, is known as hydrodynamic focusing [110]. Hydrodynamic focusing has been applied for particle sorting, alignment and counting [111], with multiple focusing as fluidic switches [112] but also for a confined patterning of metal and polyelectrolyte structures inside microfluidic channels [113-115]. Hydrodynamic focusing is an interesting method to pattern ligand arrays onto biosensors as compared with alternative microfluidic techniques such as stamping and spotting [116-118]. It is possible to guide cell and protein containing streams inside a flow-chamber and to immobilize the ligands in parallel lanes [119]. Furthermore, by removing a microfluidic PDMS structure from the substrate and applying it a second time turned by 180 degrees, more complex two-dimensional arrays can be formed [120, 121]. A recent overview about different patterning methods by means of microfluidics and was published by Situma et al. [122]. Dusseiller et al. used hydrodynamic focusing to position proteins and vesicles in two directions [123]. An alternative to hydrodynamic focusing is electrokinetic focusing in which electroosmotic-flow (EOF) is used as the fluid pumping mechanism instead of pressure driven flow. EOF is the motion of the bulk liquid in response to an applied electrical field in a capillary which is extensively used in capillary-electrophoresis systems [124]. The usage of EOF implies several advantages compared with pressure driven systems: No valves or other moving parts are involved, which allows a simple chip structure and a fast and accurate switching between different flow-rates. However, EOF is mainly usable in combination with aqueous solutions and other polar solvents, and in most cases voltages up to several 100 volts are required to generate adequate flow rates. Furthermore, electrochemical phenomena such as electrolysis and unwanted bubble formation may disturb flow behavior. To remove gas produced during the electrolysis the electrodes have to be placed outside the actual flow-structure in the open fluid reservoirs. It has been

successfully demonstrated to vary three and five parallel fluid streams in position and width inside in laminar-flow chamber by electrokinetic focusing [125, 126].

Described here is a sealed microfluidic structure which can be used to pattern two-dimensional biochemical arrays. It is not necessary to remove the flow-structure and therefore array spots are never exposed to air and are prevented from drying. Due to the mentioned advantages electrokinetic focusing is used to position two perpendicular sample containing streams inside a laminar-flow chamber.

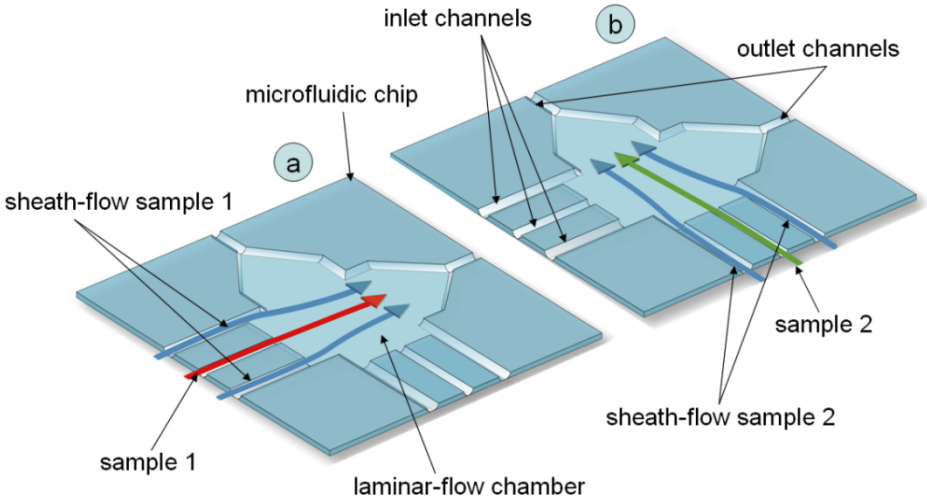


Fig. 6.1 Illustration of the principle layout of the chip. Two laminar flow streams are focused by two parallel sheath flows. These sample streams can operate in terms to coat the chip surface. (a) First, lanes are generated in one direction by steering the sample to different positions. (b) Second, perpendicular lanes are generated (b). The overlapping regions form the array. Fluid flow is achieved electroosmotically.

As illustrated in Fig. 6.1, the chip consist of a microfluidic network of six inlet channels, a wider cross-shaped flow-chamber and two outlet channels. The position and the width of two sample streams (Fig. 6.1, sample 1 and sample 2) can be varied inside the laminar-flow chamber. This is achieved by adjusting the flux ratio of the sheath flow streams sandwiching each sample stream. These sheath flow streams contain only buffer solution. The two sample streams can be operated to sequentially (Fig. 6.1, a and b) coat the chip surface. Since EOF is used for pumping the liquids the required electrical voltages have to be applied outside the actual flow structure by

electrodes inside the fluid reservoirs. During operation three voltages are calculated and applied to the electrodes in the active flow direction in real-time, while the electrodes in the perpendicular direction are set to floating (i.e., act as disconnected). To move the sample stream inside the flow chamber, the voltages applied to the sheath flow streams are controlled. Increasing one voltage and decreasing the other voltage, increases the volume flow of the first one but decreases the flow of the second sheath. This results in unequal widths of the sheath flow streams inside the chamber, thus changing the position of the sandwiched sample stream. Here the principle, fabrication and the experimental characterization of the device are described and discussed. The chip was used to verify the principle of forming a micro array by applying electrokinetic focusing of two perpendicular streams, each forming lanes on the chip surface resulting in a 2D grid. To control the required voltage settings an analytical model was applied.

## 6.3 Experimental

### 6.3.1 Microfabrication

The fabrication is described briefly since only standard cleanroom fabrication techniques were applied. Most of the cleaning and intermediate steps are not mentioned. The microfluidic chip consists of two bonded plates. The silicon top plate contains the microfluidic channels as well as inlet and outlet holes while the bottom Pyrex glass plate is left unprocessed.

To fabricate the 10 µm deep channel structure, a standard photo lithography step was carried out on a 100 mm diameter <100> silicon wafer. The developed photoresist served as an etching mask during the following deep-reactive-ion-etch (DRIE) step of silicon. After removing the photoresist the silicon wafer was coated with a 250 nm low-stress silicon-nitride (SiN) layer during a low pressure chemical vapor deposition. This SiN layer was structured after a second photo lithography step on the backside of the wafer by plasma etching to form a mask layer for the inlet and outlet holes. These through-holes were etched in a 2% KOH bath at 75 °C while the SiN layer protected the rest of the wafer. The SiN layer was removed by etching in 50% hydrofluoric acid (HF). Since silicon is a semi-conducting material it has to be completely covered with an isolating layer when applying electroosmotic flow with high voltages involved. The

isolation layer was achieved by a wet oxidation step at 1150 °C to grow a 1 µm layer of $SiO_2$. The processed oxidized silicon wafer was bonded to a Pyrex-glass wafer by anodic bonding and finally diced into single chips.

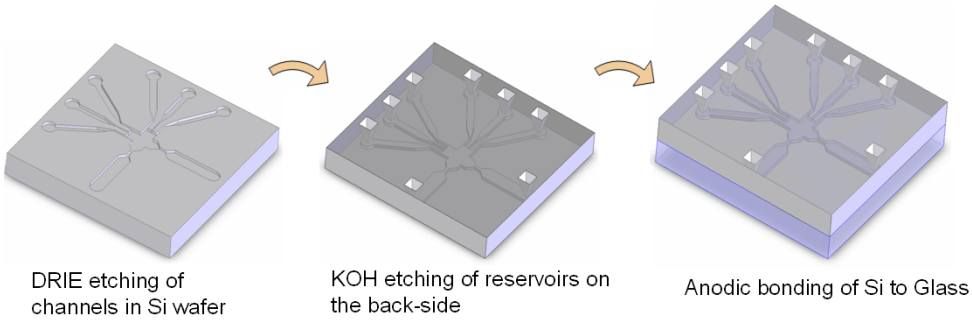


Fig. 6.2 Illustrative chip fabrication process: (1) Etching the channel network into a silicon wafer. (2) Etching the channel inlets from the wafer backside. (3) Bonding a Pyrex glass wafer to close the structure.

Fig. 6.2 illustrates the three main fabrication steps involved in the process (flow-structure etching, inlet/outlet etching and bonding). The chip size is 15 x 15 $mm^2$ and the thickness is 1 mm. The surface area for patterning e.g. bio arrays is about 1 $mm^2$ and the channel widths differ from 150 to 30 µm and the channel height is 10 µm. The fabricated microfluidic chip is shown in Fig. 6.3.a and the flow-chamber in the close-up Fig. 6.3.b.

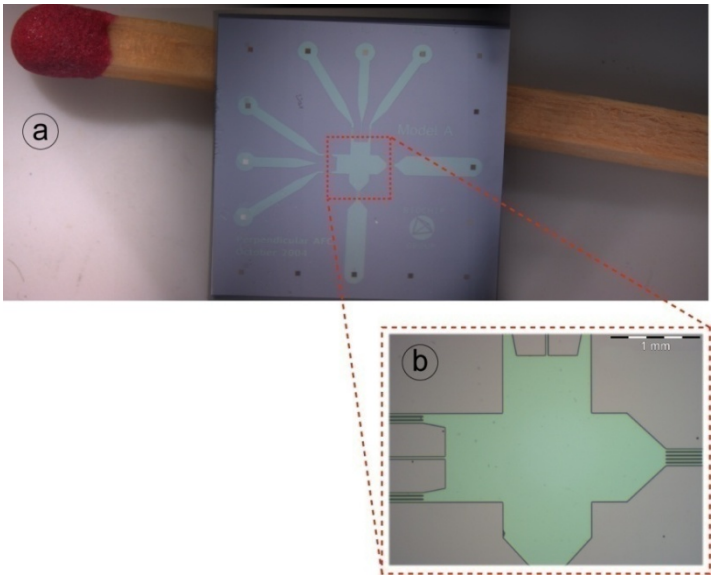


Fig. 6.3 Photographs of the fabricated chip: The chip is 15 x 15 mm² in size with a thickness of 1 mm (a). The actual flow chamber which is used for array patterning has a surface area of 1 mm² (b).

### 6.3.2 Materials

Bovine serum albumin (BSA), fluorescein isothiocyanate and Hepes were obtained from Sigma (Sigma-Aldrich Chemie BV, Zwijndrecht, The Netherlands). Rhodamine B labeled dextrane (MW 10.000) was obtained from Molecular Probes (Invitrogen BV, Breda, The Netherlands). All other chemicals were purchased from VWR International (Darmstadt, Germany) and were of analytical grade. BSA (30 mg $mL^{-1}$ in 0.5 M sodium borate, pH 9.0) was fluorescently labeled by treating it for 30 min at room temperature with (a 60-fold molar excess of) fluorescein isothiocyanate, followed by gel filtration over a PD-10 column (Amersham Biosciences, Uppsala, Sweden). A solution of 10 mM Hepes in demineralized water was prepared and adjusted to pH 8.0.

### 6.3.3 Setup and Methods

For experimental work, the flow structure was flushed several minutes with 1 M NaOH and afterwards with demineralized water to clean the channels and to ensure reproducible EOF conditions. The outside of the chip was cleaned with isopropanol

and dried with nitrogen. The fabricated chip was mounted into an in-house fabricated holder with integrated fluid reservoirs and platinum electrodes.

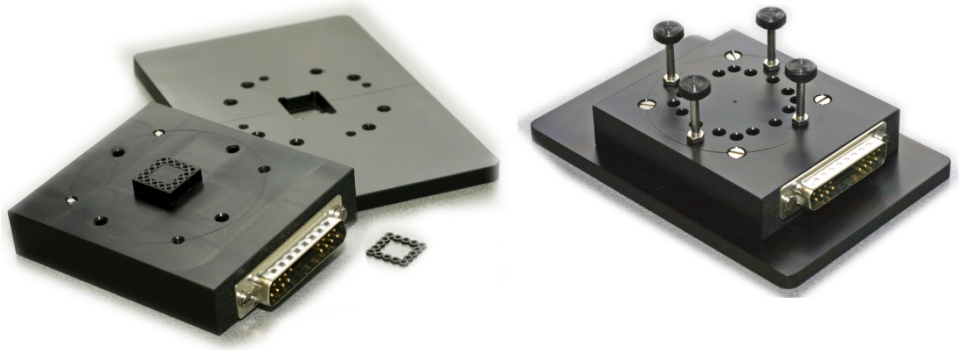

Fig. 6.4 An in-house fabricated holder was used to mount the chip on an inverted microscope with fluorescent equipment. This holder has integrated platinum electrodes for electrical connections. Sealing between the chip and the lid was achieved by a laser cut rubber plate.

The holder (see Fig. 6.4) consists of two parts which fixate the chip in-between while the glass side of the chip faces downwards to the square opening. Sealing between the chip and the holder is achieved with a laser-cut rubber plate of 1 mm thickness. All holder reservoirs were filled with 10 mM Hepes (pH 8.0) and a conventional syringe was used to apply vacuum to several reservoirs to remove air bubbles and fill the microfluidic network with the buffer solution. All reservoirs were emptied and refilled with buffer to ensure equal fluid heights. For stream visualization the sample stream reservoirs were filled with 1 mg $mL^{-1}$ Rhodamine B in 10 mM Hepes buffer and 1 mg $mL^{-1}$ Fluorescein labeled BSA in Hepes buffer, respectively. The integrated electrodes were connected to two computer controlled power supplies (IBIS 411, microfluidic control unit; IBIS Technologies B.V., Hengelo, The Netherlands) supplying eight independent voltage channels (up to 1 kV). This holder was placed on an inverted microscope (Olympus IX51, Olympus Nederland B.V. The Netherlands) equipped with a mercury lamp and appropriate fluorescent filter cubes for visualization of the fluid streams. A digital color camera (ColorView II, Soft Imaging Systems, Münster, Germany) was attached to the microscope and images were captured during experimental work with the imaging software package Analysis (analySIS 5, Soft Imaging Systems, Münster, Germany).

The positions of the two samples streams were varied by controlling the voltage settings with a in-house written Labview program (LabVIEW, National Instruments). Therefore an analytical model, which is an analogue of EOF to an electrical network, was developed and embedded into the software allowing real-time control of the sample stream positions and widths by calculating the corresponding voltage settings.

The distribution of the electrical field inside the microfluidic chip and EOF operation was simulated with the CFD-ACE+ software (CFD Research Corporation, Huntsville, USA). The microfluidic device was approximated as a 2D structure with approximately 7000 grid-cells. The simulation was performed with "no-slip conditions at walls". The electrical boundary conditions were obtained from the analytical model. Residual convergence criteria were set to $10^{-4}$. The electroosmotic mobility was set to 5x10-8 $m^2 (Vs)^{-1}$ for guiding as well as the sample stream [127].

### 6.3.4 Analytical Model

An analytical model was developed to calculate the required voltage settings for any sample stream position, velocity and width. This model is based on earlier presented results [125, 126, 128, 129]. Therefore, it is described only briefly. To simplify the calculations, the cross shaped flow chamber was neglected and a straight channel was assumed. Furthermore entrance effects were neglected. Fig. 6.5.a shows the relevant geometrical parameters which were used for the calculations. An analogy of electroosmotic flow to an electrical network was developed as illustrated in Fig. 6.5.b.

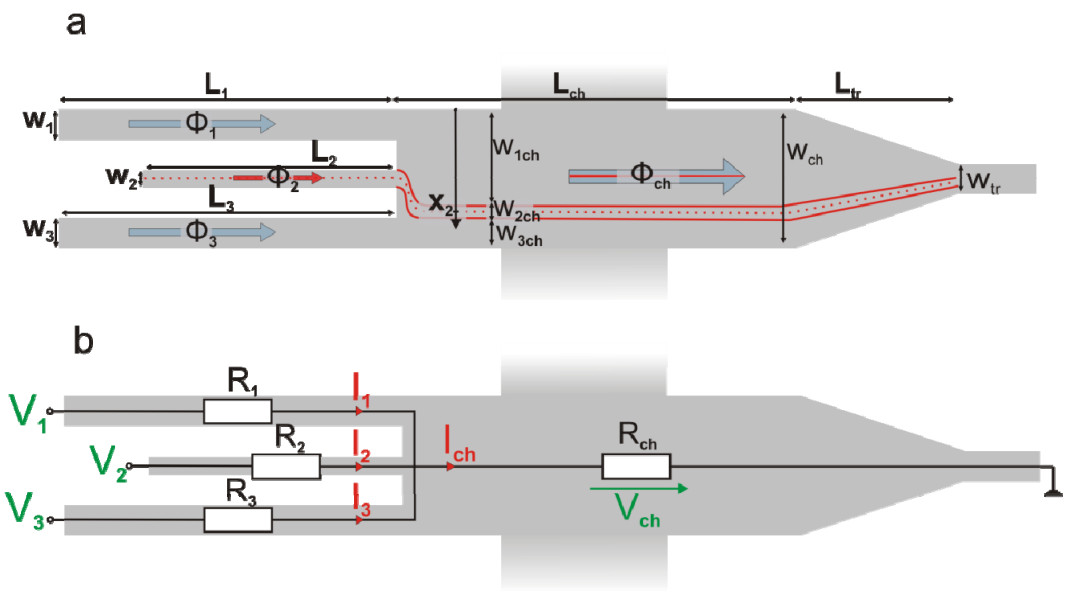


Fig. 6.5 Technical layout with relevant geometrical and flow parameters (a) To calculate the voltages required for the electroosmotic flow an electrical network was used. (b) Each channel is represented by an electrical resistance.

Due to mass conservation, the fluid stream through each inlet channel is proportional to its corresponding fluid stream inside the flow chamber. Therefore, the position $x_2$ and the width $w_{2ch}$ of the sample stream inside the chamber can be expressed by:

$$x_2 = \frac{\phi_1 + \frac{1}{2}\phi_2}{\phi_1 + \phi_2 + \phi_3} w_{ch} \tag{6.1}$$

and

$$w_{2ch} = \frac{\phi_2}{\phi_1 + \phi_2 + \phi_3} w_{ch} \tag{6.2}$$

where $w_{ch}$ is the width of the flow chamber and $\Phi_i$ the flow rate through an inlet channel.

The flow rate $\Phi_i$ through each channel is given by:

$$\phi_i = \mu_{EOF\,i} A_i \frac{V_i - V_{ch}}{L_i} \tag{6.3}$$

where $\mu_{EOFi}$ is the electroosmotic mobility, $A_i$ the cross-sectional area and $V_i$ the voltage applied to each inlet reservoir and $L_i$ the channel length.

$V_{ch}$, the voltage drop across the chamber, can be calculated using:

$$V_{ch} = \frac{\frac{V_1}{R_1} + \frac{V_2}{R_2} + \frac{V_3}{R_3}}{\frac{1}{R_{ch}} + \frac{1}{R_1} + \frac{1}{R_2} + \frac{1}{R_3}} \tag{6.4}$$

Knowing the electrical properties such as conductivity and the geometrical parameters, the electrical resistance of the channels $R_i$ and the electrical resistance of the chamber $R_{ch}$ the mentioned equations can be solved. The analytical model is a useful tool for calculating the voltages that are needed for obtaining the desired sample stream position and width.

## 6.4 Results and discussion

### 6.4.1 Experimental Array Visualization

For obtaining an impression of the flow behavior and visualizing the array geometry, two fluorescent components were chosen as flow marker, namely Rhodamine B and fluorescein labeled BSA. After prefilling the chip, Rhodamine B was added to the first sample reservoir. The sample stream thickness was focused to approximately 50 µm. Due to diverging flow lines inside the cross shaped flow chamber, the sample stream tend to broaden near the sides. Therefore, the thickness of 50 µm was only valid along the centerline of the chip. The flow velocity was set to 1 mm $s^{-1}$. For this setting 133 V was applied to the sample electrode and 180 V to the sheath flow electrodes (valid for center position). When moving the sample inside the flow chamber, the voltages applied to the sheath flow electrodes were adjusted, keeping the voltage ratio constant to prevent altering the total current and hence the velocity (Tab. 6.1).

| position | $V_1$ (V) (sheath 1) | $V_2$ (V) (sample) | $V_3$ (V) (sheath 2) |
|---|---|---|---|
| 1 | 118 | 133 | 241 |
| 2 | 133 | 133 | 226 |
| 3 | 149 | 133 | 210 |
| 4 | 164 | 133 | 195 |
| 5 (center) | 180 | 133 | 180 |
| 6 | 195 | 133 | 164 |
| 7 | 210 | 133 | 149 |
| 8 | 226 | 133 | 133 |
| 9 | 241 | 133 | 118 |

Tab. 6.1 Voltages used during experimental work. The velocity was constant at 1mm $s^{-1}$ for all settings.

As shown in Fig. 6.6.a, the Rhodamine B containing sample was sequentially positioned to nine different lanes forming the first dimension of the array. It has to be pointed out that no immobilization of Rhodamine B molecules was performed. Several photographs were taken during the experimental run and were merged to an overlay image for visualization of the sample streams. The voltage configuration was altered in the next patterning step. For this purpose, the electrical connections were changed from that of the first sample to that of the second sample and guiding channels. Now the sample containing BSA was guided to nine positions resulting in a second set of parallel lanes as shown in Fig. 6.6.b. All eighteen images were superimposed to one image to visualize the possible array geometry. In Fig. 6.6.c it can be seen, that due to the curvature flow of the sample stream the array spots are not uniformly sized and positioned. However, if the highly broadened outer streams are excluded, an acceptable micro array of 49 spots was generated. This could be a useful format for bio-assay applications. Using image based software, regions of interest (ROI) could be placed inside the generated array spots. The cross-shaped flow chamber is not ideal, since the curvature flow caused by non-parallel electrical current streamlines is broadening the flow. However, the usage of a closed system instead of earlier presented results with removable PDMS cover layers will be advantageous when using proteins and other more fragile components as drying induced denaturation of biomolecules can be prevented.

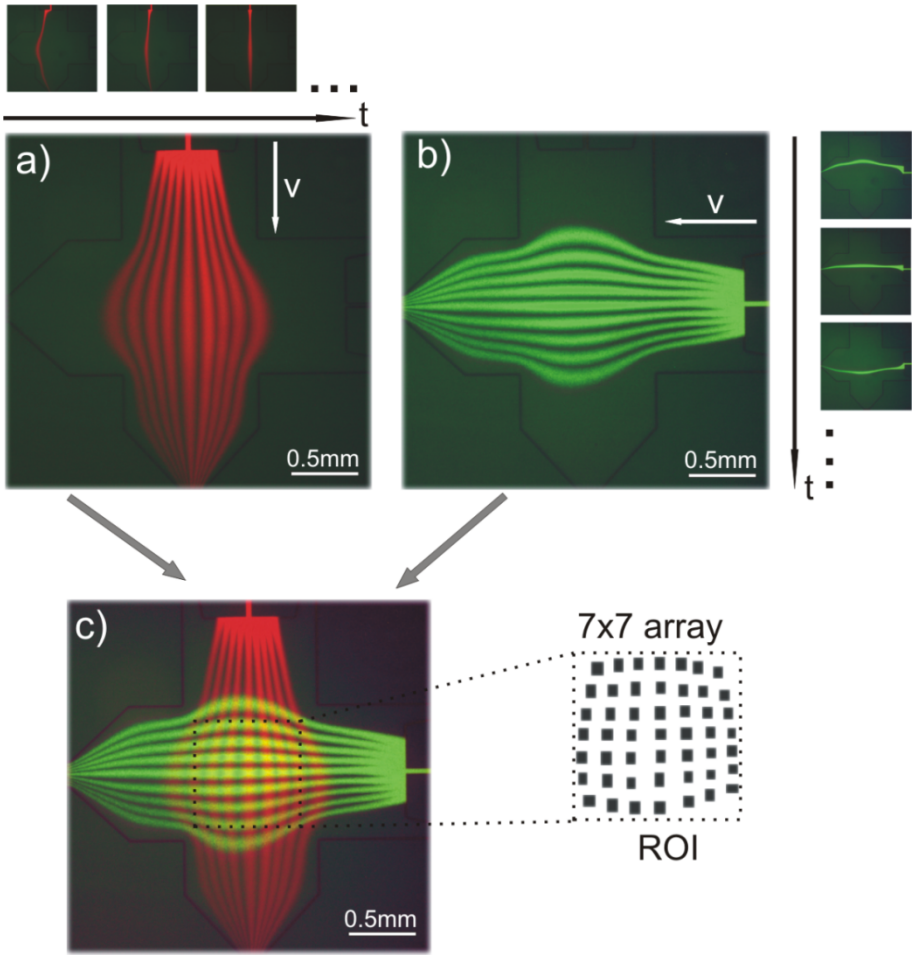


Fig. 6.6 Superimposition of several photographs taken during the experimental work. (a) 1 mg $mL^{-1}$ Rhodamine B containing sample stream was steered to nine different parallel positions. Each lane was recorded separately (illustrated by the small images above figure (a) and right to figure (b). (b) Sample containing 1 mg $mL^{-1}$ Fluorescein labeled BSA was positioned in the perpendicular direction. All images were merged to visualize the generated array. (c) Overlapping regions form the actual regions of interest (ROI).

Several principles based on combinatorial (bio) chemistry have been described in the literature which could be a relevant application for this technique. DNA-directed immobilization (DDI), for example, employs proteins tagged with specific single strands of DNA, to be hybridized to complementary DNA strands previously spotted on a solid substrate. DDI is a self-assembly method that is chemically mild and leads to relatively high protein immobilization yields and homogeneous results [130]. The use of DDI has been described for the preparation of protein microarrays that were employed in chip-based multi analyte detection [131]. The device described in the present chapter might be useful in such an approach: First by applying streams of different oligonucleotides in one direction resulting in immobilization of these oligonucleotides in distinct lanes; Next by applying streams of the DNA-tagged proteins in the perpendicular direction enabling hybridization between complementary DNA strands and the connected immobilization of the DNA-tagged proteins thereby resulting in protein microarrays. To generate a DDI based microarray, as described above, the future chip device has to be supplemented with several inlet reservoirs to enable feeding with different immobilants. The usage of electroosmotic flow allows an easy switching between the separate inlet reservoirs to immobilize different components, such as oligonucleotides. The device described here has only two separate sample reservoirs to apply an orthogonal pattern in order to demonstrate the basic functions.

When switching between various positions, crosstalk of different components might occur between adjacent spots immobilized on the surface. This will be avoided by an intermediate step, where an inlet reservoir with clean buffer solution is activated before moving the sample stream towards its next position. Crosstalk can also be caused by sample stream broadening due to diffusion which can lead to overlapping between neighboring lanes. The extent of stream broading depends on flow-rate and the diffusion constant of the applied component and can be prevented by choosing proper lane pitches.

### 6.4.2 Simulations

To verify the experimental results as well as the analytical model, the system was simulated using a 2D model of the flow structure. Fig. 6.7 shows the comparison between the simulation and the experimental result (left half: simulation, right half: experimental). Also shown is an intensity line profile from the image. These results indicate a good agreement between simulation and experimental results and, furthermore, prove the usefulness of the model in predicting stream positions. The higher background level in the right part of the intensity plot is due to the auto fluorescence caused by the silicon oxide layer inside the chip.

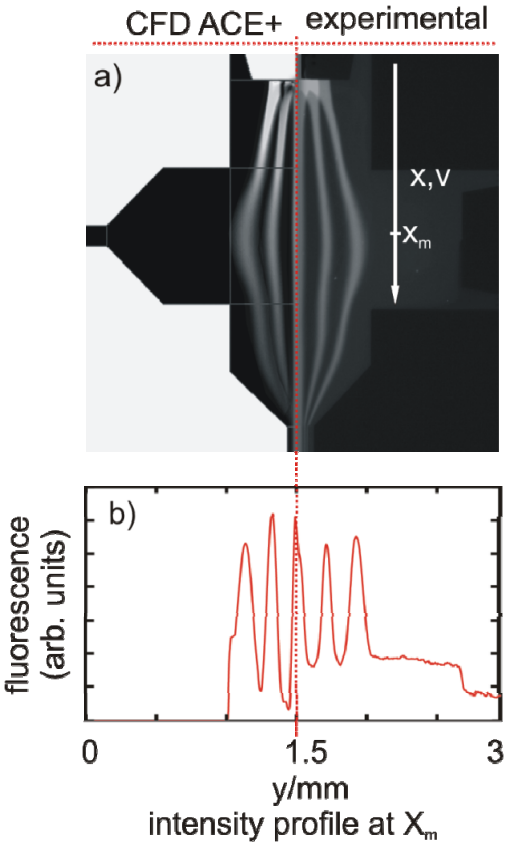


Fig. 6.7 Comparison of simulations (a, left half) with experimental results (a, right half). (b) Intensity profile measured at Xm.

The curvedness and broadening of the sample stream increases to the sides is a result of the inhomogeneous distribution of the electrical field. Since EOF stream lines are perpendicular to the electrical field lines, the flow line of a centered sample will remain straight, as can be derived from Fig. 6.8.a and b. However, when unequal voltages $V_1$ and $V_3$ are applied ($V_1 + V_3$ = constant) the sample stream is guided to the side (Fig. 6.8.c and d)., leading to a curved sample stream. Furthermore, the lower field strength and lower velocity near the sides of the flow chamber results in a broadening of the sample stream.

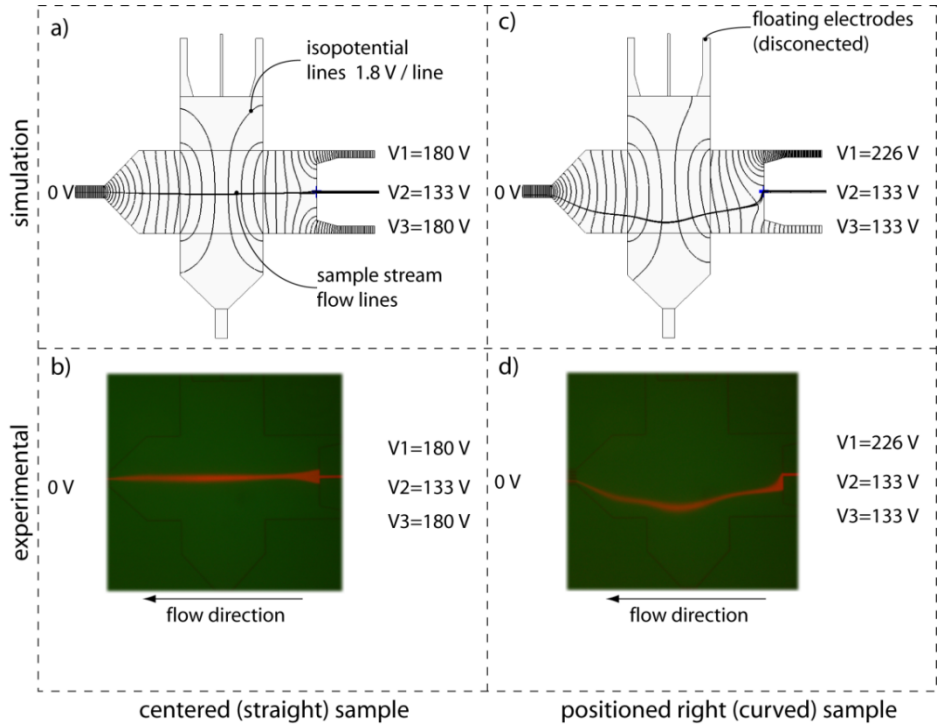


Fig. 6.8 Illustration comparing simulation with experimental results: The cross shaped flow chamber has a distribution of the electrical field with non-parallel curved field lines. Electroosmotic flow is perpendicular to the flow resulting in a curved flow stream when applying unequal voltages V1 and V3.

## 6.5 Conclusions

An EOF driven chip system that can be used for patterning a surface in an array-like manner, was demonstrated. To visualize the possible array dimensions, two fluorescent flow markers were used and images were superimposed. Two perpendicular laminar flow streams could be sequentially operated to address the chip surface with parallel lanes in a perpendicular direction which results in two overlapping grids, thus generating an array of 49 spots or more on a surface area of $1mm^2$. No immobilization was performed yet; however the technology is promising. Since electroosmotic flow is a pumping mechanism where no pumps and moving parts are involved, the setup is easy and straight forward to handle. An analytical model proved to be useful in predicting the stream positions and widths by calculating the required voltages. This technology is a new line spotting tool for generating, e.g., biochemical micro arrays without exposure of fragile biomolecules to air.

# 7 Continuous-Flow Sample Control

*In this chapter an electrokinetically driven two stream microreactor is demonstrated. Although this project was not directly related to my main research line, it allowed me an insight view in electroosmotic flow and steering with laminar flows by electrokinetic focusing. Several later developed FFE features are based on these principles. To demonstrate the capability of the chip, an application as microreactor seemed straight forward to realize, although more functions are possible. The outcome of this work was published in Microfluidics & Nanofluidics in 2005.*

## 7.1 Abstract

An adjustable diffusion-based microfluidic reactor is presented here, which is based on electroosmotic guiding of reagent samples. The device consists of a laminar-flow chamber with two separate reagent inlets. The position and the width of the two sample streams in the flow chamber can be controlled individually by changing the flow ratio of three parallel guiding buffer streams. Since electroosmotic flow is used for pumping, no external pumps or other moving parts are needed. The region where the diffusive profiles of the two sample streams overlap is used for reactions. This overlapping region can be manipulated in a predictable way by adjusting the voltages required to generate the respective electroosmotic flow. Reaction dynamics inside the microreactor is illustrated with a reactant pair of a fluorescent calcium tracer and a calcium chloride solution. An analytical model, which is an analogue of electrical circuits to electroosmotic flow was developed and embedded into the LabView control software, allowing real-time control of the microreactor. This chapter describes the simulation, fabrication and experimental characterization of the device.

## 7.2 Introduction

In the last decade, the research and development of microfluidic systems have grown rapidly, allowing the fabrication of micro-total-analysis-systems (μ-TAS) or lab-on-a-

chip devices [22, 132]. These microfluidic systems profit from their small dimension and high surface to volume ratios, allowing reaction and analysis to be fast and efficient [133, 134]. Furthermore, the energy and sample consumption in microfluidic structures are much lower compared to that in traditional macrofluidic systems. Flow in microfluidic channels is always laminar because of low Reynolds numbers [135], which makes it possible to have parallel flowstreams without turbulent mixing [136]. In such systems transversal mass transport is based on diffusion. Micro total analysis systems include several passive and active microfluidic components such as mixers and reactors. Microreactors integrated in such systems have been developed in different shapes among which the T-reactor is a well-known example [132, 136-138]. The mixing of two homogeneous solutions in a T-reactor and laminar-flow is based only on diffusion. To influence the reaction yield it is possible to vary for instance the concentrations of the reagent streams. In some applications it might be of interest to control the extent of mixing, and therefore the reaction yield in simpler way. The microreactor presented here is an adjustable diffusion-based one, which is easy to operate and fulfills these requirements. Fluid flow in this reactor is induced by electroosmotic flow (EOF), which is a simple technique used for pumping aqueous solutions through microchannels. The major advantage of using EOF is that no external pumps or other moving parts are needed. Furthermore, EOF is easy to implement and operate, especially when more miniaturized structures are involved. More complex electroosmotic fluid control became possible with the introduction of the FlowFET, an electroosmotic pumping and switching device [56]. Here, we report on the design and evaluation of a microfluidic reactor driven by EOF.

### 7.2.1 Functional Principle

In lab-on-a-chip devices, flow control is one of the most relevant issues. Electrokinetic control is a common technique used to adjust the width and the position of a sample plug for instance in capillary electrophoresis [139, 140]. Methods for controlling the position of streams (hydrodynamically induced) using parallel guiding streams in a laminar-flow chamber has been demonstrated earlier [141-143]. The idea of electrokinetic steering [144] is to control both, the position and the width of one central fluid stream (containing sample or reagent) entering a microfluidic chamber sandwiched by two parallel guiding streams. In electrokinetic steering devices only electroosmotic flow is used. The position and width of the sample stream can be

controlled by varying the flow ratio of the sample stream as well as the guiding streams. This is done by adjusting the EOF voltage settings for the streams individually. Electrokinetic steering is only possible in microsystems where turbulent mixing is absent. Since the chips contain no moving parts, the manufacturing becomes simpler. An analogue model of electroosmotic flow to electrical circuits has been developed and embedded into a LabView program for real-time control during experimental work. Measurements were found to correspond well with the respective model [144]. To investigate the possibilities of controlling multiple sample streams inside a laminar-flow chamber, a 2-sample electrokinetic steering chip has been developed. It has two sample streams and three guiding streams (Fig. 7.1). Both sample streams can be individually controlled in position and width by adjusting the EOF voltages according to the analytical model.

This 2-sample electrokinetic steering chip is used as a microreactor. The reaction occurs where the diffusive profiles of the two reagent streams overlap (Fig. 7.2).

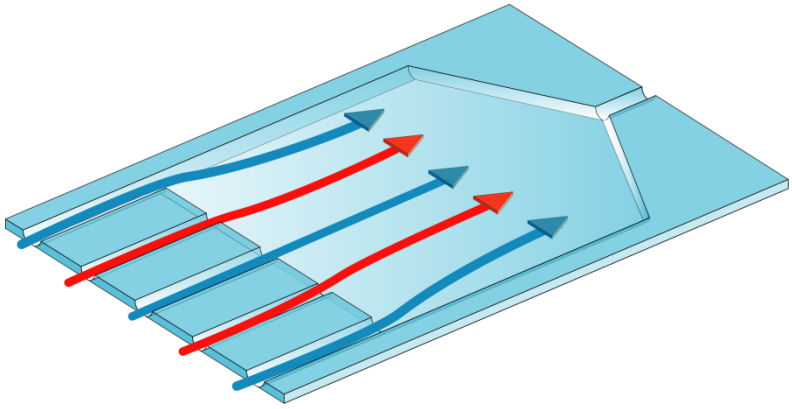

Fig. 7.1 Illustration of the 2-sample electrokinetic steering chip. The position and the width of two inner sample streams (red) can be influenced in a predictable way with the adjustment of three parallel guiding streams (blue).

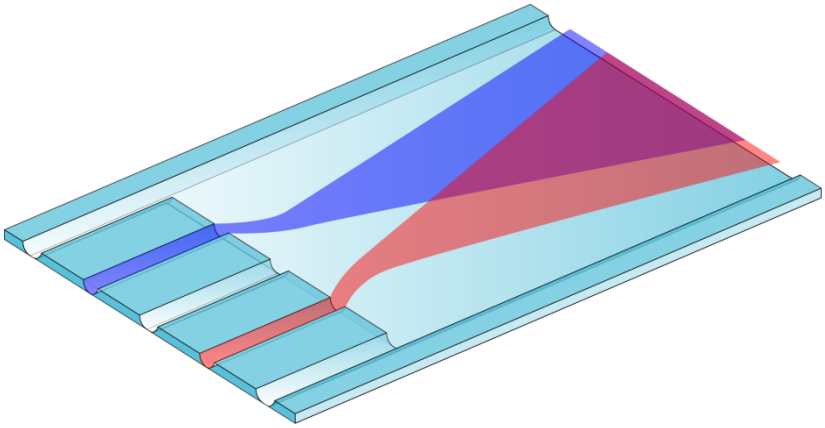

Fig. 7.2 Illustration of the 2-sample electrokinetic steering chip used as a microreactor. The region where the diffusive profiles of the two analyte streams overlap is used for reactions.

## 7.3 Experimental

### 7.3.1 Microfabrication

The microfluidic chips were fabricated at the MESA+ cleanroom facilities (Enschede, the Netherlands). Each chip consists of two glass plates: the top plate contains the channel structures, flow-chamber and the reservoir holes while the bottom plate is unprocessed. Processing of the top plate was done as follows. A 100 mm Pyrex-glass wafer (Corning 7740) was coated with 1 µm of amorphous silicon. After a standard lithography step this silicon layer was structured by $SF_6$ reactive ion etching. The silicon layer served as a mask during the following wet etching step in 10% HF to create the channel and chamber structures in the underlying glass layer. For the inlet and outlet reservoirs a second photolithography step was carried out on the back side using Ordyl BF410 resist foil. This foil was exposed to a UV light source and was developed in a sodium carbonate solution. After that, powderblasting is performed with $Al_2O_3$ particles (30 µm particle diameter) [97] to create the inlet and outlet holes. After ultrasonic cleaning in acetone and the removal of the silicon layer in 25% KOH, the wafer was chemically mechanically polished preparing the surface for the following fusion bonding step [145]. Fusion bonding of the structured wafer to another Pyrex wafer was performed at 600°C. The bonded wafers are finally diced into several microfluidic chips. Fig. 7.3 shows the design of the 2-sample electrokinetic

steering chip and Fig. 7.4 exhibits a chip manufactured from Pyrex glass according to that design.

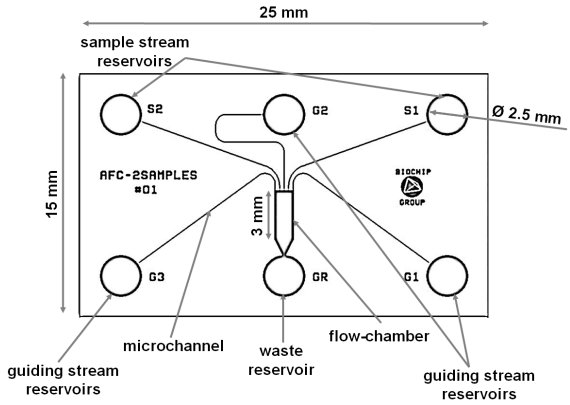


Fig. 7.3 Design of a 2-sample electrokinetic steering chip that was used for cleanroom fabrication. The chip dimensions are 15 mm x 25 mm. The chamber is 1200 µm wide and 3 mm long. The width of the three guiding stream channels is 100 µm and the width of the two sample stream channels is 50 µm. Channel and chamber height is 10µm.

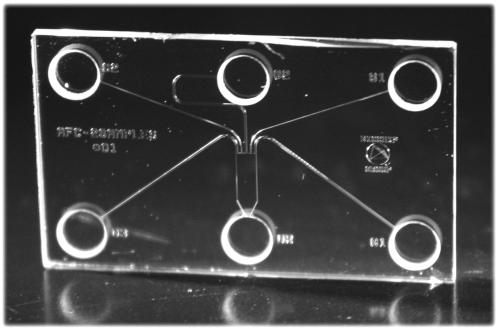

Fig. 7.4 Photograph of 2-sample electrokinetic steering chip fabricated from Pyrex glass. The size of the chip is 15 mm x 25 mm

### 7.3.2 Stream and Reaction Visualization

The visualization of streams and reaction was done using fluorescence microscopy. Bovine serum albumin (BSA) was obtained from Sigma (St. Louis, MO). BSA was fluorescently labeled by treating it with (a 60-fold molar excess of) fluorescein isothiocyanate in 0.5 M sodium borate, pH 9.0, for 30 min at room temperature followed by gel filtration over a PD-10 column. Fluo-4 pentapotassium (salt,

fluorescent calcium probe F14240) was obtained from Molecular Probes (Europe BV, Leiden, The Netherlands). HEPES buffer (prod. no. 110110) was obtained from Merck KGaA (Darmstadt, Germany). All the other chemicals were purchased from VWR International GmbH (Darmstadt, Germany) and were of analytical grade.

The 2-sample electrokinetic steering chip was placed in an in-house manufactured holder. This holder contains six reservoirs with integrated platinum electrodes connected to two high voltage sources (IBIS 411, microfluidic control unit, IBIS Technologies B.V., Hengelo, The Netherlands). The applied voltages were controlled with a LabView (LabView 7.0, National Instruments) program based on the analytical model described below. An inverted (epifluorescence) microscope (Olympus IX51) with UV light source and filter (U-MWB2 Wide-band 450 - 480 500>515, Olympus), equipped with an F-View II 12-bit digital camera (Soft Imaging System GmbH, Münster, Germany) was used. The camera control software AnalySIS (Soft Imaging System GmbH, Münster, Germany) was used to capture images and for measurements of stream positions and widths.

The glass chips were thoroughly cleaned in 1 M NaOH and then rinsed with DI water to ensure reproducible surface characteristics. Before filling, the chip was rinsed with Ethanol and dried with nitrogen. All inlet reservoirs were filled with 10 mM Hepes in demineralized water (adjusted with 0.1 M NaOH to pH 7.2). Hepes buffer was chosen, because of its low electrical conductivity to minimize the effect of Joule heating. To remove air bubbles from the channels and the chamber under pressure was applied to the reservoirs using a syringe. In the first experiment fluorescently labeled BSA (7.5 μM in 10 mM Hepes buffer) was added as a stream marker to both sample stream reservoirs. To study reaction dynamics, the calcium indicator fluo-4 (50 μM fluo-4 in 10 mM Hepes buffer, supplemented with 1 mM EDTA to bind free $Ca^{2+}$ present as contamination) was added to the reservoir of one of the sample streams and a calcium solution (10 mM $CaCl_2$ in 10 mM Hepes buffer) to the other.

## 7.4 Results and Discussion

### 7.4.1 Analytical Model

An analytical model was developed for calculating the required EOF potential settings to obtain the desired inlet flows. The developed model is based on an analogy of

electroosmotic flow to electrical circuits [146, 147]. It was developed to show the possibility of adjusting the position and width of the reactant streams individually by controlling only the applied voltages, thereby providing complete control over the reaction (zone).It is assumed that the parameters like electrical conductivity and fluid viscosity are homogeneous across the entire structure. The flow in the entire structure is driven only electroosmotically. Since there is no pressure difference applied across this structure, this Ohmic model analogy takes only the electrical field across the structure into consideration for flow rate calculations. Due to the non-uniform electrical field at the chamber entrance, it can be concluded that the velocity at the chamber entrance is different from the velocity after the flow stabilizes. It is obvious that these entrance effects cannot be completely removed. In order to simplify the calculations, entrance effects of the streams are neglected and it is assumed that the chamber velocity is uniform over the entire flow-chamber.

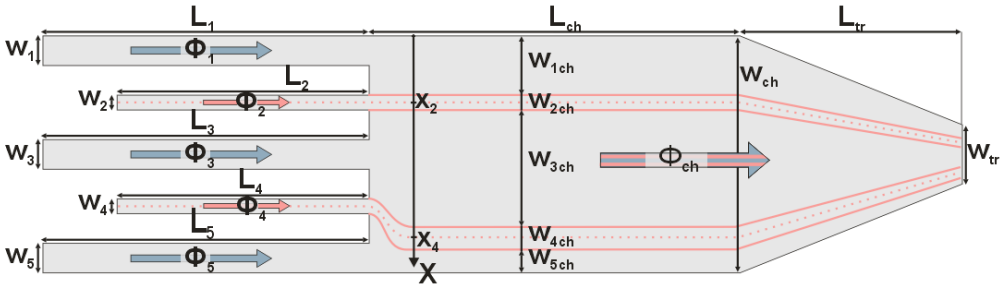


Fig. 7.5 Schematic drawing of the 2-sample electrokinetic steering chip with corresponding parameters.

Fig. 7.5 shows a schematic drawing of the 2-sample electrokinetic steering chip with all relevant geometrical and flow parameters. In order to determine the EOF potential settings it is necessary to know the corresponding channel and chamber fluxes. Due to mass conservation, the total flux $\Phi_{ch}$ inside the chamber is always the sum of the fluxes through the inlet channels:

$$\Phi_{ch} = u_{ch} A_{ch} = \sum_{i=1}^{5} \Phi_i \tag{7.1}$$

Where, $u_{ch}$ is the flow velocity inside the flow chamber and $A_{ch}$ is the cross-section of the rectangular part of the flow chamber. For clarity in calculations each channel is identified using an index $i$. It is possible to calculate each incoming flux $\Phi_i$ as a fraction

of the total flux $\Phi_{ch}$ by determining the ratio of the corresponding stream widths $W_{ich}$ (inside the chamber) to the total width of the flow chamber $W_{ch}$:

$$\Phi_i = \frac{w_{ich}}{w_{ch}} \cdot \Phi_{ch} \tag{7.2}$$

The stream widths $W_{ich}$ depends on the positions ($X_2$, $X_4$) and the widths ($W_{2ch}$, $W_{4ch}$) of the two sample streams. Therefore it is possible to replace the $W_{ich}$ in eq. (7.2) with the known parameters $X_2$, $X_4$, $W_{2ch}$ and $W_{4ch}$:

$$\Phi_1 = \frac{x_2 - \frac{w_{2ch}}{2}}{w_{ch}} \cdot \Phi_{ch} \tag{7.3}$$

$$\Phi_2 = \frac{w_{2ch}}{w_{ch}} \Phi_{ch} \tag{7.4}$$

$$\Phi_3 = \frac{x_4 - x_2 - \frac{w_{2ch}}{2} - \frac{w_{4ch}}{2}}{w_{ch}} \Phi_{ch} \tag{7.5}$$

$$\Phi_4 = \frac{w_{4ch}}{w_{ch}} \Phi_{ch} \tag{7.6}$$

$$\Phi_5 = \frac{w_{ch} - x_4 - \frac{w_{4ch}}{2}}{w_{ch}} \Phi_{ch} \tag{7.7}$$

For further calculations of the electrical voltages, the fluidic network (channels and chamber) have to be replaced by their analogous electrical resistance as shown in Fig. 7.6. Since the flow in the inlet channels is induced electroosmotically, the flux depends on the applied electrical field and the electroosmotic mobility (according to the Helmholtz-Smoluchowski equation):

$$\Phi_i = u_i A_i = \mu_{EOFi} E_i A_i = \mu_{EOFi} \frac{V_i - V_{ch}}{L_i} A_i \tag{7.8}$$

where, $u$ is the fluid velocity, $A$ the cross-section of the channel, $\mu_{EOF}$ the electroosmotic mobility, $E$ the electric field, $L$ the length of the channel, $V$ the applied voltage at an inlet reservoir and $V_{ch}$ the electrical potential at the entrance to the flow chamber. For simplification, it was assumed that the electrical field at the flow-chamber entrance is uniform (as displayed in Fig. 7.6 by the junction of the five

resistors). For a straight channel of length $L$, cross-section $A$ and which is filled with a solution of electrical conductivity $\sigma_i$, the electrical resistance is given by:

$$R_i = \frac{L_i}{\sigma_i A_i} \tag{7.9}$$

And for the flow chamber with its rectangular part (length $L_{ch}$ and cross-section $A_{ch}$) and trapezoid part (length $L_{tr}$ and outlet cross-section $A_{tr}$) electrical resistance is given by:

$$R_{ch} = \underbrace{\frac{L_{ch}}{\sigma A_{ch}}}_{\text{Rectangular}} + \underbrace{\frac{L_{tr}}{\sigma(A_{ch} - A_{tr})} \ln\left(\frac{A_{ch}}{A_{tr}}\right)}_{\text{Trapezoid}} \tag{7.10}$$

To calculate the voltage drop across the channels ($V_i$ - $V_{ch}$) and thereby the flux in each channel, the electrical potential $V_{ch}$ has to be calculated first. This can be obtained by calculating the total electrical current in the chamber $I_{ch}$:

$$I_{ch} = \sum_{i=1}^{5} I_i \quad \Rightarrow \frac{V_{ch}}{R_{ch}} = \sum_{i=1}^{5} \frac{V_i - V_{ch}}{R_i}$$

$$\Rightarrow V_{ch} = R_{ch} \cdot \sum_{i=1}^{5} \frac{V_i - V_{ch}}{R_i} \tag{7.11}$$

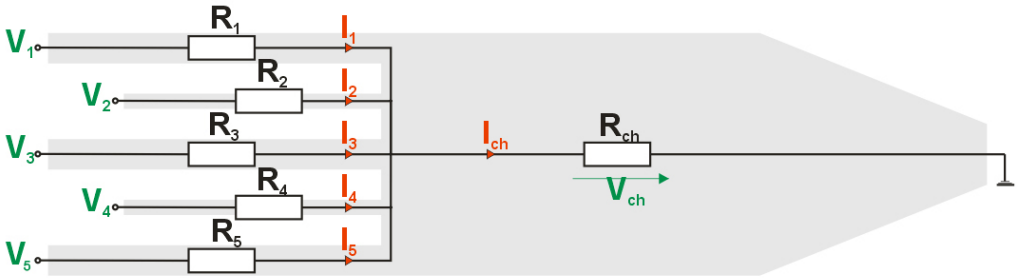


Fig. 7.6 Electrical circuit for a 2-sample electrokinetic steering chip.

With eqs. (7.8) and (7.11) it is now possible to calculate $V_{ch}$ as follows:

$$V_{ch} = \frac{R_{ch}}{\mu_{EOFi}} \cdot \sum_{i=1}^{5} \frac{\Phi_i L_i}{R_i A_i} \tag{7.12}$$

Finally, from eqs. (7.8) and(7.12), $V_i$ can be deduced:

$$V_i = \frac{\Phi_i L_i}{A_i \mu_{EOFi}} + \frac{R_{ch}}{\mu_{EOFi}} \cdot \sum_{j=1}^{5} \frac{\Phi_j L_j}{R_j A_j} \tag{7.13}$$

Using eq. (7.13) it is possible to calculate all five voltages needed to obtain any desired regime of positions, widths and velocities of the two sample streams.

### 7.4.2 Experimental Results

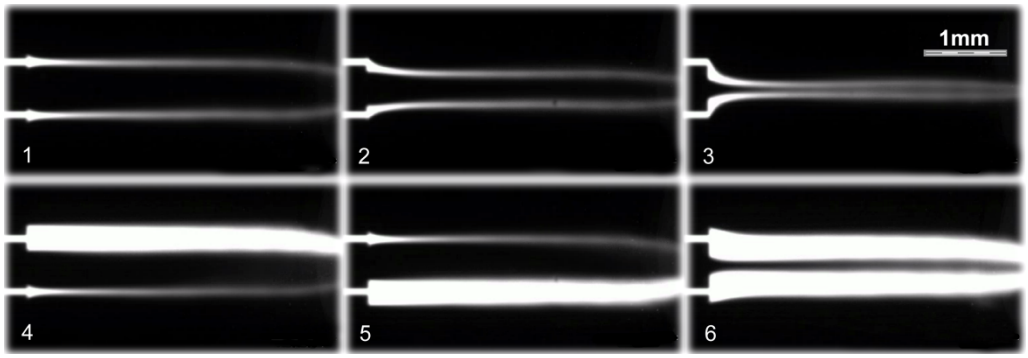


Fig. 7.7 Different stream positions and widths of the two sample streams visualized with fluorescently labeled BSA. The flow (velocity $u_{ch} \approx 750\ \mu m\ s^{-1}$) direction is from left to right.

Fig. 7.7 shows images of the 2-sample steering device working under different guiding potential settings. Positions and widths of the sample streams were changed keeping the velocity inside the flow-chamber constant (750 µm $s^{-1}$). It can be observed in the top three images (1, 2 and 3 in Fig. 7.7) that the distance between the two sample streams was reduced from 625 µm to 10 µm while maintaining the width of both sample streams at 50 µm. In image 4 of Fig. 7.7, the width of sample stream 1 was set to 200 µm and that of sample stream 2 to 50 µm. In image 5 of Fig. 7.7 the width of sample stream 1 was set to 50 µm and that of sample 2 stream to 200 µm. In image 6 of Fig. 7.7 both the streams were set to 200 µm in width and the distance between the two streams was set to 50 µm. Confirmation of the chamber velocity was done using a conventional stopwatch measurement technique. Stream positions and widths (full-width-half-maximum method) were measured using the AnalySIS software.

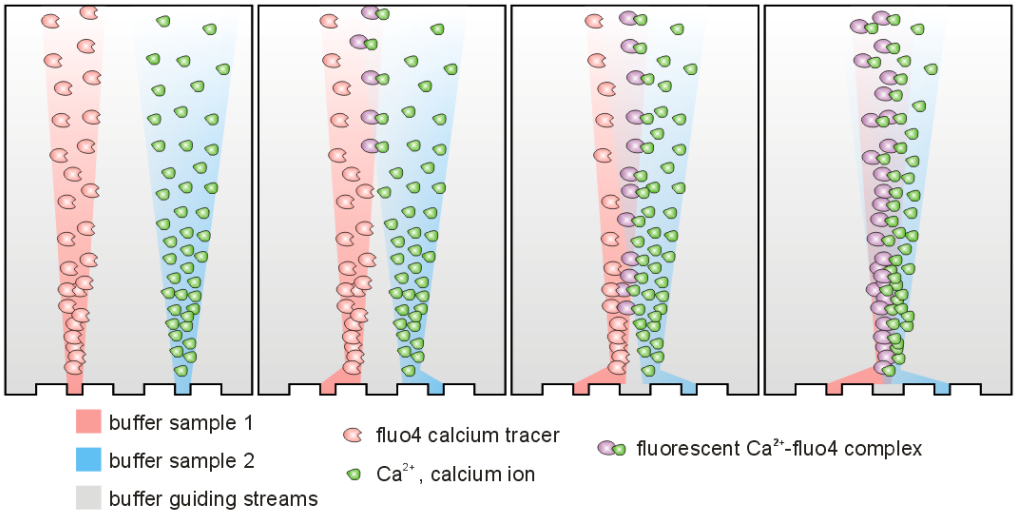


Fig. 7.8 Schematic Illustration of the microreactor with a fluorescent calcium tracer and a calcium solution as reagents.

When reacting components are added to the sample stream reservoirs, the 2-sample electrokinetic steering chip can be used as a microreactor. By adjusting the positions and the widths of the two sample streams, the overlapping region (reaction zone) of the diffusive reagent profiles can be adjusted. To show that the chip can be used as a microreactor, the following experiment was performed, which is illustrated in Fig. 7.8. First the chip was completely filled with the buffer solution. After that, one sample stream reservoir was emptied and refilled with fluo-4 (a calcium indicator). The other sample stream reservoir was filled with the $CaCl_2$ solution. The flow velocity in the chamber was set to 250 µm $s^{-1}$. After binding with calcium, fluo-4 will strongly increase its fluorescence. The fluorescence of the calcium indicator was measured with the microscope setup described in Sec. 7.3.2.

Fig. 7.9 shows a picture series with images which were taken during the experiment. In Fig. 7.9 (images 1 to 6), it can be observed that the reaction yield (fluo-4/$Ca^{2+}$ complex) became higher as the distance between the two sample streams was consistently reduced. In Fig. 7.9 in can be seen that the overlapping reaction region is asymmetric. This is due to the difference in the diffusive profiles of the fluo-4 (diffusion coefficient $D_{fluo4} \approx 2 \times 10^{-10}$ $m^2$ $s^{-1}$ [148]) as well as the calcium (diffusion coefficient $D_{Ca2+} \approx 1.6 \times 10^{-9}$ $m^2$ $s^{-1}$ [148]) reactant streams. In the reaction zone, mixing is dominated by the diffusion of $Ca^{2+}$, which is smaller than Fluo-4 and was used in

excess. It can also be observed in Fig. 7.9 that the fluo-4 indicator stream exhibits a background fluorescence when entering the reaction-chamber. This might be due to contamination of undesired calcium in the buffer solution or due to self fluorescence of the unbound fluo-4 molecule.

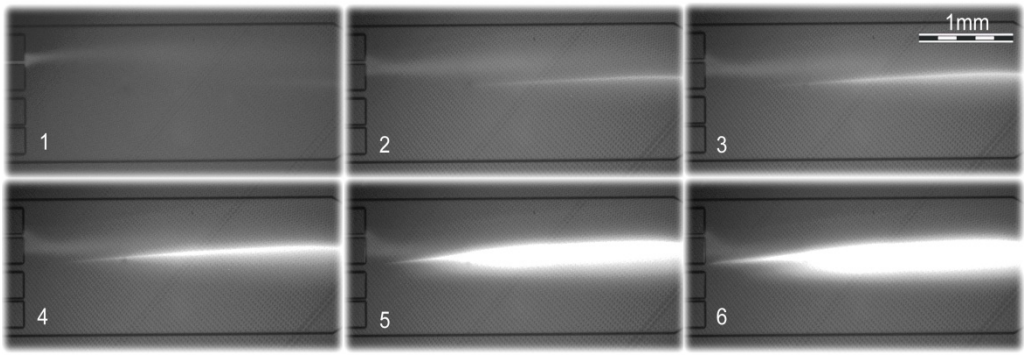


Fig. 7.9 Fluorescence microscope images showing different intensities of the reaction product: Fluo-4/ $Ca^{2+}$. From picture 1 to 6 a decrease of distance between the two reactant streams resulted in an increasing yield of the Fluo-4/ $Ca^{2+}$ complex. The flow (velocity $u_{ch} \approx 250\ \mu m\ s^{-1}$) direction is from left to right.

### 7.4.3 Simulations

In addition to the experiments, the presented microfluidic structure was simulated using the software package CFDRC (CFD Research Corporation, Huntsville, AL 35805, USA). For a chemical reaction it could be of interest to be able to vary the reaction yield without changing the reactant concentrations or flow velocity in the reaction chamber. The following simulation was performed to show the possibility of stabilizing the reaction yield even in the case of a fluctuating reactant concentration, by adjusting the positions and widths of the reactant streams.

In this simulation the overlapping region of the two diffusive sample streams (both containing the same sample with a diffusion coefficient $D=1x10^{-8}\ m^2\ s^{-1}$) was studied, for different positions and widths (of the two sample streams). This was done by calculating the variation of the concentration along the centerline of the overlapping region. The microfluidic device was approximated as a 2D structure with approximately 7000 grid-cells. The simulation was performed with “no-slip conditions at walls”. The electrical boundary conditions were obtained from the analytical model. Both sample-streams were programmed to contain an equivalent concentration of sample and to have a width of approximately 100 µm. The electroosmotic mobility

was set to $5x10^{-8}$ $m^2$ $(Vs)^{-1}$ for all guiding as well as sample streams. An overlapping region between the two sample streams was established at a velocity of 400 µm $s^{-1}$ in the flow-chamber. Fig. 7.10 illustrates three curves representing concentration profiles along the centerline of the overlapping region (in flow direction) during the simulation. Line 1 in Fig. 7.10 shows the optimal concentration profile that results in case of two identical streams (same width and concentration). Then the concentration of sample-stream 1 was reduced to 50% of the original value while the concentration of sample-stream 2 was left unchanged.

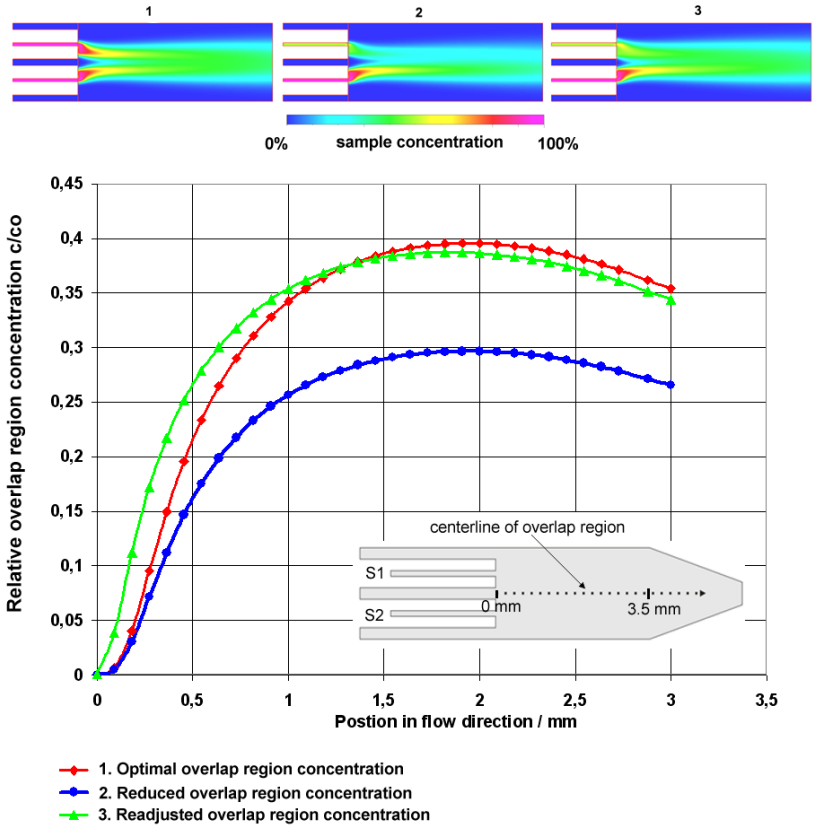


Fig. 7.10 Diagram showing three overlap region concentration profiles obtained from CFDRC simulation. Line 1 shows the optimal concentration with two identical streams. Line 2 represents the concentration after reducing the inlet concentration of stream 1 to 50% of its original value. Line 3 represents the concentration after adjusting the width and the position of stream 1 to achieve a similar concentration as in line 1. The respective stream positions and their concentrations can be seen in the top three images.

The decreased sample concentration in the first sample-stream causes a drop of the concentration, which would lead to a reduced reaction yield, in the overlapping region (Fig. 7.10, line 2) to 75% of the previous value. By changing only the width and the position of the first sample-stream, a new concentration profile was established that closely resembles the optimal concentration profile (Fig. 7.10, line 3).

## 7.5 Conclusions

An adjustable diffusion based microfluidic reactor has been designed and successfully fabricated. Electroosmotic flow was used as a pumping technique inside the channels. Due to this no external pumps or other sophisticated systems were needed. Experimental and simulation results showed that the reaction yield can be manipulated by controlling the EOF potential settings. This device allows to adjust the reaction yield inside the reaction-chamber even in case of fluctuating reactant concentrations. Since always the ratio of all inlet flows is proportionally varied, the flow-rate inside the reaction-chamber remains constant while the reaction yield is manipulated. Furthermore an analytical model, based on an electrical circuit has been developed and tested. This model makes it possible to control the position and width of reagent streams real-time in a predictable way. The chip can be used as a new component for upcoming Lab-on-a-chip or μ-TAS technology.

# 8 Hyphenation Approach: FFE-SPR

*The final goal of this thesis was to combine a miniaturized free-flow electrophoresis device for the continuous separation of proteins and surface-plasmon resonance to monitor affinity based interaction. Due to various technical problems of integrating the SPR gold region into the previously described FFE chips, an adapted chip design was introduced and new materials were applied. In this chapter the results achieved so far are shown and discussed. This chapter gives mostly aspects on fabrication, principles and the planned approach towards the proteomics-on-a-chip device.*

## 8.1 Abstract

A new hyphenated microfluidic system incorporating free-flow electrophoresis for separation purposes and surface plasmon resonance imaging as detector of the separated compounds was successfully fabricated. The principal layout is explained and certain aspects of the fabrication are given. A measuring strategy was developed applying a rheumatoid arthritis related model system based on molecular antibody-antigen interactions. This device is intended for future proteomics-on-a-chip applications; however, certain hurdles remain to be overcome.

## 8.2 Introduction

Miniaturized free-flow electrophoresis systems have recently gained interest and experimental results have demonstrated that in contrast to their large counterparts microfluidic FFE devices reach higher separation resolution and work more efficiently. The major advantage is obviously their high ability to be integrated into more complex analysis systems [95]. Although it was proposed already 15 years ago,

until now no hyphenated fully microfabricated FFE devices were introduced to the public. This was mainly due to the fact that stand-alone µ-FFE chips were and are still undergoing further development and improvement, rather than that the focus can be on more complex systems. Miniaturized FFE devices are capable of separating very low sample volumes within the nanoliters range in a very short amount of time. Because of this ability to separate nano-liter sample volumes, fluid interfacing and sample handling for further processing becomes crucial and not a straightforward task. Certainly, in disease related proteomics research high sample volumes are often rare and fast separation and analysis times are beneficial. These requirements give rise to the desire to implement a bio-chemical detection unit into the sample separation device in order to avoid further manual and offline processing. In this chapter, a new microfluidic free-flow electrophoresis chip is introduced which incorporates a surface plasmon resonance detection region to follow and monitor bio-molecular affinity based interactions after the electrophoretic separation, in order to extract relevant sample and therefore patient information. The chips were successfully fabricated and with regard to the "proteomics-on-a-chip project for monitoring autoimmune diseases", a first experimental model system was chosen, which could add insight in understanding the mechanism of autoimmune factors involved in rheumatoid arthritis disease. In recent research it was found, that serum antibodies reacting with citrullinated proteins and peptides are very sensitive and specific markers for rheumatoid arthritis [149]. Therefore, digested citrullinated fibrinogen, a common protein involved in the blood clotting process and furthermore possibly playing an important role in rheumatoid arthritis disease, was selected as the compound to be separated and detected by the FFE-SPR device. The principal layout and the experimental approach are explained in the following section.

### 8.2.1 Principle

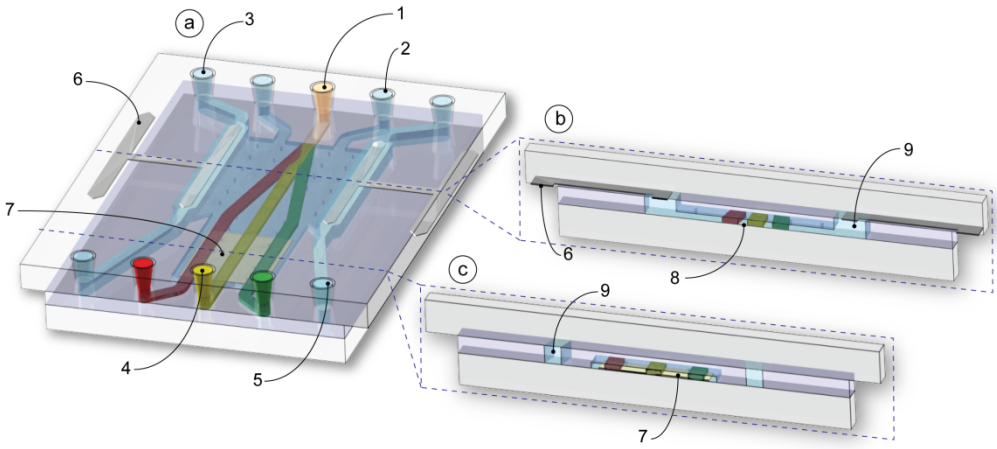


Fig. 8.1 Schematic illustration of the FFE microfluidic chip with integrated SPR sample immobilization and detection region; (a), FFE-SPR chip with three components separated; (b), cross section of the shallow separation region and deeper electrode channels; (c), cross section of the SPR detection region. (1), Sample inlet; (2), sheath flow inlet; (3) electrolyte inlet; (4), fraction outlet, (5), electrolyte outlet; (6), electrode contact pad; (7) SPR gold detection region; (8) separation region; (9) deep electrode channel with integrated Pt electrode; (dimensions are not to scale)

As shown in Fig. 8.1 the FFE-SPR chip incorporates the FFE separation region and a SPR gold monitoring region. The device has five inlets and for practical reasons five outlets. If FFZE is applied, the center inlet is used to inject the sample which is hydrodynamically focused between two sheath flow streams containing buffer solution only in order to confine the sample stream width (compare chapter 3). The two outer inlets are used to infuse the electrode solutions. If FFIEF is applied, ampholyte solutions are introduced through the three center inlets, while a solution of high pH and of low pH respectively is pumped through the flanking outer inlets (compare chapter 4). In contrast to earlier μ-FFE devices presented in this thesis, here the electrodes are placed inside the chip and no additional membranes are used to isolate the separation region from the electrodes. Instead, the two parallel outer electrode channels supplying the electrolyte surrounding the electrodes are roughly 25 times higher, than the intermediate shallow separation region (see cross sections in Fig. 8.1.b and c). In this configuration bubbles formed during electrolysis are supposed to be flushed away efficiently without disturbing the separation.

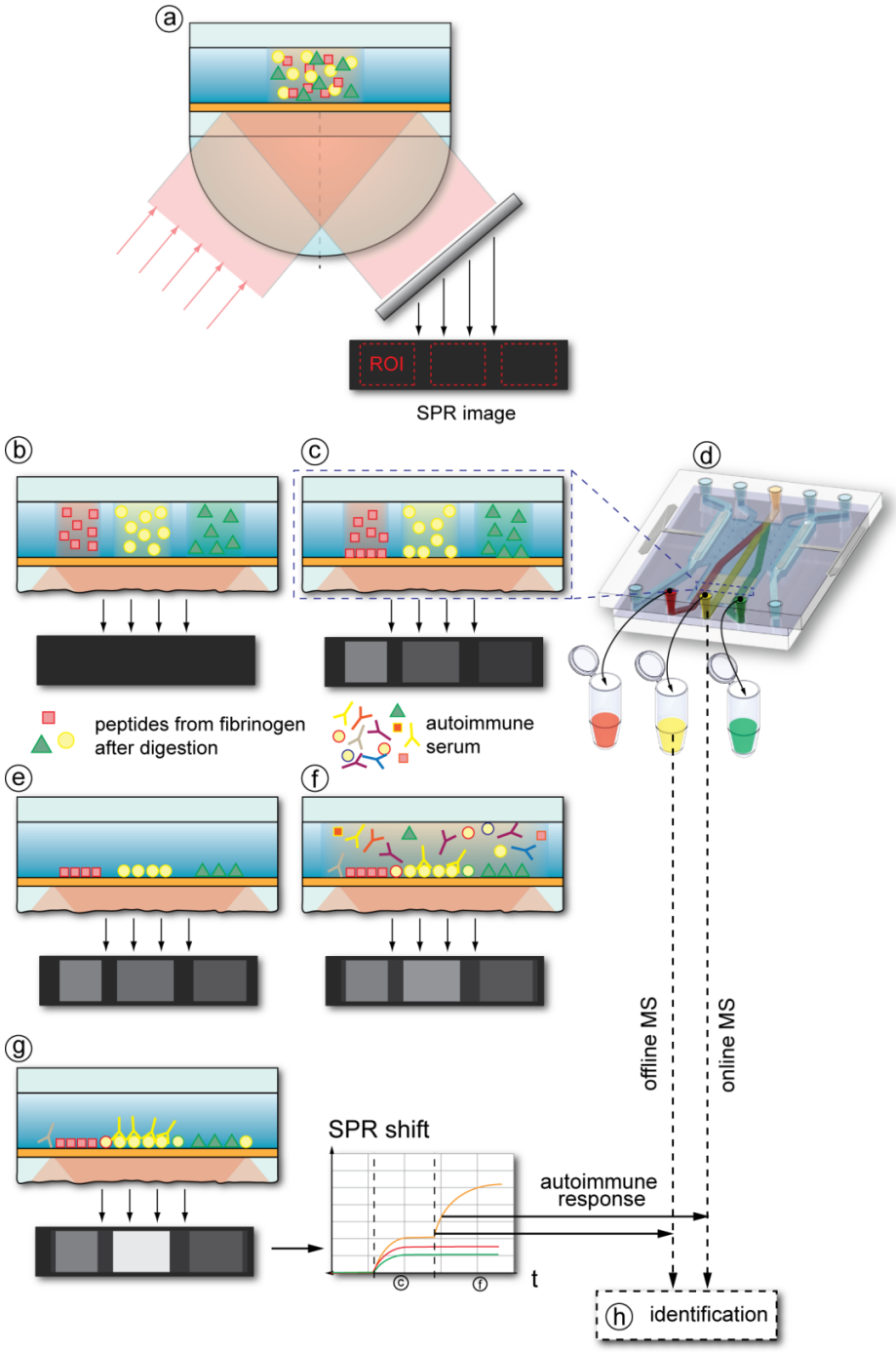
a
ROI
SPR image
b
c
d
peptides from fibrinogen
after digestion
autoimmune
serum
e
f
g
SPR shift
autoimmune
response
t
offline MS
online MS
h identification

Fig. 8.2 Illustration of the FFE-SPR approach: Towards Rheumatoid Arthritis biomarker discovery. (a-g) Various device cross-sections over the analysis period demonstrate the planned proteomics-on-a-chip approach; (a), A citrullinated and digested fibrinogen sample is injected into the FFE device and (b) separated by FFZE or FFIEF in order to achieve adjacent lanes. (c), The separated peptides become immobilized by non specific absorption on the SPR gold surface, whereby the accumulation can be followed in the SPR signal as the grey values change. (d), During separation fractions are collected in various containers (or injected directly into an MS system). (e), Flushing followed by (f) the injection of a diluted RA patient serum containing specific RA antibodies whereby biomolecular interactions can be followed real-time in the SPR sensorgram. (g), Fractions with positive response to the RA serum will be analyzed by (h) MS.

This design principle was successfully applied earlier by Fonslow et al.[50], as discussed in chapter 2.4.1**.** As an alternative to prevent bubble formation or in addition, the formation of gas bubbles can be chemically suppressed as demonstrated in chapter 5. Although the design shown here puts higher demand on the fabrication, the conductive acrylamide membranes introduced earlier in this thesis were found to have more disadvantages and were therefore not further investigated for this approach. During operation the chip was placed in an imaging SPR instrument, as illustrated in Fig. 8.5.

Eventually, the device is supposed to be applied in proteomics research (here specifically autoimmune disease research), whereby the principal analysis sequence consists of four main steps: i) separation, ii) immobilization, iii) interactions and iv) identification. This procedure is illustrated in Fig. 8.2 and described in more detail in the following.

A digested and citrullinated fibrinogen protein sample is introduced into the FF-SPR chips (Fig. 8.2.a) and the different citrullinated peptides become separated according to their mobility or isoelectric point (Fig. 8.2.b), depending on the applied FFE separation method. The fractions separated in the FFE part flow over the SPR gold region where the molecules become immobilized in adjacent lanes on top of the SPR gold surface, which can be monitored by changing gray values in the corresponding SPR image (Fig. 8.2.c). Immobilization is achieved either by simple adsorption or by appropriate more specifically binding surface coatings (not further investigated in this thesis). Furthermore, the separated fractions will be collected for further off-line analysis (Fig. 8.2.d). The immobilization is followed by a washing step (Fig. 8.2.e) and subsequently by flushing the device with patient serum containing diluted autoimmune antibodies (Fig. 8.2.f). The positive interaction of autoimmune

antibodies with the on the surface immobilized complementary antigens (here citrullinated peptides) causes a significant change in the SPR signal (Fig. 8.2.g), which is constantly monitored to furthermore extract binding-kinetics related molecule properties. Finally, the fractions collected during the separation which showed positive response to the patient serum will be further analyzed for identification purpose, e.g. by MS (Fig. 8.2.h). This can be achieved either off-line or in a more advance approach also online, e.g. by coupling the chip outlets to an ESI-MS system (not investigated here).

## 8.3 Experimental

### 8.3.1 Materials and Reagents

If not otherwise stated, all chemicals were obtained from Sigma-Aldrich-Fluka. Solutions were degassed in vacuum prior to application.

### 8.3.2 Chip Fabrication

Common in microfluidic glass chip fabrication is the thermal bonding of two glass wafers at app. 600 °C. This method was applied for most of the chips presented in this thesis. However, here a high temperature treatment would lead to deterioration of the sensitive SPR gold layer. To overcome this problem a low temperature bonding method with PDMS as an intermediate layer was chosen, as briefly explained in the following section. The fabricated FFE-SPR chip consists of three separately fabricated and finally bonded layers, as illustrated in Fig. 8.3: i) The top Borofloat glass layer (t = 1.1 mm) contains the inlets, outlets and the platinum electrodes. (ii) The intermediated PDMS layer (t = 0.4 mm) contains the separation chamber (h = 15 μm), connecting microchannels and the deeper electrode channels (h = 0.4 mm). iii) The bottom D263 glass layer (t = 1.1 mm) contains the SPR gold detection region.

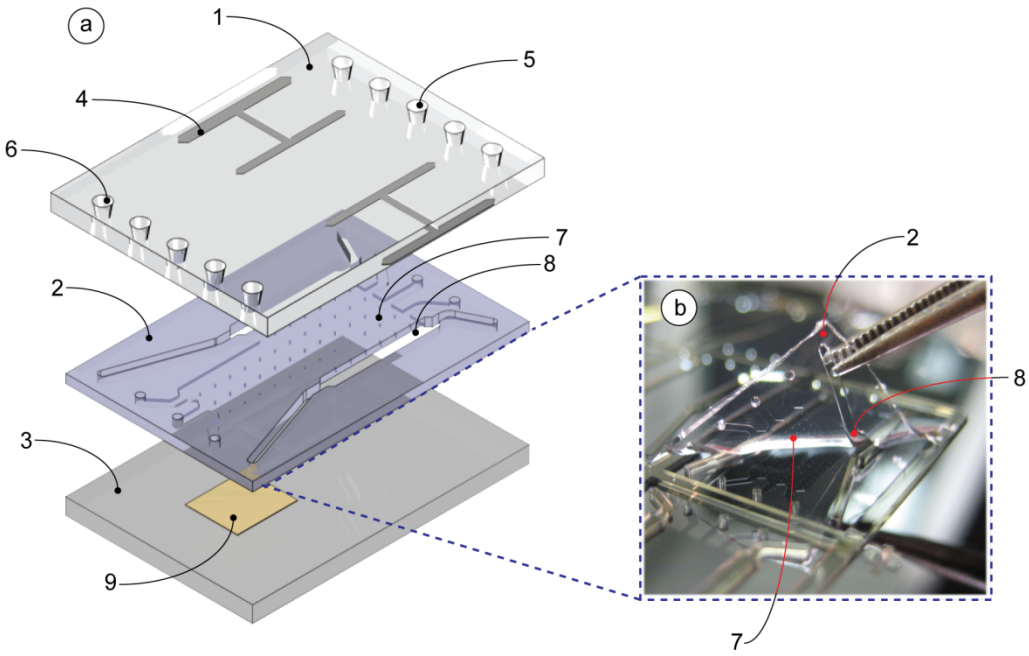


Fig. 8.3 (a) Assembly illustration of the three layer FFE-SPR chip with (b) Photograph of the intermediate PDMS chip during fabrication, in particular during the chip release from the mold; (1), 1.1 mm Borofloat glass chip; (2), 0.4 mm PDMS layer; (3), 1.1 mm D263 glass chip; (4) Pt electrodes; (5), channel inlets; (6); channel outlets; (7) 15 µm deep separation and detection region; (8), 0.4 mm deep electrode channel; (9); SPR gold surface; (dimensions are not to scale)

i) For the top layer a photolithography step was carried out to transfer the pattern of the electrodes onto the surface of the top Borofloat 33 glass wafer (Schott Jenaer Glas, Germany). Subsequently a 10 nm chromium adhesion layer was sputtered on top of the wafer followed by a 190 nm platinum layer. A lift-off in acetone was performed, leaving the platinum electrodes on the surface. A powder blasting step was performed with 30 µm diameter $Al_2O_3$ particles to create the inlet and outlet holes for fluidic connections. For more details the reader is referred to relevant references [97, 98]. Finally the wafer was diced into separate chips of 14.5 mm x 18.5 mm. The fabrication of the top-layer and the SU8 mold wafer was carried out by Lionix (Lionix Bv, The Netherlands).

ii) To fabricate the intermediate PDMS layer a mold was created applying soft lithography techniques using the photo resist SU8. Therefore, a silicon wafer was first coated with a 15 µm thick layer of SU8 and the pattern of separation chamber and

inlet channels transferred by photolithography. A layer of SU8 of 400 µm thickness was then spun on top of the first layer and the pattern of the electrode regions was transferred by photolithography. After appropriate backing steps, both SU8 layers were developed removing the unexposed regions and leaving a two layer relief-like structure. The fabricated SU8 wafer was placed in an in-house developed PDMS molding press. A 10:1 mixture of PDMS monomer and cross linker was prepared by thoroughly mixing and degassing and filled into the molding press covering the entire SU8 surface. A transparency foil followed by a thin metal plate was placed on top of the SU8 mold. By applying pressure to this sandwiched molding structure, surplus PDMS was squeezed out leaving a PDMS layer of well defined thickness as soon as the transparency foil reached the highest SU8 structure. The molding press was placed at 80 °C for 1 hour to cure the PDMS. Afterwards, the SU8 wafer including the PDMS layer was removed from the molding press. The chip design included a square border of SU8 allowing an easy "ready to use" PDMS chip release, as shown in Fig. 8.3.b, with no need for cutting out the chips or punching additional holes. For more details on the so called soft-lithography fabrication process one is referred to recent literature [150, 151].

iii) For the bottom chip layer, a standard photolithography step was carried out on a D263 glass wafer to transfer the pattern of the SPR gold region. Subsequently, an adhesion layer of titanium followed by the SPR gold layer was evaporated onto the glass wafer. The evaporation of the SPR gold was carried out by Ssens (Ssens Bv, The Netherlands). A lift-off in acetone was performed leaving the defined gold regions on the surface. Finally the wafer was diced into separate chips of 12.5 mm x 18.5 mm in size.

All chip layers were placed in a plasma oxidizer (50% oxygen, 110 W output) and exposed to plasma for 10 seconds [152]. Consequently, the activated PDMS surface and the cleaned glass surfaces allowed for a direct and permanent bonding of all three layers, whereby the alignment was performed manually, with the final chip shown in Fig. 8.4. To prevent a collapsing of the shallow separation region during bonding, an array of micro pillars was included into the design to enhance the mechanical stability.

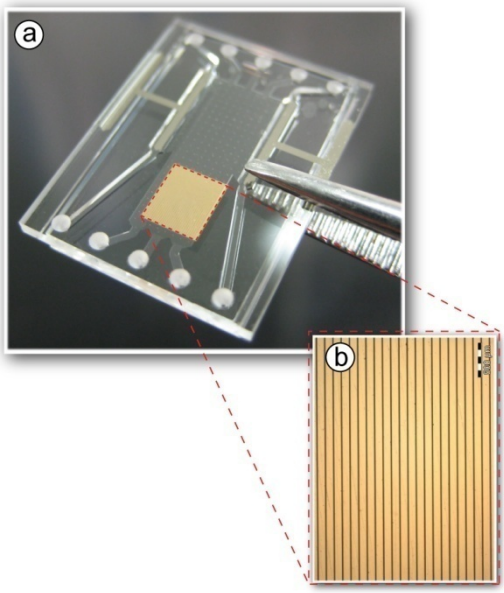


Fig. 8.4 (a), Photograph of the fully assembled FFE-SPR chip. The chip is 14.5 mm x 18.5 mm in dimensions with a thickness of 2.6 mm. The top plate overlaps the sandwiched PDMS layer and the bottom glass chip by 1 mm on both sides to allow the electrodes to be contacted from the bottom side. (b) Inset photograph of the SPR gold region (surface: 4 mm x 3.5 mm). To avoid short circuiting the gold surface is divided into adjacent 100 µm wide separate lanes with 10 µm spacing.

### 8.3.3 Setup and Methods

The fabricated chips were placed in an in-house fabricated holder with an integrated glass hemisphere matching the refractive index of the bottom glass chip of the FFE-SPR device, as shown in Fig. 8.5 (with an old chip design, later discarded). Syringe pumps (CMA/102, Microdialysis, Sweden) were used to control the flow rates. 1 mL glass syringes (Microdialysis, Sweden) were filled with the required solutions and connected via glass capillaries (Aurora, The Netherlands) and Nanoport connectors (Upchurch Scientific, USA) to the in-house fabricated chip holder. The two integrated platinum electrodes were connected to a power supply (HVS448-3000, Labsmith, USA). Power supply and syringe pumps were controlled in real-time with a personal computer and Labview software (National Instruments). The holder was placed inside the imaging surface plasmon resonance instrument (iSPR-IBIS, IBIS Technologies B.V., The Netherlands).

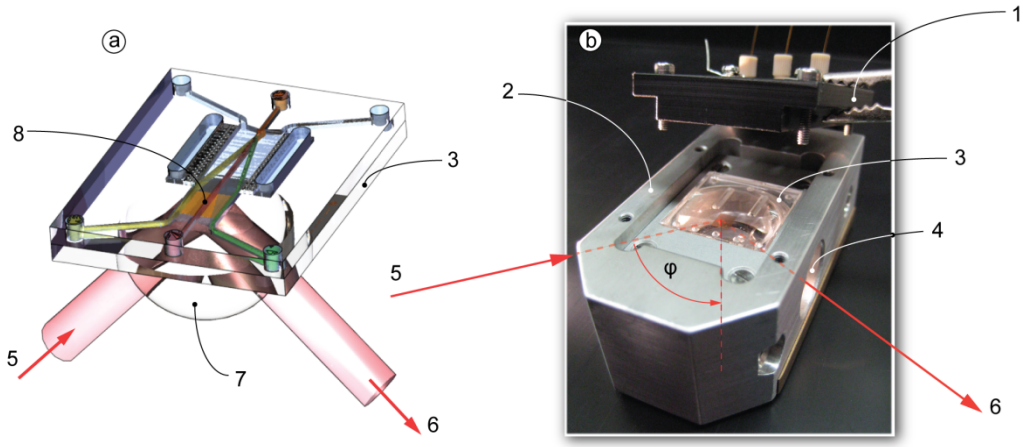


Fig. 8.5 (a) Illustration of the FFE-SPR microfluidic chip with hemisphere and light path; (b) Photograph of the chip holder; (1), holder lid with electrode capillary connections; (2), chip holder/slider to be inserted into the SPR instrument; (3), FFE-SPR chip (here old concept, later discarded); (4), holder opening for light path; (5), incoming polarized monochromatic light beam; (6), reflected light beam towards CCD chip; (7), hemisphere; (8), SPR gold region;

## 8.4 Results and Discussion

As described in the introduction chapter, the SPR signal is dependent on the refractive index near the measurement surface, in fact the generated plasmons penetrate as far as several 100 nm into the solution. Therefore not only molecules adsorbed to the surface as commonly applied in proteomics research cause changes of the SPR signal but also fluids of different refractive index can be easily visualized. This approach was followed as a first preliminary experiment to test the FFE-SPR equipment, whereby isopropanol was used as a sample stream and water as sheath flows, as shown in Fig. 8.6. For this purpose an earlier fabricated FFE-SPR chip entirely manufactured from glass was applied. This chip included a similar SPR gold region as described earlier in this chapter and the FFE separation device with permeable acrylamide membranes as described in chapter 3. Unfortunately, the implementation of the SPR gold region into this glass FFE chip and the required 400-600 °C (glass-glass) bonding temperature caused significant changes to the gold properties and therefore to the SPR capability. We concluded that titanium from the underplaying adhesion layer migrated into the 60 nm thick SPR layer. This approach was eventually rejected and with the search for alternative low-temperature chip bonding methods, finally we developed the

multilayer chip presented in section 8.3.2 which is more suitable for upcoming experiments. Due to this, the fabrication of this primary chip and observed phenomena are not further discussed in this thesis.

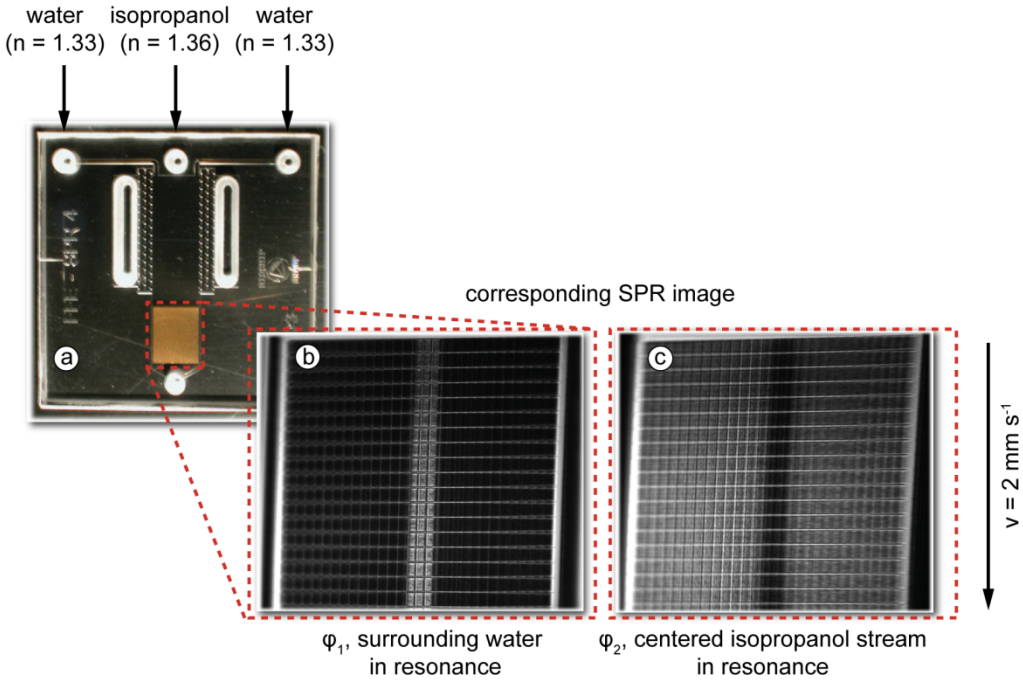


Fig. 8.6 Preliminary experimental results showing the SPR signal of isopropanol hydrodynamically focused between water. (a), photograph of the FFE-SPR chip (chip design later discarded); (b), incident light angle $\Phi_1$ = 68 deg: SPR image showing the surrounding water in resonance; (c), incident light angle $\Phi_2$ = 70 deg: SPR image showing the centered isopropanol stream in resonance.

It can be clearly seen in Fig. 8.6 that the sample (ethanol n = 1.36) solution and the surrounding water cause different light reflection intensities. In Fig. 8.6.b the light incident angle was set to 68 deg which is the SPR resonance angle for water in the applied system. Due to that, the gold region covered with water shows the lowest light reflection intensity. In Fig. 8.6.c the light incident angle was set to 70 deg which is the SPR resonance angle for isopropanol in the applied system. This angle shift caused a reversed situation. Now the light reflection intensity of the surrounding water was higher than the sandwiched ethanol stream. The above experiments clearly show that the measurement equipment works and the on-line measurement principle functions, but no separation was performed.

## 8.5 Conclusions

A new microfluidic chip was developed which will be utilized for proteomics-on-a-chip research. The chip contains a continuous separation region based on FFE and a SPR detection gold area. We furthermore developed a new biomarker discovery approach to get more insight in rheumatoid arthritis. In future this chip will be used for sample separation and affinity based interaction studies. Here we showed the successful fabrication of this device and preliminary results demonstrate the functionality of the device. Several hurdles still have to be taken when considering realistic patient samples and their high protein complexity. However, the results shown so far are promising and haven't been demonstrated so far.

# 9 Conclusions and Recommendations

*This chapter gives overall conclusions on the results achieved within the four year research project on developing a microfluidic FFE device and integrating a SPR detection region for e.g. monitoring bio-molecular interactions. Furthermore, recommendations for future developments and related projects are discussed.*

## 9.1 Conclusions

As defined in the project goals, microfluidic free-flow electrophoresis was chosen as the separation method for the proteomics-on-a-chip device. Although a miniaturized FFE device was introduced to the public already in 1993 and frequent innovations within this field led to further improvements, the published results until 2004 seemed insufficient in terms of reliability, separation efficiency and capacity to be effectively used in our project. Therefore, it was of main importance to first develop an improved FFE chip, prior to the planned implementation of a biochemical detection unit.

With the application of a new membrane structure to separate separation region and electrode compartments, namely a photo polymerized acrylamide gel, we could successfully develop a new glass-glass microfluidic FFE chip. These conductive membranes flanking the separation chamber prevented gas bubbles formed during electrolysis from disturbing the separation. Furthermore, this principle proved to be efficient in terms of voltage efficiency. The chip device was successfully characterized by the rapid separation of various fluorescent dyes in free-flow zone electrophoresis and free-flow isoelectric focusing within seconds and below. For the first time a sample steering method during FFZE was demonstrated allowing selection of specific fractions. This was achieved by controlling the sheath flow-rates which hydrodynamically focused the sample stream. Furthermore, in contrast to previous

publications on FFIEF where parts of the pH gradient were inaccessible, the device shown here was capable of separating within a full wide range pH gradient (pH 3-11).

Since IEF separation methods are commonly used in proteomics research, an improved glass FFE chip had to be developed in order to enhance the separation capability especially for FFIEF. This was indeed achieved by incorporating additional sheath flows and the application of a pre-separated ampholyte buffer system. This led to drastically improved separation times and increased peak capacity and results not exceeded so far.

Although the devices mentioned above performed well in terms of separation, the mechanical stability of the acrylamide membranes turned out to be insufficient for prolonged use at flow velocities higher than 4 mm $s^{-1}$. Therefore the flow velocity was usually limited to avoid breakage of the membranes and resulting leakage. As a consequence a redesigned FFE chip was investigated. As a new feature, surface electrodes were integrated into the closed separation chamber allowing for higher flow rates. The generation of gas bubbles caused by electrolysis was successfully suppressed by adding an alternative redox-couple. Instead of the reduction and oxidization of water molecules, the electrical current was conducted by the oxidization and reduction of quinhydrone. This approach was limited in terms of electrical current, allowing only for certain applications such as FFZE, where usually lower currents are involved.

With respect to the planned integration of SPR, a third chip concept was introduced which included the SPR sensing region. This three layer glass-PDMS-glass chip allowed for room temperate bonding. This was necessary to avoid temperature related damage to the gold sensor, which turned out to be a critical issue in our previous FFE chips. Furthermore, an elegant solution with deep electrode channels and a shallow separation region (adapted from literature) was applied in order to prevent gas bubbles from entering the separation region. The chip was successfully fabricated. A measurement approach was developed for a first proteomics-on-a-chip experiment, with respect to the final project goal: Proteomics-on-a-chip for monitoring autoimmune diseases.

In general we can conclude, that technological advances and developments in the field of microfluidic FFE as presented not only in this thesis but also in other recent reports, have led to great and promising improvements. Innovations still occur and the

possibilities for more complex analytical μ-FFE based systems, rather than pure separation devices as proposed already many years ago seem more realistic now.

In addition to the FFE research we also investigated two proteomics-on-a-chip related continuous flow devices. In order to allow multiple sample streams, a new chip was introduced in which two laminar flow streams were independently controlled in order to perform bio-chemical reactions and assays. This steering method, although based purely on electrokinetic effects, was related to the sample steering performed during FFFZ. The capability of the device was tested with a calcium tracer compound in the first reactant/sample stream and a calcium chloride solution in the second stream. The results clearly indicate that the devices allowed for a full reaction intensity control. With respect to more biochemical investigations-related approaches the device was not further investigated. However, a similar technology was applied for a related chip designed to be applied for a microfluidic array spotting method. In this chip two perpendicular independent sample streams could be used to sequentially coat the surface in order to create a bio-chemical sensing array, for possible integration in the FFE-SPR device. The principle was tested with a set of fluorescent dyes but not further investigated.

## 9.2 Recommendations and Proposals for Further Investigations

### 9.2.1 FFE+SPR Chip – Technical Issues

In order to overcome deterioration of the sensitive SPR gold layer during thermal bonding, as described in chapter 8.3.2, a three layer (glass-PDMS-glass) chip was developed and fabricated. However, first observations showed that the shallow separation region and connecting channels (app. 15 µm in height) collapsed easily when pressure was applied to the top glass layer. This problem, caused by the high elasticity of PDMS, was known. However, it was expected to be a minor issue due to the more rigid glass-PDMS-glass sandwich structure. This problem puts high demands on a suitable chip holder. We see three feasible solutions to this problem:

i) The replacement of the sandwiched PDMS layer by an alternative more rigid material. Dry film resist technology, as successfully demonstrated by Vulto et al. [153], allows for multilayer microfluidic channel structures with no need for high temperature bonding. Furthermore, the stiffness of the material is certainly sufficient to avoid a collapse of the channels and the fabrication could be performed completely on wafer scale, in contrast to the single chip bonding procedure described here. PDMS was chosen in the first place due to the availability of the fabrication technology, material and full control over the channel and chip height.

ii) The redesign of the current chip layout in order to allow for the use of commercially available, Nanoport connectors (Upchurch, USA) which would avoid the compression of the sandwiched PDMS layer, since the connectors could be glued on top of the glass layer. Certainly an elegant solution, however reusability of these connectors is rather difficult and it would require an increased chip surface in order to place minimal 5 assemblies (see Fig. 9.1.a).

iii) A specially fabricated chip holder which fixates the assembled chip at two levels. The chip is placed in the SPR instrument slider, as shown in Fig. 8.5.b with the bottom chip plate in contact with the optical hemisphere. In addition, the overlapping edge of the chip top glass plate is placed on a supporting structure to transfer pressure forces caused by capillary connectors to the chip holder, as illustrated in Fig. 9.1.b. Certainly, this approach would require a difficult and precise chip alignment inside the holder.

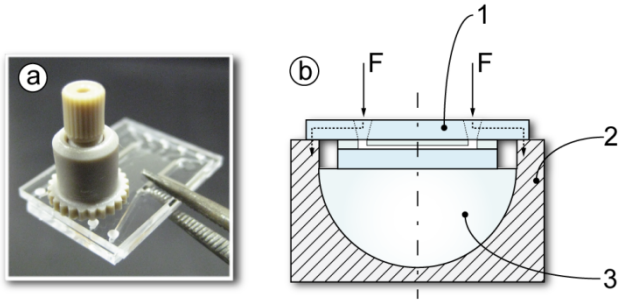


Fig. 9.1 (a) Photograph of the microfabricated FFE+SPR chip with a commercially available Upchurch Nanoport connecter. Although, the compression of the sandwiched PDMS layer could be avoided, a larger chip surface would be necessary. (b) Schematic chip holder configuration in order to transfer pressure forces caused by the chip holder lid (not shown here) to the surrounding structure. (1), three layer glass-PDMS-glass chip; (2), chip and hemisphere holder; (3) hemisphere;

### 9.2.2 Cascaded Free-Flow Electrophoresis

In order to achieve multidimensional separations or to increase overall separation performance, the coupling of several FFE units seems promising. Though difficult to realize on a large scale, due the enormous amount of fluid connections necessary, several microfluidic connected FFE units can be easily fabricated on one substrate, as successfully demonstrated by Albrecht et al. [60]. This and similar approaches especially in combination with the described FFE steering capability (as demonstrated in chapter 3.4.2) would allow for new multidimensional continuous flow separation methods. An example of such a cascaded FFZE-FFIEF device can be seen in Fig. 9.2. In such a system sample compounds separated in the first stage according to their charge to size ratio, could be steered towards a specific outlet connected to a second separation stage where pI based separation is performed. If e.g. proteins are separated in a wide pH gradient in the first dimension, a connected second FFIEF unit with a narrow pH gradient would allow for an increase in resolution in a specific pH range.

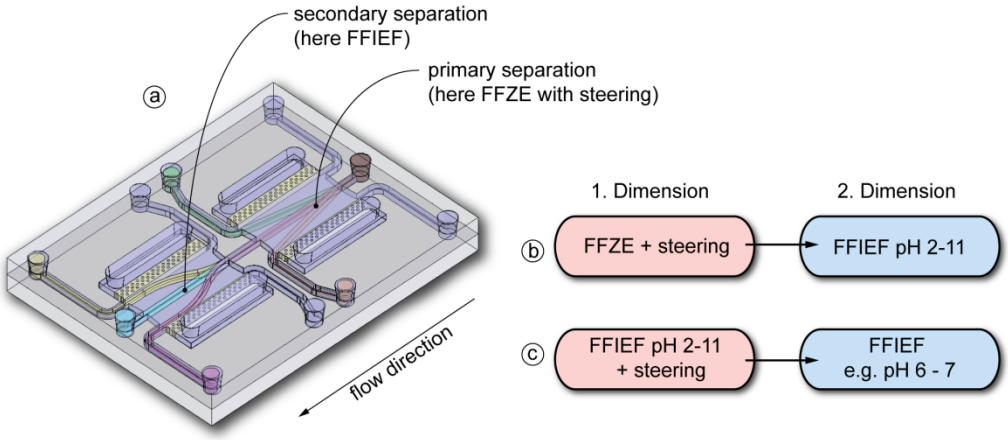


Fig. 9.2 (a) Illustration of a cascaded FFE system in which a FFZE unit with steering capability is connected to a FFIEF separation unit for 2D separations. (b) FFZE+FFIEF: Samples separated by FFZE according to their charge/size ratio can be steered to the FFIEF unit for pI based separations. (c) FFIEF+FFIEF: Fractions separated by FFIEF in wide range pH gradient can be steered to a FFIEF unit with a narrow pH gradient to increase resolution within a specific pH range.

### 9.2.3 FFZE of Whole Blood Samples

Free-flow electrophoretic separations have been applied to many different substances, among them also cell suspensions and cell fragments. As an excursion we performed FFZE of whole blood samples in order to separate red blood cells. Particular interest was put in the possible separation of human red bloods carrying transformed myoglobin, as can be observed in the sickle cell disease. Conventional large scale FFE separations were successfully applied to such blood samples as shown in Hannig [16]. However, a conventional FFE system can only be used as a preparative separation method to purify patient samples. In contrast to that, in a microfluidic FFE system, e.g., a simple conductivity sensor implemented in the outlet channels would allow for direct counting of healthy (biconcave shaped cells) and deformed sickel shaped red blood cells as illustrated in Fig. 9.3.

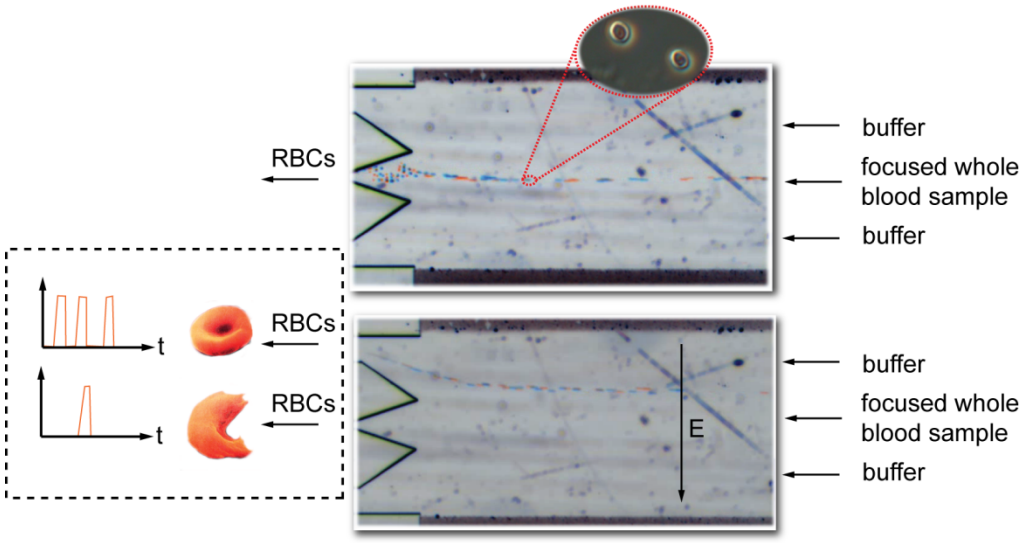


Fig. 9.3 Preliminary experimental results obtained during FFZE of whole blood. When the electrical field was applied the negatively charged RBC moved towards the anode. A method is proposed in which FFZE with integrated conductivity detection is used to separate and count healthy cells and sickle cells in order to obtain disease related information.

# References


1. Lewin, B., *Genes IX*. 2008: Jones and Bartlett Publishers.

2. Fields, S., *PROTEOMICS: Proteomics in Genomeland.* Science, 2001. **291**(5507): p. 1221-1224.

3. Freire, S.L.S. and A.R. Wheeler, *Proteome-on-a-chip: Mirage, or on the horizon?* Lab Chip, 2006. **6**: p. 1415-1423.

4. Lion, N., T.C. Rohner, L. Dayon, I.L. Arnaud, E. Damoc, N. Youhnovski, Z.-Y. Wu, C. Roussel, J. Josserand, H. Jensen, J.S. Rossier, M. Przybylski, and H.H. Girault, *Microfluidic systems in proteomics.* Electrophoresis, 2003. **24**(21): p. 3533-3562.

5. Visser, N.F.C. and A.J.R. Heck, *Surface plasmon resonance – mass spectrometry in proteomics.* Expert Review of Proteomics, 2008. **in press**.

6. Lokate, A.M.C., J.B. Beusink, G.A.J. Besselink, G.J.M. Pruijn, and R.B.M. Schasfoort, *Biomolecular Interaction Monitoring of Autoantibodies by Scanning Surface Plasmon Resonance Microarray Imaging.* J. Am. Chem. Soc., 2007. **129**(45): p. 14013-14018.

7. Beusink, J.B., A.M.C. Lokate, G.A.J. Besselink, G.J.M. Pruijn, and R.B.M. Schasfoort, *Angle-scanning SPR imaging for detection of biomolecular interactions on microarrays.* Biosensors and Bioelectronics, 2008. **23**(6): p. 839-844.

8. Figeys, D. and D. Pinto, *Proteomics on a chip: Promising developments.* Electrophoresis, 2001. **22**(2): p. 208-216.

9. Schasfoort, R.B.M., *Proteomics-on-a-chip:the challenge to couple lab-on-a-chip unit operations.* Expert Review of Proteomics, 2004. **1**: p. 123-132.

10. Koster, S. and E. Verpoorte, *A decade of microfluidic analysis coupled with electrospray mass spectrometry: An overview.* Lab Chip, 2007. **7**(11): p. 1394-1412.

11. Bier, M., *Electrophoresis*. 1967, New York: Academic Press.

12. Shaw, D.J., *Electrophoresis*. 1969, London: Academic Press.

13. Li, D., *Electrokinetics in Microfluidics*. 2004, Amsterdam: Elsevier, Academic Press.

14. Hannig, K., *Die trägerfreie kontinuierliche Elektrophorese und ihre Anwendung.* Z. Anal. Chem., 1961. **181**(181): p. 244-254.

15. Bauer, J., ed. *Special Issue on free-flow electrophoresis, Electrophoresis 1998, 19, 1057-1235*.

16. Hannig, K. and H.G. Heidrich, *Free-flow Electrophoresis*. 1990, Darmstadt: GIT Verlag.

17. Weber, G. and P. Bocek, *Recent developments in preparative free flow isoelectric focusing.* Electrophoresis, 1998. **19**(10): p. 1649-1653.

18. Weber, P.J.A., G. Weber, and C. Eckerskorn, *Protein Purification using free-flow electrophoresis*, in *Purifying Proteins for Proteomics: A Laboratory Manual*, R.J. Simpson, Editor. 2003, Cold Spring Harbor Laboratory Press: New York.

19. Mazereeuw, M., C.M.d. Best, U.R. Tjaden, H. Irth, and J.v.d. Greef, *Free Flow Electrophoresis Device for Continuous On-Line Separation in Analytical Systems. An Application in Biochemical Detection.* Anal. Chem., 2000. **72**: p. 3881-3886.

20. Chartogne, A., U.R. Tjaden, and J.V.d. Greef, *A free-flow electrophoresis chip device for interfacing capillary isoelectric focusing on-line with electrospray mass spectrometry.* Rapid Commun. Mass Spectrom., 2000. **14**: p. 1269–1274.

21. Tudos, A.J., G.A.J. Besselink, and R.B.M. Schasfoort, *Trends in miniaturized total analysis systems for point-of-care testing in clinical chemistry.* Lab Chip, 2001. **1**: p. 83-95.

22. Dittrich, P.S., K. Tachikawa, and A. Manz, *Micro Total Analysis Systems. Latest Advancements and Trends.* Anal. Chem., 2006. **78**: p. 3887-3908.

23. Manz, A. and J.C.T. Eijkel, *Miniaturization and chip technology. What can we expect?* Pure Appl. Chem., 2001. **73**(10): p. 1555-1561.

24. Das, C. and Z.H. Fan, *Effects of separation length and voltage on isoelectric focusing in a plastic microfluidic device.* Electrophoresis, 2006. **27**(18): p. 3619-3626.

25. Pamme, N., *Continuous flow separations in microfluidic devices.* Lab Chip, 2007. **7**(12): p. 1644-1659.

26. Baker, D.R., *Capillary electrophoresis*. 1995, New York: John Wiley and Sons Inc.

27. Krivánková, L. and P. Bocek, *Continuous free-flow electrophoresis.* Electrophoresis, 1998. **19**(7): p. 1064-1074.

28. Roman, M.C. and P.R. Brown, *Free-Flow Electrophoresis.* Anal. Chem., 1994. **66**(2): p. 86A-94A.

29. Kasicka, V., Z. Prusík, and J. Pospísek, *Conversion of capillary zone electrophoresis to free-flow zone electrophoresis using a simple model of their correlation.* J. Chromatogr. A, 1992. **608**: p. 13-22.

30. Kasicka, V., Z. Prusik, P. Sazelova, J. Jiracek, and T. Barth, *Theory of the correlation between capillary and free-flow zone electrophoresis and its use for the conversion of analytical capillary separations to continuous free-flow preparative processes: Application to analysis and preparation of fragments of insulin.* J. Chromatogr. A, 1998. **796**(1): p. 211-220.

31. Raymond, D.E., A. Manz, and H.M. Widmer, *Continuous Sample Pretreatment Using a Free-flow Electrophoresis Device Integrated onto a Silicon chip.* Anal. Chem., 1994. **66**: p. 2858-2865.

32. Gebauer, P. and P. Bocek, *A new type of migrating zone boundary in electrophoresis: 1. General description of boundary behavior based on electromigration dispersion velocity profiles.* Electrophoresis, 2005. **26**(2): p. 453-462.

33. Raymond, D.E., A. Manz, and H.M. Widmer, *Continuous Separation of High Molecular Weight Compounds Using a Microliter Volume Free-Flow Electrophoresis Microstructure.* Anal. Chem., 1996. **68**: p. 2515-2522.

34. Kohlheyer, D., G.A.J. Besselink, S. Schlautmann, and R.B.M. Schasfoort, *Free-flow zone electrophoresis and isoelectric focusing using a microfabricated glass device with ion permeable membranes.* Lab Chip, 2006. **6**: p. 374-380.

35. Fonslow, B.R. and M.T. Bowser, *Optimizing Band Width and Resolution in Micro-Free Flow Electrophoresis.* Anal. Chem., 2006. **78**: p. 8236-8244.

36. Kohlheyer, D., J.C.T. Eijkel, S. Schlautmann, A. van den Berg, and R.B.M. Schasfoort, *Microfluidic High Resolution Free-Flow Isoelectric Focusing.* Anal. Chem., 2007. **79**(21): p. 8190-8198.

37. Albrecht, J.W. and K.F. Jensen, *Micro free-flow IEF enhanced by active cooling and functionalized gels.* Electrophoresis, 2006. **27**: p. 4960-4969.

38. Wang, Q., H.D. Tolley, D.A. LaFebre, and M.L. Lee, *Analytical equilibrium gradient methods.* Anal. Bioanal. Chem., 2002. **373**: p. 125-135.

39. Righetti, P.G., *Isoelectric focusing: theory, methodology and applications*. Laboratory Techniques, ed. T.S. Work and R.H. Burdon. Vol. 11. 1983, Amsterdam: Elsevier Biomedical.

40. Bocek, P., M. Deml, P. Gebauer, and V. Dolnik, *Analytical Isotachophoresis*. 1988, Weinheim: Verlag Chemie.

41. Everaerts, F.M., K.L. Beckers, and T.P.E.M. Verheggen, *ISOTACHOPHORESIS - Theory, Instrumentation and Applications*. J. Chromatogr. Lib. Vol. 6. 1976, Amsterdam: Elsevier.

42. Gebauer, P. and P. Bocek, *Theory of zone separation in isotachophoresis: A diffusional approach.* Electrophoresis, 1995. **16**(1): p. 1999-2007.

43. Kuhn, R., S. Hoffstetter, and K.H. Wagner, *Free-flow electrophoresis for the purification of proteins: II. Isoelectric focusing and field step electrophoresis.* Electrophoresis, 1990. **11**(11): p. 942-947.

44. Stone, V.N., S.J. Baldock, L.A. Croasdell, L.A. Dillon, P.R. Fielden, N.J. Goddard, C.L.P. Thomas, and B.J.T. Brown, *Free flow isotachophoresis in an injection moulded miniaturised separation chamber with integrated electrodes.* J. Chromatogr. A, 2007. **1155**: p. 199-205.

45. Zhang, C.-X. and A. Manz, *High-Speed Free-Flow Electrophoresis on Chip.* Anal. Chem., 2003. **75**: p. 5759-5766.

46. Xu, Y., C.X. Zhang, D. Janasek, and A. Manz, *Sub-second isoelectric focusing in free flow using a microfluidic device.* Lab Chip, 2003. **3**: p. 224-227.

47. Janasek, D., M. Schilling, J. Franzke, and A. Manz, *Isotachophoresis in Free-Flow Using a Miniaturized Device.* Anal. Chem., 2006. **78**: p. 3815-3819.

48. de Jesus, D.P., L. Blanes, and C.L. do Lago, *Microchip free-flow electrophoresis on glass substrate using laser-printing toner as structural material.* Electrophoresis, 2006. **27**: p. 4935-4942.

49. Fonslow, B.R. and M.T. Bowser, *Free-Flow Electrophoresis on an Anodic Bonded Glass Microchip.* Anal. Chem., 2005. **77**: p. 5706-5710.

50. Fonslow, B.R., V.H. Barocas, and M.T. Bowser, *Using Channel Depth To Isolate and Controle Flow in a Micro Free-Flow Electrophoresis Device.* Anal. Chem., 2006. **78**: p. 5369-5374.

51. Kobayashi, H., K. Shimamura, T. Akaida, K. Sakano, N. Tajima, J. Funazaki, H. Suzuki, and E. Shinohara, *Free-flow electrophoresis in a microfabricated chamber with a micromodule fraction separator: Continuous separation of proteins.* J. Chromatogr. A, 2003. **990**(1-2): p. 169-178.

52. Lu, H., S. Gaudet, M.A. Schmidt, and K.F. Jensen, *A Microfabricates Device for Subcellular Organelle Sorting.* Anal. Chem., 2004. **76**: p. 5705-5712.

53. Song, Y.A., S. Hsu, A.L. Stevens, and J. Han, *Continuous-Flow pI-Based Sorting of Proteins and Peptides in a Microfluidic Chip Using Diffusion Potential.* Anal. Chem., 2006. **78**(11): p. 3528-3536.

54. Janasek, D., M. Schilling, A. Manz, and J. Franzke, *Electrostatic induction of the electric field into free-flow electrophoresis devices.* Lab Chip, 2006. **6**: p. 710-713.

55. Takamura, Y., H. Onoda, H. Indokuchi, A. Oki, and Y. Horiike, *Low-voltage electroosmosis pump for stand-alone microfluidics devices.* Electrophoresis, 2003. **24**: p. 185-192.

56. Schasfoort, R.B.M., S. Schlautmann, J. Hendrikse, and A. van den Berg, *Field-Effect Flow Control for Microfabricated Fluidic Networks.* Science, 1999. **286**(5441): p. 942-945.

57. Matsumoto, H., N. Komatsubara, C. Kuroda, N. Tajima, E. Shinohara, and H. Suzuki, *Numerical simulation of temperature distribution inside microfabricated free flow electrophoresis module.* Chem. Eng. J., 2004. **101**(1-3): p. 347-356.

58. Malmstrom, J., H. Lee, A.I. Nesvizhskii, D. Shteynberg, S. Mohanty, E. Brunner, M. Ye, G. Weber, C. Eckerskorn, and R. Aebersold, *Optimized Peptide Separation and Identification for Mass Spectrometry Based Proteomics via Free-Flow Electrophoresis.* J. Proteome Res., 2006. **5**(9): p. 2241-2249.

59. Fu, R., B. Xu, and D. Li, *Study of the temperature field in microchannels of a PDMS chip with embedded local heater using temperature-dependent fluorescent dye.* Int. J. Therm. Sci., 2006. **45**(9): p. 841-847.

60. Albrecht, J.W., J. El-Ali, and K.F. Jensen, *Cascaded Free-Flow Isoelectric Focusing for Improved Focusing Speed and Resolution.* Anal. Chem., 2007. **79**(24): p. 9364-9371.

61. Schasfoort, R.B.M., *Proteomics-on-a-chip: the challenge to couple lab-on-a-chip unit operations.* Expert Rev. Proteomic., 2004. **1**: p. 123-132.

62. Janasek, D., J. Franzke, and A. Manz, *Scaling and the design of miniaturized chemical-analysis systems.* Nature, 2006. **442**: p. 374-380.

63. Hoffmann, P., U. Häusig, P. Schulze, and D. Belder, *Microfluidic Glass Chips with an Integrated Nanospray Emitter for Coupling to a Mass Spectrometer.* Angew. Chem. Int. Edit., 2007. **46**(26): p. 4913-4916.

64. Belder, D., M. Ludwig, L.-W. Wang, and M.T. Reetz, *Enantioselective Catalysis and Analysis on a Chip.* Angew. Chem. Int. Edit., 2006. **45**(15): p. 2463-2466.

65. Kohlheyer, D., G.A.J. Besselink, S. Schlautmann, and R.B.M. Schasfoort, *An integrated system approach for protein discovery using miniaturized free-flow electrophoresis and surface plasmon resonance imaging*, in *Nanotech 2006*. 2006: Montreux, Switzerland.

66. Homola, J., *Present and future of surface plasmon resonance biosensors.* Anal. Bioanal. Chem., 2003. **377**(3): p. 528-539.

67. Dolník, V., S. Liu, and S. Jovanovich, *Capillary electrophoresis on microchip.* Electrophoresis, 2000. **21**(1): p. 41-54.

68. Uchiyama, K., H. Nakajima, and T. Hobo, *Detection method for microchip separations.* Anal. Bioanal. Chemistry, 2004. **379**(3): p. 375-382.

69. Hannig, K., *Die trägerfreie kontinuierliche Elektrophorese und ihre Anwendung.* Z. Anal. Chem., 1961(181): p. 244-254.

70. Barrolier, J., E. Watzke, and H. Gibian, *Einfache Apparatur für die trägerfreie präparative Durchlaufelektrophorese* Z. Naturforsch., 1965(13b): p. 238-252.

71. Obermaier, C., V. Jankowski, C. Schmutzler, J. Bauer, R. Wildgruber, M. Infanger, J. Köhrle, E. Krause, G. Weber, and D. Grimm, *Free-flow isoelectric focusing of proteins remaining in cell fragments following sonication of thyroid carcinoma cells.* Electrophoresis, 2005. **26**(11): p. 2109-2116.

72. Hoffstetter-Kuhn, S. and R.K.H. Wagner, *Free flow electrophoresis for the purification of proteins: I. Zone electrophoresis and isotachophoresis.* Electrophoresis, 1990. **11**(4): p. 304-309.

73. Weber, G. and P. Bo, *Recent developments in preparative free flow isoelectric focusing.* Electrophoresis, 1998. **19**(10): p. 1649-1653.

74. Poggel, M. and T. Melin, *Free-flow zone electrophoresis: A novel approach and scale-up for preparative protein separation.* Electrophoresis, 2001. **22**(6): p. 1008-1015.

75. Weber, G., M. Islinger, P.W. Christoph, and E.A. Völkl, *Efficient separation and analysis of peroxisomal membrane proteins using free-flow isoelectric focusing.* Electrophoresis, 2004. **25**(12): p. 1735-1747.

76. Bosse, M.A. and P. Arce, *Role of Joule heating in dispersive mixing effects in electrophoretic cells: Convective-diffusive transport aspects.* Electrophoresis, 2000. **21**(5): p. 1026-1033.

77. Kobayashi, H., K. Shimamura, T. Akaida, K. Sakano, N. Tajima, J. Funazaki, H. Suzuki, and E. Shinohara, *Free-flow electrophoresis in a microfabricated chamber with a micromodule fraction separator: Continuous separation of proteins.* J. Chromatogr. A, 2003. **990**(1-2): p. 169.

78. Chun, H., T.D. Chung, and H.C. Kim, *Cytometry and Velocimetry on a Microlfuidic Chip Using Polyelectrolytic Salt Bridges.* Anal. Chem., 2005. **77**: p. 2490-2495.

79. Lee, G.B., B.H. Hwei, and G.R. Huang, *Micromachined pre-focused MxN flow switches for continuous multi-sample injection.* J. Micromech. Microeng., 2001. **80**: p. 3863-3866.

80. Knight, J.B., A. Vishwanath, J.P. Brody, and R.H. Austin, *Hydrodynamic focusing on a silicon chip:mixing nanoliters in microseconds.* Phys. Rev. Lett., 1998. **80**: p. 3863-3866.

81. Kohlheyer, D., G.A.J. Besselink, R.G.H. Lammertink, S. Schlautmann, S. Unnikrishnan, and R.B.M. Schasfoort, *Electro-osmotically controllable multi-flow microreactor.* Microfluidics and Nanofluidics, 2005. **1**(3): p. 242-248.

82. Vidic, J., A. Podgornik, and A. Strancar, *Effect of the glass surface modification on the strength of methacrylate monolith attachment.* J. Chromatogr. A, 2005. **1065**(1): p. 51.

83. Cui, H., K. Horiuchi, P. Dutta, and C.F. Ivory, *Isoelectric Focusing in a Poly(dimethylsiloxane) Microfluidic Chip.* Anal. Chem., 2005. **77**(5): p. 1303-1309.

84. Horka, M., T. Willimannb, M. Blumb, P. Nordingb, Z. Friedlc, and K. Slais, *Capillary isoelectric focusing with UV-induced fluorescence detection.* J. Chromatogr. A, 2001. **916**: p. 65-71.

85. Soulet, N., H.R.-d. Balmann, and V. Sanchez, *Continuous flow isoelectric focusing for purification of proteins.* Electrophoresis, 1998. **19**: p. 1294-1299.

86. Lion, N., T.C. Rohner, L. Dayon, I.L. Arnaud, E. Damoc, N. Youhnovski, Z.-Y. Wu, C. Roussel, J. Josserand, H. Jensen, J.S. Rossier, M. Przybylski, and H.H. Girault, *Microfluidic systems in proteomics.* Electrophoresis, 2003. **24**: p. 3533-3562.

87. Chartogne, A., U.R. Tjaden, and J.V.d. Greef, *A free-flow electrophoresis chip device for interfacing capillary isoelectric focusing on-line with electrospray mass spectrometry.* Rapid. Commun. Mass Spectrom., 2000. **14**: p. 1269-1274.

88. Albrecht, J., S. Gaudet, and K.F. Jensen. *Rapid Free-Flow Isoelectric Focusing via Novel Electrode Structures*. in *9th International Conference on Miniaturized Systems for Chemistry and Life Sciences (μ-TAS2005)*. 2005. Boston, USA.

89. Albrecht, J. and K.F. Jensen. *Multi-Stage Free-Flow Isoelectric Focusing for Enhanced Separation Speed and Resolution*. in *μ-TAS 2006*. 2006. Tokyo, Japan.

90. Giddings, J.C. and K. Dahlgren, Sep. Sci., 1971. **6**: p. 345-356.

91. Cifuentes, A. and H. Poppe, *Rectangular Capillary Electrophoresis: Some Theoretical Considerations.* Chromatographia, 1994. **39**: p. 391-404.

92. Lammertink, R.G.H., S. Schlautman, G.A.J. Besselink, and R.B. M.Schasfoort, *Recirculation of Nanoliter Volumes within Microfluidic Channels* Anal. Chem., 2004. **76**: p. 3018-3022.

93. Giddings, J.C., *The Role of Lateral Diffusion as a Rate-Controlling Mechanism in Chromatography.* J. Chromatogr., 1961. **5**: p. 46-60.

94. Craig, D.B., B.K. Wetzl, A. Duerkop, and O.S. Wolfbeis, *Determination of picomolar concentrations of proteins using novel amino reactive chameleon labels and capillary electrophoresis laser-induced fluorescence detection.* Electrophoresis, 2005. **26**: p. 2208-2213.

95. Kohlheyer, D., J.C.T. Eijkel, A. van den Berg, and R.B.M. Schasfoort, *Miniaturizing free-flow electrophoresis - A critical review.* Electrophoresis, 2008. **29**: p. 977-993.

96. van der Schoot, B. and P. Bergveld, *An Isfet-Based Microliter Titrator Integration of a Chemical Sensor-Actuator System.* Sensors and Actuators, 1985. **8**: p. 11-22.

97. Wensink, H. and M.C. Elwenspoek, *Reduction of sidewall inclination and blast lag of powder blasted channels.* Sensors and Actuators A: Physical, 2002. **102**(1-2): p. 157-164.

98. Schlautman, S., H. Wensink, R. Schasfoort, M. Elwenspoek, and A.v.d. Berg, *Powder-blasting technology as an alternative tool for microfabrication of capillary electrophoresis chips with integrated conductivity sensors.* J. Micromech. Microeng., 2001. **11**: p. 386-389.

99. Gear, A.R.L., *Rhodamine 6G.* J. Biol. Chem., 1974. **11**: p. 3628-3637.

100. Rubinstein, I., ed. *Physical Electrochemistry*. 1995, Marcel Dekker, Inc.: New York.

101. Vijayan, M. and V. Krishnan, *Electrocatalytic oxidation of hydroquinone on a polypyrrole-coated glassy carbon electrode.* Electroanalysis, 1995. **7**(2): p. 197-198.

102. Bockris, J.O.M. and A.K.N. Reddy, *Modern Electrochemistry 1 - Ionics*. 1998, New York: Plenum Press.

103. Martin, M.M. and L. Lindqvist, *The pH dependence of fluorescein fluorescence.* Journal of Luminescence, 1975. **10**(6): p. 381-390.

104. Pérez-Ruiz, T., C. Martínez-Lozano, A. Sanz, and E. Bravo, *Separation of fluorescein dyes by capillary electrophoresis using β-cyclodextrin.* Chromatographia, 1998. **48**(3): p. 263-267.

105. Vilkner, T., D. Janasek, and A. Manz, *Micro Total Analysis Systems. Recent Developments.* Anal. Chem., 2004. **76**: p. 3373-3386.

106. Erickson, D. and D. Li, *Integrated microfluidic devices.* Analytica Chimica Acta, 2004. **507**(1): p. 11.

107. Huikko, K., R. Kostiainen, and T. Kotiaho, *Introduction to micro-analytical systems: bioanalytical and pharmaceutical applications.* European Journal of Pharmaceutical Sciences, 2003. **20**(2): p. 149.

108. Sato, K., A. Hibara, M. Tokeshi, H. Hisamoto, and T. Kitamori, *Microchip-based chemical and biochemical analysis systems.* Advanced Drug Delivery Reviews, 2003. **55**(3): p. 379.

109. Reynolds, O., *On the experimental investigation of the circumstances which determine whether the motion of water shall be direct or sinuous, and the law of resistance in parallel channels.* Phil. Trans. Roy. Soc., 1883. **174**: p. 935-982.

110. Knight, J.B., A. Vishwanath, J. P.Brody, and R.H. Austin, *Hydrodynamic Focusing on a Silicon Chip: Mixing Nanoliters in Microseconds.* Phy. Rev . Let., 1998. **80**(17): p. 3863-3866.

111. Dittrich, P.S. and P. Schwille, *An integrated Microfluidic System for Reaction, High-Sensitivity Detection, and Sorting of Fluorescent Cells and Particles* Anal. Chem., 2003. **75**: p. 5767-5774.

112. Lee, G.B., B.H. Hwei, and G.R. Huang, *Micromachined pre-focused MxN flow switches for continuous multi-sample injection.* J. Micromech. Microeng., 2001. **11**: p. 654-661.

113. Kenis, P.J.A., R.F. Ismagilov, S. Takayma, and G.M. Whitesides, *Fabrication Inside Microchannels Using Fluid Flow.* Acc. Chem. Res., 2000. **33**(12): p. 841-847.

114. Kenis, P.J.A., R.F. Ismagliov, and G.M. Whitesides, *Microfabrication Inside Capillaries Using Multiphase Laminar Flow Patterning.* Science, 1999. **285**: p. 83-85.

115. Shchukin, D.G., D.S. Kommireddy, Y. Zhao, T. Cui, G.B. Sukhorukov, and Y.M. Lvov, *Polyelectrolyte Micropatterning Using a Laminar Flow Microfluidic Device.* Adv. Mater., 2004. **16**(5): p. 389-393.

116. Bernard, A., B. Michel, and E. Delamarche, *Micromosaic Immonuassays.* Anal. Chem., 2001. **73**: p. 8-12.

117. Juncker, D., H. Schmid, A. Bernard, I. Caelen, B. Michel, N.d. Rooij, and E. Delamarche, *Soft and rigid two-level microfluidic networks for patterning surfaces.* J. Micromech. Microeng., 2001. **11**: p. 532-541.

118. T.Chiu, D., N.L. Jeon, S. Huang, R.S. Kane, C.J. Wargo, I.S. Choi, D.E. Inger, and G.M. Whitesides, *Patterned deposition of cells and proteins onto surfaces by using three-dimensional microfluidic systems.* Proc. Natl. Acad. Sci. USA, 1999. **97**(6): p. 2408-2413.

119. Regenberg, B., U. Krühne, M. Beyer, L.H. Pedersen, M. Simón, O.R.T. Thomas, J. Nielsen, and T. Ahl, *Use of laminar flow patterning of miniaturized biochemical assays.* Lab Chip, 2004. **4**: p. 654-657.

120. Brevig, T., U. Krühne, R.A. Kahn, T. Ahl, M. Beyer, and L.H. Pedersen, *Hydrodynamic guiding for addressing subsets of immobilized cells and molecules in microfluidic systems.* BMC Biotechnology, 2003. **3**(10).

121. Takayma, S., J.C. McDonald, E. Ostuni, M.N. Liang, P.J.A. Kenis, R.F. Ismagilov, and G.M. Whitesides, *Patterning cells and their enviroment using multiple laminar fluid flows in cappillary networks.* Proc. Natl. Acad. Sci. USA, 1999. **96**: p. 5545-5548.

122. Situma, C., M. Hashimoto, and S.A. Soper, *Merging microfluidics with microarray-based bioassays.* Biomolecular Engineering, 2006. **23**: p. 213-231.

123. Dusseiller, M.R., B. Niederberger, B. Städler, D. Falconnet, M. Textor, and J. Vörös, *A novel crossed microfluidic device for the precise positioning of proteins and vesicles.* Lab Chip, 2005. **5**: p. 1387-1392.

124. Effenhause, C.S., G.J. Bruin, and A. Paulus, *Integrated chip-based capillary electrophoresis.* Electrophoresis, 1997. **18**: p. 2203-2213.

125. Besselink, G.A.J., P. Vulto, R.G.H. Lammertink, S. Schlautmann, A.v.d. Berg, W. Olthuis, G.H.M. Engbers, and R.B.M. Schasfoort, *Electroosmotic guiding of sample flows in a laminar flow-chamber.* Electrophoresis, 2004. **25**: p. 3705-3711.

126. Kohlheyer, D., G.A.J. Besselink, R.G.H. Lammertink, S. Schlautmann, S. Unnikrishnan, and R.B.M. Schafoort, *Electroosmotically controllable multi-flow microreactor`*. Microfluidics & Nanofluidics, 2005. **1**(3): p. 242-248.

127. Lion, N., T.C. Rohner, L. Dayon, I.L. Arnaud, E. Damoc, N. Youhnovski, Z.-Y. Wu, C. Roussel, J. Josserand, H. Jensen, J. Rossier, M. Przybylski, and H. H.Girault, *Microfluidic systems in proteomics.* Electrophoresis, 2003. **24**: p. 3533-3562.

128. Ajdari, A., *Steady flows in networks of microfluidic channels: building on the analogy with electrical circuits.* C. R. Physique, 2003. **5**: p. 539-546.

129. Qiao, R. and N.R. Aluru, *A compact model for electroosmotic flows in microfluidic devices.* J. Micromech. Microeng., 2002. **12**: p. 625-635.

130. Wacker, R., H. Schröder, and C.M. Niemeyer, *Performance of antibody microarrays fabricated by either DNA-directed immobilization, direct spotting, or streptavidin-biotin attachment: a comparative study.* Biochemistry, 2004. **330**: p. 281-287.

131. Wacker, R. and C.M. Niemeyer, *DDI-µFIA-A readily configurable microarray-fluorescence immunoassay based on DNA-directed immobilization of proteins.* ChemBioChem, 2004. **5**: p. 453-459.

132. Haswell, S.J. and V. Skelton, *Chemical and biochemical microreactors.* TrAC Trends in Analytical Chemistry, 2000. **19**(6): p. 389-395.

133. Fletcher, P.D.I., S.J. Haswell, and V.N. Paunov, *Theoretical considerations of chemical reactions in micro-reactors operating under electroosmotic and electrophoretic control.* The Analyst, 1999. **124**: p. 1273-1282.

134. Haswell, S.J., R.J. Middleton, B. O'Sullivan, V. Skelton, P. Watts, and P. Styring, *The application of micro reactors to synthetic chemistry.* Chemical Communications, 2001(5): p. 391-398.

135. Brody, J.P., P. Yager, R.E. Goldstein, and R.H. Austin, *Biotechnology at low Reynolds numbers.* Biophys. J., 1996. **71**(6): p. 3430-3441.

136. Weigl, B.H. and P. Yager, *Silicon-microfabricated diffusion-based optical chemical sensor.* Sensors and Actuators B: Chemical, 1997. **39**(1-3): p. 452-457.

137. Baroud, C.N., F. Okkels, L. Ménétrier, and P. Tabeling, *Reaction-diffusion dynamics: Confrontation between theory and experiment in a microfluidic reactor.* Physical Review E, 2003. **67**(6): p. 060104.

138. Yunus, K., C.B. Marks, A.C. Fisher, D.W.E. Allsopp, T.J. Ryan, R.A.W. Dryfe, S.S. Hill, E.P.L. Roberts, and C.M. Brennan, *Hydrodynamic voltammetry in microreactors: multiphase flow.* Electrochemistry Communications, 2002. **4**: p. 579-583.

139. Lin, J.-Y., L.-M. Fu, and R.-J. Yang, *Numerical simulation of electrokinetic focusing in microfluidic chips.* Micromech. Microeng., 2002. **12**: p. 955-961.

140. Sinton, D., L. Ren, and D. Li, *A dynamic loading method for controlling on-chip microfluidic sample injection.* Journal of Colloid and Interface Science, 2003. **266**: p. 448-456.

141. Dittrich, P.S. and P. Schwille, *An Integrated Microfluidic System for Reaction, High-Sensitivity Detection, and Sorting of Fluorescent Cells and Particles.* Anal. Chem., 2003. **75**(21): p. 5767-5774.

142. Knight, J.B., A. Vishwanath, J.P. Brody, and R.H. Austin, *Hydrodynamic Focusing on a Silicon Chip: Mixing Nanoliters in Microseconds.* Phy. Rev. Let., 1998. **80**(17): p. 3863.

143. Lee, G.B., B.H. Hwei, and G.R. Huang, *Micromachined pre-focused MxN flow switches for continuous multi-sample injection.* Journal of Micromechanics and Microengineering, 2001. **11**: p. 654-661.

144. Besselink, G.A.J., P. Vulto, R.G.H. Lammertink, S. Schlautmann, A.v.d. Berg, W. Olthuis, G.H.M. Engbers, and R.B.M. Schasfoort, *Electroosmotic guiding of sample flows in a laminar flow chamber.* Electrophoresis, 2004. **25**(21-22): p. 3705-3711.

145. Fan, Z.H. and D.J. Harrison, *Micromachining of capillary electrophoresis injectors and separators on glass chips and evaluation of flow at capillary intersections.* Anal. Chem., 1994. **66**(1): p. 177-184.

146. Ajdari, A., *Steady flows in networks of microfluidic channels: building on the analogy with electrical circuits.* Comptes Rendus Physique, 2004. **5**(5): p. 539-546.

147. Qiao, R. and N.R. Aluru, *A compact model for electroosmotic flows in microfluidic devices.* Journal of Micromechanics and Microengineering, 2002. **12**: p. 625-635.

148. Song, H., M.R. Bringer, J.D. Tice, C.J. Gerdts, and R.F. Ismagilov, *Experimental test of scaling of mixing by chaotic advection in droplets moving through microfluidic channels.* Applied Physics Letters, 2003. **83**(22): p. 4664-4666.

149. Migliorini, P., F. Pratesi, C. Tommasi, and C. Anzilotti, *The immune response to citrullinated antigens in autoimmune diseases.* Autoimmunity Reviews, 2005. **4**(8): p. 561-564.

150. Rogers, J.A. and R.G. Nuzzo, *Recent progress in soft lithography.* Materials Today, 2005. **8**(2): p. 50-56.

151. Xia, Y. and G.M. Whitesides, *Soft Lithography.* Angew. Chem. Int. Edit., 1998. **37**(5): p. 550-575.

152. Jo, B.-H., L.M.V. Lerberghe, K.M. Motsegood, and D.J. Beebe, *Three-Dimensional Micro-Channel Fabrication in Polydimethylsiloxane (PDMS) Elastomer.* Journal of Micromechanical Systems, 2000. **9**: p. 76-81.

153. Vulto, P., N. Glade, L. Altomare, J. Bablet, L.D. Tin, G. Medoro, I. Chartier, N. Manaresi, M. Tartagnia, and R. Guerrieria, *Microfluidic channel fabrication in dry film resist for production and prototyping of hybrid chips.* Lab Chip, 2005. **5**: p. 158-162.

# Summary

This thesis describes the results of the four years research project to develop a new microfluidic chip for applications in proteomics analysis. The research was driven by the need for new analytical tools for proteomics research, here in particular tools to help understanding autoimmune diseases such as rheumatoid arthritis. In order to cope with the high complexity and diversity of proteomics related research microfluidic systems and in particular separation devices offer new possibilities such as highly decreased separation times, low sample volumes and increased separation resolution. Furthermore, the integration of sensors into such systems would lead to autonomously working analytical systems, often referred to as labs-on-a-chip.

The focus was put on the development of a new microfluidic free-flow electrophoresis chip with the final goal of implementing a surface plasmon resonance detection region for the separation and detection of specific proteins. Free-flow electrophoresis is the continuous separation of substances injected into a thin carrier flow with an electrical field applied perpendicular to the flow. Surface plasmon resonance is an optical label-free detection method for various substances, allowing real time monitoring of affinity based interactions. In essence more focus was directed to the free-flow electrophoresis techniques but integration with SPR imaging was realized. A patent was filed for this hyphenated FFE-SPR device and the work resulted in seven journal contributions. Four different miniaturized free-flow electrophoresis chips and two additional continuous flow devices were developed and successfully characterized whereby promising results could be obtained.

A new free-flow electrophoresis microchip with integrated permeable membranes was demonstrated, and different substances were separated by free-flow zone electrophoresis, free-flow isoelectric focusing and free-flow field step electrophoresis. This chip contained a new type of membranes enabling a stable carrier flow with a perpendicular electrical current. Due to this chip configuration, the device performance and efficiency were superior to recently published alternative systems in terms of separation resolution and sample capacity. The results furthermore indicate that even better results are possible. Analytes were separated and focused within hundreds of milliseconds whereby only nanoliters of samples were consumed. In addition, a new sample steering method was demonstrated during free-flow zone

electrophoresis, allowing the specific sorting of various components. As an alternative, a free-flow electrophoresis chip was developed with integrated platinum electrodes, whereby the generation of gas bubbles caused by electrolysis was successfully suppressed by chemical means. Gas bubbles generated by electrolysis are major concern in free-flow electrophoresis systems in general leading to distorted separation. Based on the results, a fourth free-flow chip was developed with an integrated surface plasmon resonance gold detection region. Although fabrication was successful, certain hurdles, in particular surface chemistry issues still remain to be overcome to perform separation and real-time detection of biological samples within this hyphenated micro device. A strategy for proteomics-on-a-chip was developed aiming at the separation of antigens that play a role in autoimmune diseases. In addition two new continuous flow microfluidic chips were developed allowing for continuous biochemical reactions or surface patterning applications. These devices could be of further interest in future, in particular in more complex analytical systems related to proteomics-on-a-chip.

# Samenvatting

Dit proefschrift beschrijft de resultaten van een vierjarig onderzoek ten behoeve van de ontwikkeling van een nieuwe microfluidische chip voor proteoomanalyse. Om een beter inzicht te krijgen in autoimmuunziekten zoals rheumatoide arthritis, is er behoefte aan nieuwe analytiche detectiemethoden om de hoge complexiteit en diversiteit van proteoom-gerelateerd onderzoek aan te kunnen. Hier bieden microfluidische systemen nieuwe voordelen zoals een kortere scheidingstijd, een verhoogde resolutie, en kleinere monstervolumes. Verder leidt de integratie van sensoren in zulke microfluidische chips tot autonoom werkende analytische systemen, laboratorium-op-een-chip genaamd.

De focus heeft gelegen op de ontwikkeling een nieuwe microfluidische free-flow elektroforese chip, met als uiteindelijk doel de implementering hierin van een gebied voor oppervlakte plasmon resonantie, voor de scheiding en detectie van specifieke eiwitten. Free-flow elektroforese, is de continue scheiding van deeltjes die geinjecteerd worden in een vloeistof dragerstroom door middel van een elektrisch veld dat loodrecht op de vloeistofstroom staat. Oppervlakte plasmon resonantie is een optische techniek om direct en zonder label deeltjes te detecteren tijdens op affiniteit gebaseerde interacties. In essentie is er het onderzoek gericht gewest op de realisatie van een goed FFE system waarbij de integratie van SPR niet uit het oog is verloren. Een octrooi is aangevraagd op het FFE-SPR combinatie technieken en zeven tijdschrift artikelen zijn publiceert. Vier verschillende geminiaturiseerde free-flow elektroforese en twee continuous-flow chips ontwikkeld en gekarakteriseerd waarbij veelbelovende resultaten zijn behaald.

Een nieuwe free-flow elektroforese microchip met geïntegreerde doorlaatbare membranen is gedemonstreerd en verschillende substanties zijn gescheiden met free flow zone elektroforese, isoelektrische focusering en free-flow field step elektroforese. Deze chip bevat een nieuw type membraan dat voor een stabiele vloeistof dragerstroom zorgt bij inschakeling van een orthogonale elektrische stroom. Door het ontwerp van deze chip zijn het behaalde resultaat en de effectiviteit superieur aan eerder gepubliceerde systemen ten aanzien van het scheidend vermogen en de capaciteit. De behaalde resultaten laten zien dat het maximaal haalbare nog niet is bereikt. Substanties werden gescheiden en geconcentreerd in enkele honderden milliseconden waarbij slechts nanoliters materiaal werden verbruikt. Daarnaast is een

nieuw monster aansturings mechanisme gedemonstreerd tijdens de free-flow zone elektroforese, waardoor de afzonderlijke fracties op te vangen zijn. De gasbelvorming in een free-flow elektroforese chip met platina elektrodes is succesvol chemisch onderdrukt. De gasbelvorming door elektrolyse is een groot probleem in free-flow elektroforese systemen aangezien het de scheiding verstoort. Een vierde free-flow electroforese chip met een geïntegreerd goud gebied voor oppervlakte plasmon resonantie is ontwikkeld aan de hand van de eerder behaalde resultaten. Hoewel de fabrikage van deze geïntegreerde microchip succesvol is verlopen, moeten er nog verschillende problemen worden opgelost vooral op het gebied van oppervlakte chemie, voordat een scheiding en directe detectie van biologische monsters gedemonstreerd kunnen worden. Er is een strategie ontworpen voor proteoom analyse-op-een-chip met als doel de scheiding van antilichamen die een belangrijke rol spelen in autoimmuunziekten. Daarnaast zijn ook nog twee continuous flow microfluidische chips ontwikkeld ten behoeve van continue biochemische reacties of oppervlaktebehandelingen. Deze chips kunnen interessante toepassingen hebben in de meer complexe analytische sytemen gerelateerd aan proteoom analyse-op-een-chip toepassingen.

# Abbreviations

| | |
|---|---|
| µ-FFE | microfluidic free-flow electrophoresis |
| µ-TAS | micro total analysis system |
| 2D GE | two dimensional gel electrophoresis |
| ASS | acetylsalicylic acid |
| BSA | bovine serum albumin |
| CE | capillary electrophoresis |
| CFD | computational fluid dynamics |
| CIEF | capillary isoelectric focusing |
| DDI | DNA-directed immobilization |
| DNA | deoxyribonucleic acid |
| DRIE | deep reactive ion etching |
| EDL | electrical double layer |
| EOF | electroosmotic flow |
| FFE | free-flow electrophoresis |
| FFFSE | free-flow field step electrophoresis |
| FFIEF | free-flow isoelectric focusing |
| FFITP | free-flow isotachophoresis |
| FFZE | free-flow zone electrophoresis |
| FITC | fluorescein isothiocyanate |
| $H_2Q$ | hydroquinone |
| HPLC | high performance liquid chromatography |
| HPMC | hydroxypropyl methyl cellulose |
| HSA | human serum albumin |
| IEF | isoelectric focusing |
| IPA | isopropyl alcohol |
| KOH | potassium hydroxide |
| LOC | lab-on-a-chip |

| | |
|---|---|
| m-FFE | mini free-flow electrophoresis |
| MS | mass spectrometry |
| MW | molecular weight |
| PDMS | polydimethylsiloxane |
| pI | isoelectric point |
| PMMA | poly(methyl methacrylate), acrylic glass |
| POC | point of care |
| Q | p-benzoquinone |
| QH | quinhydrone |
| RA | rheumatoid arthritis |
| ROI | region of interest |
| SPR | surface Plasmon resonance |

# List of Publications

**Journal articles**

D.R. Zalewski, D. Kohlheyer, S. Schlautmann and J.G.E. Gardeniers, *Synchronized, continuous flow zone electrophoresis.* **Analytical Chemistry 2008**, revision submitted

D. Kohlheyer, J.C.T. Eijkel, S. Schlautmann, A. van den Berg, and R.B.M. Schasfoort, *Bubble-free operation of a microfluidic free-flow electrophoresis chip with integrated Pt electrodes*. **Analytical Chemistry 2008**, published online, DOI: 10.1021/ac800275c

D. Kohlheyer, J.C.T. Eijkel, A. van den Berg, and R.B.M. Schasfoort, *Miniaturizing Free-Flow Electrophoresis - A critical Review*. **Electrophoresis, 2008,** 29, 977-993

D. Kohlheyer, S. Unnikrishnan, G.A.J. Besselink, S. Schlautmann, and R.B.M. Schasfoort, *A microfluidic device for array patterning by perpendicular electrokinetic focusing.* **Microfluidics and Nanofluidics 2007,** published online, DOI: 10.1007/s10404-007-0217-9

D. Kohlheyer, J.C.T. Eijkel, S. Schlautmann, A. van den Berg, and R.B.M. Schasfoort, *Microfluidic High-Resolution Free-Flow Isoelectric Focusing*. **Analytical Chemistry, 2007**. 79(21): p. 8190 - 8198

D. Kohlheyer, G.A.J. Besselink, S. Schlautmann, and R.B.M. Schasfoort, *Free-flow zone electrophoresis and isoelectric focusing using a microfabricated glass device with ion permeable membranes.* **Lab on a Chip, 2006**. 6(3): p. 374-380.

D. Kohlheyer, G.A.J. Besselink, R.G.H. Lammertink, S. Schlautmann, S. Unnikrishnan, and R.B.M. Schasfoort, *Electro-osmotically controllable multi-flow microreactor*. **Microfluidics & Nanofluidics, 2005**. 1(3): p. 242-248.

**Patent**

D. Kohlheyer and R.B.M. Schasfoort, System and Method for Separating, *Analysing, Detecting and/or Determining Particles in a Liquid Sample Flow*, **WO2007008064**, STW, **2007**.

**Conference contributions**

D. Kohlheyer, J.C.T. Eijkel, S. Schlautmann, van den Berg, A. and R.B.M. Schasfoort, *Microfluidic free-flow electrophoresis for proteomics on a chip*, MSB **2008**, Berlin, Germany

D. Kohlheyer, J.C.T. Eijkel, S. Schlautmann, A.van den Berg, and R.B.M. Schasfoort, *Rapid and high resolution Free Flow Isoelectric Focusing in a glass microchip*, in Nanotech Montreux 2007. **2007**: Montreux, Switzerland.

D. Kohlheyer, G.A.J. Besselink, S. Schlautmann, and R.B.M. Schasfoort, *Microfluidic free-flow Electrophoresis and isoelectric focusing for proteomics on a chip*, in Exploring new FRONTIERS in bio/nano. **2007**: Zermatt, Switzerland.

D. Kohlheyer, G.A.J. Besselink, S. Schlautmann, and R.B.M. Schasfoort, *An integrated system approach for protein discovery using miniaturized free-flow electrophoresis and surface plasmon resonance imaging*, in Nanotech Montreux 2006. **2006**: Montreux, Switzerland.

D. Kohlheyer, S. Schlautmann, G.A.J. Besselink, and R. Schasfoort, *Microfabricated free-flow electrophoresis device with integrated salt bridge* in 4th International Symposium on Separations in the Biosciences. **2005**: Utrecht, The Netherlands.

D. Kohlheyer, R.G.H. Lammertink, G.A.J. Besselink, S. Schlautmann, and R.B.M. Schasfoort. *Laminar Flow Microarray Patterning by Perpendicular Electrokinetic Focusing*. in Micro Total Analysis Systems **2005**. Boston, USA: Royal Society of Chemistry.

D. Kohlheyer, G.A.J. Besselink, S. Schlautmann, and R.B.M. Schasfoort, *Free-Flow-Electrophoresis chip with microfabricated salt-bridges*, in 3rd Gordon Research Conference on the Physics and Chemistry of Microfluidics. **2005**: Oxford, UK

D. Kohlheyer, R.G.H. Lammertink, S. Schlautmann, G.A.J. Besselink, and R.B.M. Schasfoort, *Reaction and Diffusion Dynamics in Address Flow Format*, in Netherlands Catalysis and Chemistry Conference. **2004**: Noordwijkerhout, The Netherlands.

D. Kohlheyer, R.G.H. Lammertink, G.A.J. Besselink, S. Schlautmann, and R.B.M. Schasfoort. *Electroosmotically controllable multiflow microreactor*. in 8th International Conference on Miniaturized Systems for Chemistry and

Life Sciences **2004**. Malmö, Sweden: Royal Society of Chemistry.

D. Kohlheyer, R.G.H. Lammertink, S. Schlautmann, G.A.J. Besselink, P. Vulto, and R.B.M. Schasfoort. *Reaction and Diffusion Dynamics in a Microfluidic Format*. in MRS Spring Meeting. **2004**. San Fransisco, USA: Mater. Res. Soc.

**Lectures**

D. Kohlheyer, *Microfluidic free-flow electrophoresis for proteomics on a chip,* University of Leipzig, Germany, December 7, **2007**

D. Kohlheyer, *Microfluidic tools for lab-on-a-chip applications*, Aachen University of Applied Sciences, Germany, November 30, **2007**

D. Kohlheyer, *An integrated system approach for protein discovery using miniaturized free-flow electrophoresis and surface Plasmon resonance imaging, Becton & Dickinson Diagnostics*, Munich Martinsried, Germany, March 23, **2007**

D. Kohlheyer, *Microfluidic free-flow electrophoresis for pre-fractioning and sorting of proteins,* Bionano Forum*,* University of Twente, The Netherlands, May 2, **2006**

# Acknowledgements

In 2003, at the time of joining the Biochip group lead by Richard Schasfoort for an internship and later, during my final thesis project at the FH Aachen, I had no real idea about how research would be like. But Inspired by my former professor for micro-technology Prof. Dr. Klaus-Peter Kämper, I had made up my mind to work in the area of BIOMEMS, although I didn't know much about it at that time. Today, five years later, I definitely can say that I did choose the right research field and place.

Multidisciplinary research is crucial in this field, and research can only be carried out in cooperation and intense interaction with a broad range of different scholars, industrialists and practitioners. It is my great pleasure to thank all of them, colleagues and project partners, for their immense support and constant encouragement that helped me in making this project a success. In particular, I would like to mention a few of them to whom I owe a special debt of gratitude for their inspiration, patience, understanding and guidance.

Richard, I would like to thank you for offering me this position in your proteomics-on-a-chip project and in your group. I truly enjoyed the space and the freedom you provided for me. I was always excited by your optimism and the power of your imagination during our discussions. (Dr. Richard Schasfoort)

Albert, I thank you for being my (third and final) promoter and for offering us a new home in your research group, BIOS. Especially during the last year I experienced a boost in research quality and supervision. (Prof. Dr. Albert van den Berg)

Special thanks go to my supervisors Geert and Jan who always kept reading and commenting my work and who were available when I had questions or doubts at any time. Although Geert left to start an industrial career, he frequently passes by for discussions and talks. Both of you were tremendously helpful and l always appreciated your contributions. Jan, I always thought research is about creating movies and images, however, you made me understand that there is much more. Geert, luckily you made me aware of the environment which blood cells like; I was already afraid something might be wrong with my blood. (Dr. Jan Eijkel, Dr. Geert Besselink)

What would this research have been without Stefan and Hans? Without you, there would have been many make-shift solutions with scotch-tape and the belief that

things would work somehow. Hans, despite your pieces of wisdom such as “komt wel goed”, “niet te laat maken”, “slaap erover” and more, you created technical solutions other researchers just dream of. From scratch you fabricated fantastic tools and holders sometimes within few days which came close to industrial products, rather than temporary research installations. Stefan, I cannot even imagine how many wafers and chips you produced for my project, but I guess hundreds. Although, in the beginning I wanted to do most of the cleanroom work by myself, soon I realized that eight years of cleanroom experience are not beatable. You always did an excellent job and you were always there for helpful discussions, coffee breaks and to join for the FC. Thank you, Hans and Stefan, for putting ideas and plans in practice so perfectly. (Dipl. Ing. Stefan Schlautmann, Hans de Boer)

I would like to thank Vinod and his whole research group and former colleagues in BPE. I felt at home in your group and enjoyed not only the coffee breaks and funny “uitjes” but also the extremely conducive working environment. Here at BIOS I certainly miss your newly build chemical lab which is exceptional. (Prof. Dr. Vinod Subramaniam)

I like to thank all the former and current Biochip people: I think we had a great time, especially during our endless penthouse coffee breaks, where the best research ideas were born, although some people would have appreciated a higher level of discussion. Looking back, I almost forgot about certain problems such as moving the lab three times or finding the right group and supervisor. Thanks to Arnoud for improving my dutch: “op de markt…”, Dawid for theoretical support, Bianca for help with biochemistry, Rob for doing the SEM analysis, Ganesh, Remco, Björn and others. Last but not least I thank Sandeep for his great contribution while he did his master thesis as part of my project.

I like to thank the whole Proteomics-on-a-Chip team for support and help. It was a pleasure to attend the project meetings and to see who is connected to whom within this project.

I would like to thank Dr. Gerhard Weber and colleagues from BD Diagnostics for their interest, kind support and generous supply of reagents.

Thanks to all (new) BIOS colleagues. I still didn’t get used to those strict coffee times.

Dietrich Kohlheyer, May 2008